

AD-A122 683

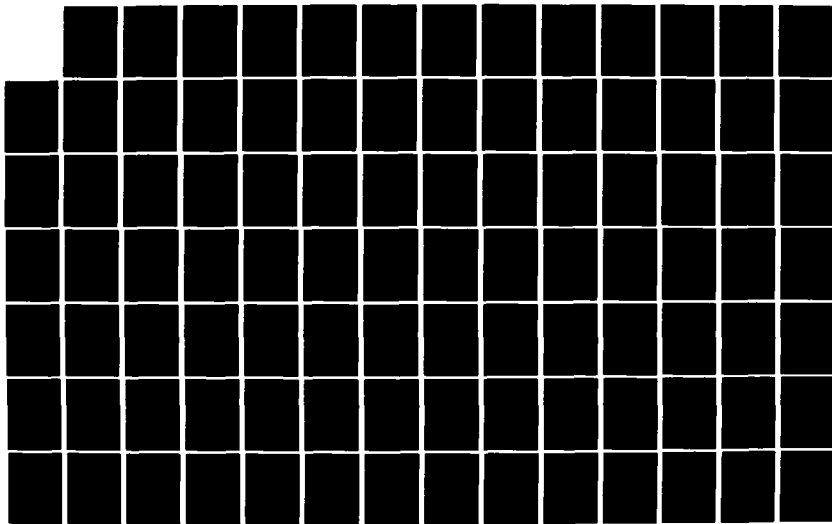
CERENKOV MASER AND CERENKOV LASER DEVICES(U) DARTMOUTH
COLL HANOVER N H DEPT OF PHYSICS AND ASTRONOMY
J E WALSH DEC 82 ARO-16572. 3-PH DAAG29-79-C-8283

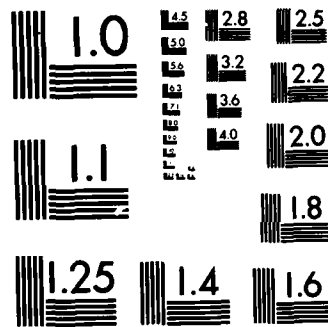
1/3

UNCLASSIFIED

F/G 28/5

NL





MICROCOPY RESOLUTION TEST CHART
NATIONAL BUREAU OF STANDARDS-1963-A

AD A 122683

FILE COPY

SECURITY CLASSIFICATION OF THIS PAGE (When Data Entered)

REPORT DOCUMENTATION PAGE		READ INSTRUCTIONS BEFORE COMPLETING
1. REPORT NUMBER 16572.3-PH	2. GOVT ACCESSION NO. AD-A122683	3. REPORT DATE 10 Sep 79 - 9 Sep 82
4. TITLE (and Subtitle) Cerenkov Maser and Cerenkov Laser Devices		5. TYPE OF REPORT Final
7. AUTHOR(s) John E. Walsh		8. CONTRACT OR GRANT NUMBER DAAG29 79 C 0203
9. PERFORMING ORGANIZATION NAME AND ADDRESS Dartmouth College Hanover, NH 03755		10. PROGRAM ELEMENT PROJECT AREA & WORK UNIT NUMBERS
11. CONTROLLING OFFICE NAME AND ADDRESS U. S. Army Research Office Post Office Box 12211 Research Triangle Park, NC 27709		12. REPORT DATE Dec 82
14. MONITORING AGENCY NAME & ADDRESS (if different from Controlling Office)		13. NUMBER OF PAGES 239
		15. SECURITY CLASS. (of this report) Unclassified
		15a. DECLASSIFICATION/DOWNGRADING SCHEDULE
16. DISTRIBUTION STATEMENT (of this Report) Approved for public release; distribution unlimited.		
17. DISTRIBUTION STATEMENT (of the abstract entered in Block 20, if different from Report) NA		
18. SUPPLEMENTARY NOTES The view, opinions, and/or findings contained in this report are those of the author(s) and should not be construed as an official Department of the Army position, policy, or decision, unless so designated by other documentation.		
19. KEY WORDS (Continue on reverse side if necessary and identify by block number) masers lasers Cerenkov radiation power sources		
20. ABSTRACT (Continue on reverse side if necessary and identify by block number) Four documents, which together serve as a review of experimental verification and the theoretical description of stimulated Cerenkov masers, is presented. Multi-hundred KW power levels have been obtained in the longer mm wavelength range and significant power at wavelengths shorter than 1.5 mm have been observed. The relations between resonator dimensions and beam parameters which determine wavelength, gain, and output power, have been established.		

CERENKOV MASER AND CERENKOV LASER DEVICES

Final Report: Department of the Army Contract

DAAG 29-79-C-0203

09/10/79 - 09/09/82

* * *

Prepared by

John E. Walsh

Department of Physics & Astronomy

Dartmouth College

Hanover, N.H. 03755

* * *

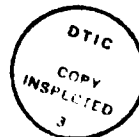
Contents

Abstract

- I. Introduction
- II. Published Abstracts
- III. Technical Reports

Abstract

Four documents, which together serve as a review of experimental verification and the theoretical description of stimulated Cerenkov masers, is presented. Multi-hundred KW power levels have been obtained in the longer mm wavelength range and significant power at wavelengths shorter than 1.5 mm have been observed. The relations between resonator dimensions and beam parameters which determine wavelength, gain, and output power, have been established.



A

I. Introduction

This final report covers research carried out during the period 09/01/79 to 09/09/82 under U.S. Army Contract DAAG 29-79-0203. The principle goal of the work was the development of high power Cerenkov sources in the lower mm wavelength range. It was demonstrated that a Cerenkov maser, which consists of a mildly relativistic electron beam and a tubular dielectric resonator, is capable of producing power at the multi-hundred KW level with efficiencies in the ten percent range. A detailed discussion of this device is found in Section III c), Characterization of a Cerenkov Maser, by S. Von Laven. Also contained in Section III are a general review of the process of stimulated Cerenkov radiation, and a paper which examines the concept of submm FIR-tunable Cerenkov devices. Published abstracts are reproduced in Section II.

II. Published Abstracts

1. Stimulated Raman Scattering from Electron Beams in Dielectric Resonators, K. Busby, K. Felch, R.W. Layman, and J. Walsh, Bull. Am. Phys. Soc. 24, 607 (1979).
2. A Cerenkov-Raman Radiation Source, K. Busby, K. Felch, R. Layman, J. Walsh, IEEE International Conference on Plasma Science, June, 1979.
3. Generation of Millimeter Microwaves Using the Cerenkov Interaction, K. Felch, K. Busby, J. Walsh, and R. Layman, Bull. Am. Phys. Soc. 24, 1076 (1979).
4. Multiple Frequency Output of a Raman Maser with a Magnetic Wiggler Pump, K. Busby, K. Felch, R. Layman, D. Kapilow, and J. Walsh, IEEE International Conference on Plasma Science, May, 1980.
5. Stimulated Cerenkov Radiation at Lower mm Wavelengths, J. Walsh, D. Kapilow, R. Layman, D. Speer, J. Branscum, D. Wise, and C. Hanna, Bull. Am. Phys. Soc. 25, 949 (1980).
6. Stimulated Cerenkov Radiation Experiments, J. Walsh, R. Layman, J. Branscum, J. Golub, D. Speer, and D. Wise, IEEE International Conference on Plasma Science, May, 1981.
7. The Generation of Coherent Millimeter Microwaves by Cerenkov Radiation, K. Busby, R. Layman, K. Felch, D. Kapilow, J. Walsh, Bull. Am. Phys. Soc. 26, 797 (1981).
8. Relativistic Beam Propagation in a Dielectric Lined Waveguide, J. Branscum, J. Walsh, and R. Layman, Bull. Am. Phys. Soc. 26, 798 (1981).
9. Power Characterization of a Cerenkov Maser, S. Von Laven, J. Branscum, J. Golub, R. Layman, D. Speer, and D. Wise, Bull. Am. Phys. Soc. 26, 936 (1981).
10. Cerenkov Masers: A Possible Plasma Heating Source, J. Walsh, J. Branscum, J. Golub, R. Layman, D. Speer, S. Von Laven, 11th Anomalous Absorption Conference, Montreal, Canada, June 1981.
11. Millimeter Wave Generation with a Relativistic Electron Beam, R. Layman, J. Branscum, and J. Walsh, Bull. Am. Phys. Soc. 27, 93 (1982).
12. A Two-Stage Cerenkov Oscillator, J. Walsh, S. Von Laven, R. Layman, E. Garate, and R. Cook, Bull. Am. Phys. Soc. 27, 1017 (1982).

April 23-26, 1979

Stimulated Raman Scattering from Electron Beams
in Dielectric Resonators. K. BUSBY, K. FELCH, R.W.
LAYMAN, J.E. WALSH, Dartmouth College.*--The addition
of a dielectric resonator to an electron beam Raman
scattering experiment can dramatically shorten the wave-
length of the output radiation. Well above the guide
cutoff frequency the output wavelength λ_s is:

$$\lambda_s = \lambda_p (1 - \beta_o n) / \beta_o$$

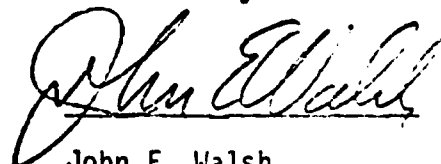
where λ_p is the pump ripple length and β_o is average
electron beam velocity. A combination Cerenkov-Raman
scattering experiment has been designed to test this
reduction. We use a tubular dielectric resonator and a
rippled magnetic field as a pump field. The effective
intensity of the pump field is approximately 20 MW/cm².
This together with electron beam voltages and currents
of 100-200 KV and 10 A respectively will lead to stimu-
lated Cerenkov-Raman growth lengths of .2-.5 cm⁻¹. The
device performance will be discussed.

*Work supported in part by U.S. Army Grant #DAAG39-78-
C-0032 and in part by U.S.AFOSR Grant # 77-3410

Prefer Oral Session

Appendix II

Submitted by:



John E. Walsh
Dartmouth College
Hanover, N.H. 03755

A Cerenkov-Raman Radiation Source. K. BUSBY,
K. FELCH, R.W. LAYMAN, J.E. WALSH, Dartmouth College.*
—Stimulated Raman Scattering from an electron beam in
a dielectric medium shows a number of interesting and
potentially useful features¹. In a dielectric the
particle velocity can exceed the speed of light and
hence there are two possible dispersion curves along
which energy and momentum can be conserved. Further-
more, in the neighborhood of the Cerenkov velocity
threshold very large Doppler shifts can be obtained
and thus this interaction can be the basis of a short
wavelength radiation source.

In order to test the potential of such a
device an experiment which uses a mildly relativistic
electron beam, a dielectric resonator, and a rippled
magnetic field for a pump wave has been constructed.
The transverse component of the magnetic field is
approximately 300 G which implies an effective pump
wave intensity of 20 MW/cm².

With beam voltages between 100 and 200 KV and
beam currents in the 10A range, operation in the
lower and middle part of the mm wave length region of
the spectrum is anticipated. The performance of the
device will be discussed.

*Work supported in part by U.S. Army Grant #DAAG39-78-
-C0032 and in part by U.S.AFOSR Grant # 77-3410

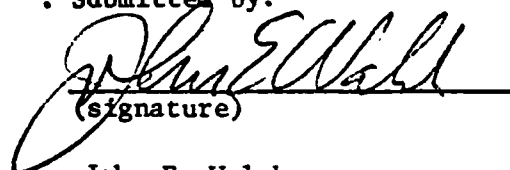
1. J.E. Walsh, G. Crew, Bull. Am. Phys. Soc. 23, 748,
(1978)

Appendix III

. Subject category number:

- . () Prefer oral session
. () Prefer poster session
. (x) No preference
. () Special requests for
placement of this
abstract
-
-
-

. Submitted by:


(signature)

John E. Walsh

(same name typewritten)

Department of Physics

(full address)

Wilder Hall

Dartmouth College

Hanover, N.H. 03755

. I am member of the Committee
on Plasma Science and Appli-
cations:

() yes (x) no

Abstract Submitted
For the Twenty-first Annual Meeting
Division of Plasma Physics
November 12 to 16, 1979

Subject Category Number 4.8

Generation of Millimeter Microwaves Using the Cerenkov Interaction. K. Felch, K. Busby, J.E. Walsh, and R.W. Layman, Dartmouth College.*--Earlier experiments involving the Cerenkov interaction between a relativistic electron beam and a dielectric loaded waveguide yielded 6 mm microwaves.¹ These experiments indicated that microwaves of significantly shorter wavelengths might be possible using the same procedures. The present experiments extend the previous attempts into the 3 mm range. Methods by which shorter wavelengths are achieved using the Cerenkov interaction and the short wavelength limit of such techniques will be discussed. Results of the latest experimental investigations will be presented.

*Work supported in part by U.S. Army Grant #DAAG39-78-C-0032 and in part by U.S. AFOSR Grant #77-3410.

¹K. Felch, K. Busby, J.E. Walsh, and R.W. Layman, Bull. Am. Phys. Soc. 23, 749 (1978).

() Prefer Poster Session

(X) Prefer Oral Session

() No Preference

() Special Requests for placement of this abstract:

() Special Facilities Requested (e.g., movie projector)

Submitted by:

Kevin Lee Felch
(signature of APS member)

Kevin Lee Felch
(same name typewritten)

H B 6127, Dartmouth College,
(address) Hanover, N.H. 03755

This form, or a reasonable facsimile, plus Two Xerox Copies must be received NOT LATER THAN FRIDAY, AUGUST 17, 1979 at the following address:

Division of Plasma Physics Annual Meeting
Mrs. Marianne Weissenburger
Plasma Physics Laboratory
P.O. Box 451
Princeton, N.J. 08540

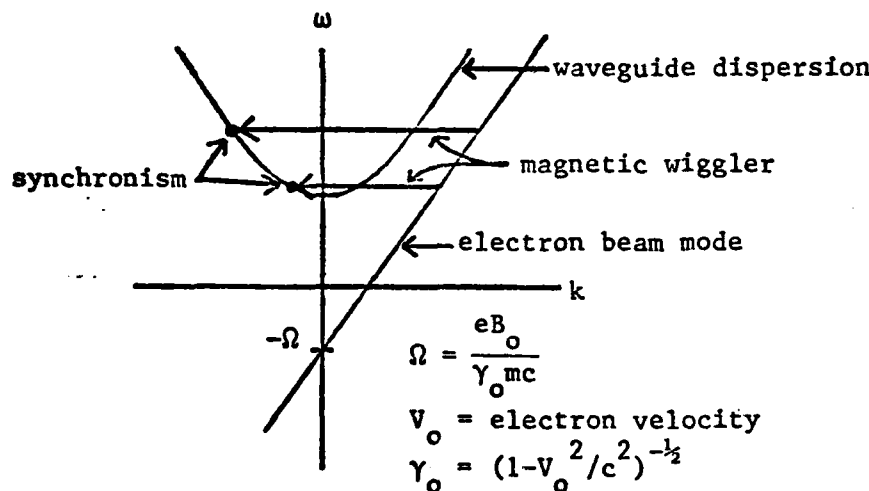
May 19-21, 1980

Multiple Frequency Output of A Raman Maser With A Magnetic Wiggler Pump. K. BUSBY, K. FELCH, R.W. LAYMAN, D. KAPLOW, J.E. WALSH, Dartmouth C.**--Microwave output at two

distinct frequencies from a Raman maser has been observed. The microwave production is due to the interaction of a 40-100 KeV, 10 A electron beam with a 0.9 cm period, zero frequency, magnetic wiggler field. The undulations are a 15% perturbation to the guiding magnetic field. The interaction takes place within a waveguide.

The electron velocities are too low to interact with the fundamental wavelength, $\lambda_p = 0.9$ cm, undulations, but the electrons do interact with higher harmonic wavelengths. Only the odd harmonics need be considered since the magnetic wiggler appears approximately as a square wave.

As shown in the figure, synchronism occurs when the negative energy cyclotron beam mode dispersion ($\omega_b = -\Omega + kv_0$) couples to the magnetic wiggler dispersion ($\omega_{\text{pump}} = 0$, $k_{\text{pump}} = 2\pi n/\lambda_{\text{pump}}$, $n = 1, 3, 5, \dots$) such that the waveguide dispersion is satisfied. The two horizontal lines are the third and fifth harmonics of the magnetic wiggler dispersion.



With 73 KeV electrons, $B_0 = 6200$ gauss, and a TE₀₁ cutoff frequency of 29.1 GHz, the frequencies at synchronism are 30 and 48 GHz, the observed frequencies are 29 and 42 GHz. Convective instabilities at $(+|\omega|, +|k|)$ are possible, but are at higher frequency.

Gain calculations, in the collective regime, for the Raman interaction between a relativistic electron beam and a static magnetic wiggler field will be presented. Waveguide effects will be included.

*Submitted by R.W. Layman

**Supported in part by U.S. Army Grant#DAAC30-78-C-0032 and in part by U.S. AFOSR Grant # 77-3410.

Please refer to "Last Call for Papers" announcement for instructions in preparing your abstract.

• Subject category number:

25

- (X) Prefer oral session
- () Prefer poster session
- () No preference
- () Special requests for placement of this abstract

If more than one session is offered, we want to be in the first session.

• Submitted by:

R.W. Layman
(Signature)

R.W. Layman
(same name typewritten)

Physics Department
(full address)

Dartmouth College

Hanover, NH 03755

- I am a member of the Committee on Plasma Science and Applications

() yes

(X) no

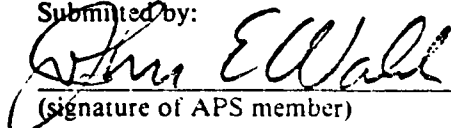
Abstract Submitted
For the Twenty-second Annual Meeting
Division of Plasma Physics
November 10 to 14, 1980

Subject Category Number 4.8

Stimulated Cerenkov Radiation at Lower mm
Wavelengths, J. WALSH, D. KAPLOW, R. LAYMAN, D. SPEER,
J. BRANSCUM, D. WISE and C. HANNA, Dartmouth College--
Stimulated Cerenkov radiation is generated by a mildly
relativistic electron beam dielectric resonator
combination. The 200KV, 5-10A 1 usec electron beam
pulse is produced by a transformer and a pulse forming
network. The radiation is contained in two modes, the
first in the 4-8 mm region and the second between 1 and
2 mm. The operating wavelength is determined by the
beam voltage and the resonator dimensions. The wave-
lengths are measured with internal reflection filters,
cutoff filters, and a mechanically tuned Fabry-Perot
resonator. The effects on device performance of a
variety of quasi-optical feed back and mode control
techniques will be discussed.
Supported in part by the Army Research Office Grant #
DAAG29-79C-0203.

- ☐ Prefer Poster Session
- ☒ Prefer Oral Session
- ☐ No Preference
- ☐ Special Requests for placement
of this abstract:
- ☐ Special Facilities Requested
(e.g., movie projector)

Submitted by:


(signature of APS member)

John E. Walsh

(same name typewritten)

Dartmouth College

(address)

This form, or a reasonable facsimile, plus *Two Xerox Copies* must be received NOT LATER
THAN WEDNESDAY, AUGUST 13, 1980 at the following address:

Division of Plasma Physics Annual Meeting
Ms. Diane Miller
Jaycor
P.O. Box 370
Del Mar, California 92014

Abstract submitted for the
1981 IEEE INTERNATIONAL CONFERENCE ON PLASMA SCIENCE
May 18-20, 1981

Stimulated Cerenkov Radiation Experiments.

J.E. WALSH, J. BRANSCUM, J. GOLUB, D. SPEER, D. WISE, and R. LAYMAN, Dartmouth College. *--An electron beam generator with a voltage range of up to 400 kv and an output current of 0.1A to 20A has been used to conduct stimulated Cerenkov radiation experiments. A tubular quartz dielectric resonator is used as a slow wave structure for TM_{0n} waves which interact synchronously with the electron beam. Using a series of resonator designs coherent oscillations have been obtained in the wavelength range between 1.5 cm and 1.5 mm. Power output at the longer wavelengths is in the range of tens of kws while that at shorter wavelengths it is approximately one kw. At the present time the beam is collected on a mirror set at a 45° angle to the end of the resonator. The mirror reflects the output through a collimating lens to a Fabry-Perot interferometer.

A description of the apparatus and experiments with various resonator parameters such as dielectric constant, radial dimensions and length will be described. A discussion of theory and the correlation of theory and experiment will be presented.

*Work supported in part by U.S. Army Grant #DAAG 29-79-C0203

Please refer to "First and Final Call for Papers" announcement for instructions in preparing your abstract.

● Subject category name:
High Power Microwave
Generation

● Subject category number:

17

- () Prefer oral session
- () Prefer poster session
- (X) No preference
- () Special requests for placement of this abstract

● Submitted by:

R.W. Layman
(Signature)

R.W. Layman

(same name typewritten)

Physics Department

(full address)

Dartmouth College

Hanover, N.H. 03755

● I am a member of the Committee on Plasma Science and Applications:

() yes (x) no

which is linearly dependent on the well depth D , and instability in D affects the stability of the ν resonance. A lower potential with greater stability should allow us to obtain a single proton linewidth of 0.005 Hz limited by detection circuit damping. Comparison of proton and electron cyclotron resonances yield a preliminary mass ratio $m_p/m_e = 1836.15300(25)$ where the uncertainty has been increased by 0.1 ppm to cover a possible systematic error.¹ This value is 20 times more accurate than our previously reported value.²

¹R.S. Van Dyck, Jr., P.B. Schwinberg, and S.H. Bailey in *Atomic Masses in Fundamental Constants 6* (Plenum, 1980).

²R.S. Van Dyck, Jr., and P.B. Schwinberg, to be published in *Bull. Am. Phys. Soc.* **26** (1981).

SESSION E: SPECTROSCOPY

Saturday morning, 18 April 1981

Salisbury Labs, Room 121 at 9:00 A.M.

T. H. Keil, presiding

E1 An Exact Solution to the Problem of Self-Diffusion Via the Vacancy Mechanism in the Sudden Jump Approximation. B. GRALLA and L. GUNTER, Tufts U.--An exact solution has been obtained for the problem of self-diffusion by the vacancy mechanism in the sudden jump approximation.¹ The probability distribution function $P(\vec{r}, t)$ for locating a marked atom at a lattice position \vec{r} at a time t can be expressed as an integral. The theory is relevant over time scales on the order of the mean jump time or greater. Therefore, not only can we obtain the diffusion constant but we can also calculate the effect of self-diffusion of a Mössbauer atom on the Mössbauer spectrum. In the case of the linear chain we have a solution in terms of known functions. In particular the mean square displacement $\langle r^2 \rangle$ of a marked atom is proportional to $t^{1/2}$ as t approaches infinity, which is a well-known result.² The Bardeen-Herring correlation factor f for the diffusion constant for a square lattice has been found equal to $(\pi-1)^{-1}$, in agreement with the value obtained by Schoen and Lowen³ using direct combinatorial techniques. Work is in progress in calculating the correlation factors for three-dimensional lattices and on calculating the corresponding Mössbauer spectra.

¹M.C. Ditar Ure and P.A. Flinn, *Phys. Rev.* **15B**, 1261 (1977).

²D.L. Huber, *Phys. Rev.* **B15**, 533 (1977).

³A.H. Schoen and R.W. Lowen, *Bull. Am. Phys. Soc.* **5**, 280 (1960).

E2 Optical Detection of Stored Mg^+ Ions in an RF Trap. W. NAGOURNEY and H. BEDERSON, Univ. of Washington.--We have observed fluorescence from the $3^2S_{1/2}$ to $3^2P_{1/2}$ transition at 2794 Å of Mg^+ ions contained in a small RF trap ($2z = 1.0$ cm, $2r = 0.1$ cm). The ions were trapped in a well about 10 volts deep by application of a 2.0 volt RF potential at 11 MHz between the ring and end caps. The 2794 Å source was a frequency doubled, cavity stabilized single frequency commercial dye laser producing about 1 uW focussed to a 0.7 mm spot diameter. Viscous cooling of the ions in a 10^{-7} Torr He buffer gas was necessary for observation of the strongest signals (4×10^4 counts/s). We estimate that about 10⁴ ions were observed. At much lower pressures ($< 10^{-8}$ Torr) we have observed small numbers of ions (< 10 , estimated) for short times (up to 20 sec). We are currently attempting to radiatively cool the ions by down tuning the laser; our ultimate goal is to observe a single Mg^+ ion cooled to considerably below room temperature. This work is supported by the ONR.

E3 Fastest Rabi Frequency Measurement with $n=0.1$ in QED. H. SCHMIDT and G. GUNTER, Univ. of Washington.--From $t = 0$ to 1 sec the electron in the $n=0$ state is subjected to a microwave pulse whose frequency and amplitude were varied. The Rabi frequency was measured by the Rabi method and the Rabi frequency was found to be 1.0×10^6 Hz and the Rabi frequency was found to be 1.0×10^6 Hz.

$\nu(12) > \dots$ refer to the $n=0 \rightarrow 1$, $n=1 \rightarrow 2$, ... transitions spaced by 150 Hz, and $\nu(01)$ is adjusted for a $n=0 \rightarrow 1$ Rabi frequency of 50 Hz. Now, after a successive imperfect adiabatic fast passages moving the electron from $n=0 \rightarrow 1$, $1 \rightarrow 2$, $2 \rightarrow 3$, ... the exciting resonance effectively becomes the synchrotron mechanism, the frequency of the motion following $\nu(t)$. The corresponding n increase is easily observed via a ν shift of ± 1 Hz. For the electron initially in $n=1$, on the other hand, the first adiabatic fast passage moves it into $n=0$ at which it remains as the $n=1 \rightarrow 2$ transition cannot proceed. In an alternate faster scheme the n -state energy is selectively multiplied in $\nu(10)$ used by the inhomogeneous field of a microwave at $\nu(01) = 30$ kHz. The excitation band is carefully adjusted from $\nu(01)$ to $\nu(10) = 30$ kHz. Now, on the average, the $n=1$ state energy is multiplied $\times 100$ while the $n=0$ state energy remains the same. Detection is again via mass increase. We thank the National Science Foundation for support.

SESSION F: NUCLEAR/PARTICLE PHYSICS

Saturday morning, 18 April 1981

Olin Hall, Room 107 at 9:00 A.M.

V. Bluemel, presiding

F1 Achromatic Proton Microbeam. F. W. MARTIN, Microscopy Associates, Inc. and R. GOLOSKE, Argonne Polytechnic Institute.--An achromatic quadrupole lens doubler is being evaluated as a means of forming finely focused ion beams. Experimental measurements indicate that a small image broadens less than 5 microns when the energy of transmitted protons is varied from 550 to 800 keV. A chromatic aberration coefficient of less than 0.4 cm is derived. Typical measurements of beam dimension, made using the Rutherford backscattering technique, will be presented. Procedures will be discussed for minimizing parasitic first- and second-order aberrations by electrical rotation of the principal sections of a lens* and by means of an off-center aperture placed to give orthogonal measurement of the undesired hexapole field component. An open house will be held at the WPI Van de Graaf Laboratory (Physics building, basement, south end, Room 004) on Saturday, April 18, 11-12 noon.

*F. W. Martin, 3rd International Conference on Ion Implantation, Kingston, Canada, July 1980.

F2 The Role of Excited State Polarizabilities in Inelastic Collisions. E. POLLACK and J. STEVENS, Univ. of Conn.--In $A^{++} + B \rightarrow A^+ + B^+$ collisions the incident potential at large r is $V = -2ae^2/r^4$, where a is the polarizability of the ground state of B . This attractive potential crosses Coulomb repulsive curves of final exothermic $A^+ + B^+$ states and may populate them. The potential for $A^{++} + B^+$ is given by $V^* = -2a^*e^2/r^4$, where a^* is the polarizability of the excited state B^+ . At infinite separation V^* lies above V by the excitation energy of B . Since a^* is much larger than a (see ref. 1 as an example), V^* will cross V at known interparticle separation and provide an intermediate state which crosses and may excite high lying levels of $A^+ + B^+$. A similar model is applicable to $A^{++} + B_2$ collisions. The $A^+ + B + A + B^+$ case may also be analyzed with a related model. The effect of the repulsive core will be discussed. The model will be compared with experimental results.

*Supported by the Army Research Office and the University of Connecticut Research Foundation.

¹E. Pollack, E. J. Robinson, and B. Bederson, *Phys. Rev.* **134**, A1210 (1964).

F3 The Generation of Coherent Millimeter Microwaves by Nonlinear Interaction. H. SCHMIDT, G. GUNTER, and G. GUNTER, Univ. of Washington.--Fast Rabi method and the Rabi frequency was found to be 1.0×10^6 Hz and the Rabi frequency was found to be 1.0×10^6 Hz.

relativistic electron beam accelerated along the axis of a dielectric lined waveguide has produced coherent Cerenkov radiation at kilowatt power levels in the millimeter region. Theory, a description of the experimental apparatus, and some experimental results will be presented.

Work supported in part by U.S. Army Grant No. DAAG-29-79-CO 2030.

F4 Relativistic Beam Propagation in a Dielectric Lined Waveguide. J. BRANSON, J.E. WALSH, P.W. LAYMAN, Dartmouth College, Hanover, N.H. 03755--Relativistic electron beams propagating along the axis of a dielectric lined cylindrical waveguide have been shown to produce coherent millimeter radiation.¹ Surface charge collecting on the dielectric liner causes problems of beam dynamics which could limit the practical uses of this process. Experiments demonstrating the effects of charge collection and some possible solutions will be described.

1. K. Felch, K. Busby, R. Layman, and J. Walsh, Bull. Am. Phys. Soc. **24**, 1076 (1979).

Work Supported in part by U.S. Army Grant No. DAAG-29-79-CO 2030.

F5 Cerenkov-Cyclotron Instability. J. GOLUB and J.E. WALSH, Dartmouth College, Hanover, N.H. 03755--It has been shown that a slow cyclotron wave propagating along an electron beam, both in a dielectric medium, is unstable.¹ A slow space charge wave propagating at the Cerenkov angle in a similar system is also unstable. We have investigated the off-angle propagation of a slow cyclotron wave. The system is shown to be unstable at a wavelength given by

$$\lambda = (8n-1)/(\Omega_c/2\pi c)$$

where $\beta = v/c$ is the relative beam velocity; n is the index of refraction of the dielectric; and Ω_c is the relativistic cyclotron frequency. A small signal temporal growth rate has been derived for propagation at a general angle. At the Cerenkov angle, using realistic experimental parameters and $\lambda = 500\mu\text{m}$, this growth rate is approximately one order of magnitude greater than that of the on-angle case. Potential application of this instability to some practical free electron laser systems will be discussed.

1. D. Kapilow and J.E. Walsh, Bull. Am. Phys. Soc., **25**, 6 (1980).

Supported in part by The Office of Naval Research Grant #N00014-79-C-0760.

SESSION G: GRAVITATION/COSMOLOGY

Saturday morning, 18 April 1981
Olin Hall, Room 223 at 9:00 A.M.
H. W. Hisinger, presiding

G1 Mechanism of Electromagnetic Radiation.*
H. W. HISINGER, Worcester Polytechnic Institute.--Mach's principle asserts that inertial effects are caused not by acceleration relative to some reference frame but by acceleration relative to the rest of the mass of the universe; however, experimental confirmation of this principle is precluded largely by the impossibility of removing that ambient mass or of shielding a system from its effect. The corresponding electromagnetic principle would attribute radiation by a charge to acceleration relative to the ambient charge. An experiment will be described that can, in principle, investigate the mechanism of electromagnetic radiation: does a charge radiate because it has absolute acceleration or because it has an acceleration relative to other charges. The possible results of such an

experiment and their interpretation will also be discussed.

*Submitted by L. R. Ram-Mohan

G2 A New View of the Solar System - Part I. HAROLD P. SCHWELDE, Retired. The solar system has a new number 38.932 with dimensions of kms/sec in the plane of the ecliptic. The Newtonian relation for orbital bodies is a limiting form of the expression derived. Jupiter has an influential role. A non-linear relation is quantized where $P^2 \propto (n + \frac{1}{2})^3$ is a constant. With K as the constant, where K has the value unity and takes care of the dimensions, R_0 has the value of 0.012262 A. U. The number n takes integral values while P is the period in sidereal tropical years. The value of n for Venus and Earth are 70 and 97 respectively. Values of n for such diverse bodies as "Object Kowal", Halley's comet and Ceres are 1867, 1749 and 269. The number $(n + \frac{1}{2}) \times R_0$ gives the average semi-major axes. The secular variations for the outer planets are discussed.

G3 Quarks and Particles. HAROLD P. SCHWELDE, Retired. Kinematic considerations of the masses of particles show intriguing results. Phase paths for Pions and Kaons are indicated. A derived number 0.511004091 is considered as the mass of the electron, in Mev/c² and a number of about 100 ev/c² is obtained which is perhaps related to the electron neutrino. Relations are given for the proton and the neutron. The twin primes centered at 138 and 1020 play a role. Rational fractions same as the alleged fractionally charged quarks appear naturally. Elliptic functions, particularly the Weierstrass relations, are revealing. A fundamental relation is easily suitable to cover many types of forces.

SESSION H: GENERAL

Saturday morning, 18 April 1981
Olin Hall, Room 126 at 9:00 A.M.
P. Glanz, presiding

H1 Association of Hemoglobins as Studied by Intensity Fluctuation Spectroscopy. K. J. LAGATTUTA, Univ. of Connecticut -- (1) Normal adult hemoglobin (HbA) exists in vivo as a tetramer, two chains of which are of the α form and two chains of which are β . The extent of the association of these four chains into tetramer, in vitro, was measured by intensity fluctuation spectroscopy (IFS) and a pH dependent reaction equilibrium constant deduced. Results are compared with values obtained by other methods. (2) Formation of multi-tetrameric aggregates of HbA is found to occur, in vitro, at low ionic strength. The average size of an aggregate and the dispersion in sizes was determined by IFS. Indications of limited aggregation at very high ionic strength was also observed. (3) Application of IFS to studies of so-called sickling hemoglobins (HbS) will be discussed. The formation of the sol phase of deoxy-HbS may be preceded by states of limited aggregation. These states should be amenable to study by IFS.

*K. J. LaGattuta, et al., Biophys. J. **33**, 63 (1981).

H2 Hand Held Calculators in Quantitative Analysis of Speckle. R. J. ... recent advances in speckle metrology based on the concept of projection matrices, lead to the development

Abstract Submitted
For the Twenty-third Annual Meeting
Division of Plasma Physics
October 12 to 16, 1981

Category Number and Subject Microwave Generation - 4.8

☐ Theory ☒ Experiment

Power Characterization of a Cerenkov Maser*.

S. VON LAVEN, J. BRANSCUM, J. GOLUB, R. LAYMAN,
D. SPEER, D. WISE, Dartmouth College --Stimulated
Cerenkov radiation is generated by a mildly relativ-
istic electron beam in a waveguide which is partially
filled with dielectric. Substantial levels of output
power have been generated at wavelengths varying
between 1.5 and 10 mm. The beam energies range from
100 to 250 keV, and the currents from 15 to 20A.
Pulse widths are of the order of 1 μ sec. Beam power
to microwave power conversion efficiencies of 1 to
5% have been achieved to date. At the present time
the system runs as a self oscillator with feedback
provided by the relatively small reflection from the
end of the tubular quartz guide. The overall cavity
Q in this case is low and oscillation commences only
at relatively high gain levels. In order to better
control the feedback, a number of quasi-optical
cavity and output coupling schemes have been tested.
The effects of these on output power and wavelength
will be presented and discussed.

*Work supported by ARO Contract number DAAG29-79-C-
0203.

☒ Prefer Poster Session

☐ Prefer Oral Session

☐ No Preference

☐ Special Requests for placement
of this abstract:

☐ Special Facilities Requested
(e.g., movie projector)

Submitted by:

Scott Von Laven

(signature of APS member)

Scott Von Laven

(same name typewritten)

Dartmouth College, Hanover,

NH 03755 (address)

This form, or a reasonable facsimile, plus Two Xerox Copies must be received NO LATER THAN
Thursday, July 9, 1981, at the following address:

Division of Plasma Physics Annual Meeting
c/o Ms. Joan M. Lavis
Grumman Aerospace Corporation
105 College Road East
Princeton, New Jersey 08540

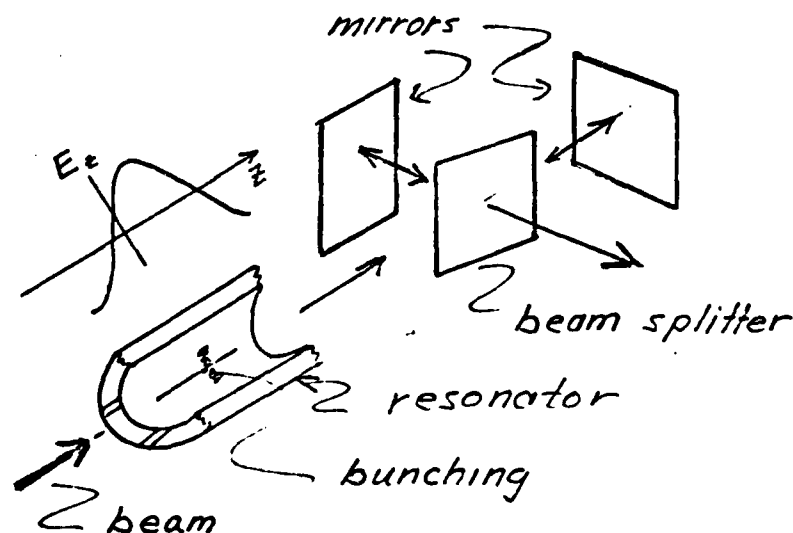
11th Anomalous Absorption Conference in Montreal, Canada
Cerenkov Masers: A Possible Plasma Heating Source

J. Walsh, J. Branscum, J. Golub, R.W. Layman,
D. Speer, S. Von Laven

Dartmouth College
Hanover, N.H.

A Čerenkov maser consists of an electron beam, a dielectric resonator and output coupling optics. The beam velocity can exceed the phase velocity of the wave in this system, and when it does, a coherent instability leads to beam bunching and a transfer of energy to the wave. The field in the beam channel is also evanescent. The decay rate, however, scales as k/γ where k is the axial wavenumber of the wave and γ is the ratio of the energy of the electron and its rest mass. Hence by using mildly relativistic electron beams ($\gamma = 1.1-1.6$) good beam-to-wave coupling can be obtained in the lower mm part of the spectrum. Depending upon their complexity and ultimate performance characteristics, devices of this kind may have a number of applications in plasma diagnostics and heating.

In order to test the basic ideas underlying such devices, a high-voltage (400 Kv max.) pulse transformer-based e-beam generator has been used to drive tubular quartz resonators. At the present time, coherent output has been obtained over the range 10mm-1.5mm. A summary of theoretical expectations and recent experimental results will be presented.



Čerenkov Maser

3 J. C. Phillips, Covalent Bonding in Crystals, Molecules, and Polymers (U. of Chicago Press, 1969); H. Watanabe as cited in ref. 1.

D3 Nonlinear screening of negative point charges in diamond, silicon, and germanium. P. CSAVINSZKY and K.R. BROWNSTEIN, Univ. of Maine.--Cornolti and Resta¹ (CR) have recently formulated a Thomas-Fermi (TF) theory of nonlinear impurity screening in semiconductors. CR have obtained the spatially-variable dielectric function for charges $\pm 1e_0$, $\pm 4e_0$ (e_0 is the proton charge) embedded in pure diamond, Si and Ge. The nonlinear results differ importantly from the results of the linearized TF theory². We have previously solved the nonlinear TF equation of CR by an equivalent variational principle³. We have used a two-parameter trial solution and considered the cases of $+1e_0$, $+2e_0$, $+3e_0$ and $+4e_0$ in pure diamond Si and Ge. We have now extended our variational approach to the negative charges $-1e_0$, $-2e_0$, $-3e_0$, and $-4e_0$ in the above semiconductors⁴. Our analytic results, using again a two-parameter trial solution, agree remarkably well with the numerical results of CR.

¹F. Cornolti and R. Resta, Phys. Rev. B **17**, 3239 (1978).

²R. Resta, Phys. Rev. B **16**, 2717 (1977).

³P. Csavinszky and K.R. Brownstein, Phys. Rev. B (to be published).

⁴P. Csavinszky and K.R. Brownstein, Phys. Rev. B (to be published).

D4 Phonon Conduction in Elastically Anisotropic Cubic Crystals. A.K. McCurdy, Worcester Polytechnic Institute.-- Striking differences in the boundary-scattered phonon conductivity are predicted along the principal axes of cubic crystals. The results are due to phonon focusing arising from elastic anisotropy. Normalized curves of phonon conductivity have been calculated for samples of square cross-section as a function of the elastic anisotropy $A = 2C_{44}/(C_{11}-C_{12})$ and the elastic ratio C_{12}/C_{11} . Anisotropies of more than 50% are possible for different rod axes. Silicon and calcium fluoride, materials in which this anisotropy was first reported, are shown to be very favorable materials to demonstrate this anisotropy. For silicon and calcium fluoride samples of rectangular cross-section the thermal conduction is shown to depend upon the crystallographic orientation and width ratio of the side faces for samples with the same $\langle 110 \rangle$ rod axis. Results are expressed in a convenient form for predicting the phonon conductivity of elastically anisotropic crystals given the linear dimensions, the density and the elastic constants.

D5 Equilibrium Configuration of an Ethylene Monolayer Adsorbed on Graphite by Eric Ehrhardt, Larry Pratt, Howard Patterson¹ (University of Maine, Orono, Maine 04469) and Larry Passell (Brookhaven National Laboratory, Upton, N.Y. 11973).

In this talk we will describe computer calculations which have been carried out to determine the equilibrium configuration of an ethylene monolayer physisorbed on graphite. A four sublattice structure was assumed from the results of elastic neutron scattering studies. In the calculation we have included ethylene-ethylene interaction as well as the ethylene-graphite substrate interactions. Our results for ethylene adsorbed on graphite are very similar to those of Fusilier, Gillis, and Raich² for nitrogen adsorption on graphite. That is, the ethylene molecules show a herringbone pattern with the ethylene C-C axis almost perpendicular to the graphite basal plane.

1. Research partially supported by NSF, Department of Materials Research DMR 77-07140.

2. C. R. Fusilier, N. S. Gillis and J. D. Raich, Solid State Communications **25**, 747 (1978).

SESSION E: CONDENSED MATTER (EXPERIMENT)

Saturday morning, 3 October 1981

Room 141 Bennett at 8:45 A.M.

James Hutchison, presiding

E2 Cerenkov Radiation as a Source of Millimeter Radiation. J. BRANSCUM, J. WALSH*-- An electron moving with a velocity greater than the phase velocity of an electromagnetic wave produces radiation. This situation can be achieved physically in a number of ways, one of which is to have the electron move through (or near) a dielectric. The resultant radiation is known as Cerenkov radiation. This phenomenon may be used as the basis of a practical millimeter-infrared radiation source. Three problems must be considered: 1) method for making $\omega/ck < 1$. 2) dependence of beam-wave coupling on k , γ , and position. 3) method of insuring that energy moves into the wave from the beam. The first problem is solved by using a dielectric resonator with internal reflection types of modes. The second is approached by examining the phase-velocity dependence of the strength of the electric field which is undergoing total internal reflection. The third problem is approached by constructing a dielectric Fabry-Perot resonator. Each component will be discussed briefly.

*Supported in part by Office of Naval Research Grant # N000-16-79-C-0760.

E3 Millimeter Wave Generation with a Relativistic Electron Beam. R.W. LAYMAN, J. BRANSCUM, and J. WALSH* -- Production of electromagnetic radiation in the 35 to 150 GHz range by a mildly relativistic electron beam accelerated along the axis of a dielectrically lined cylindrical waveguide has been reported elsewhere¹. This process shows potential as a tunable source of high power millimeter radiation. Results of experimental work to demonstrate this possibility will be described.

1. K. Felch, K. Busby, R. Layman, and J. Walsh, Bull. Am. Phys. Soc. **24**, 1076 (1981).

*Work supported in part by U.S. Army Research Office Grant # DAAG-29-79-C-0203.

E4 Evidence of Bifurcation Universality for First Sound Subharmonic Generation in Superfluid He⁴. C.W. SMITH, D.A. FARRIS, and M.J. TEJWANI, University of Maine, Orono.-- Measurement of the subharmonic responses of superfluid helium-4 to ultrasound at 3 MHz is reported. A matched pair of PZT4 thickness mode transducers are positioned parallel on a common axis in an open geometry. One transducer is employed as a first sound source and the other as a receiver. The received signal is Fourier analyzed. Several subharmonic frequencies (f_0/n , where $n = 2, 3, 4, \dots$) of the applied frequency f_0 are observed above specific sound thresholds. Preliminary results for $n = 2, 4, 8$ have been analyzed in terms of the bifurcation theory for a nonlinear system in transition to chaos¹. To within experimental error the thresholds for the onset of the subharmonics agree with the theoretically predicted value of the universal geometric convergence constant, 4.7. Comparison of the observed decrease in the amplitude of successive subharmonics with theoretical prediction, the sequence $n = 3, 6, 12$ and apparent phase-locking behavior are currently under investigation.

*Supported by NSF, DMR8005358 and AFOSR, NP 80-151.

¹M.J. Fergenbaum, J. Stat. Phys. **19**, 25 (1978).

E5 Photoacoustic Studies of Iodine Vapor. A. BRAN, M. SARLANCUE and B. DI SANTO, Boston College. We constructed a photoacoustic apparatus, using an acoustical cylindrical cavity operating in a longitudinal mode and used molecular iodine vapor as specimen and Argon as buffer gas to study the photoacoustic characteristics of the system. The iodine molecules, excited periodically

Abstract Submitted
For the Twenty-Fourth Annual Meeting
Division of Plasma Physics
November 1 to 5, 1982

4.8 Microwave Generation

Category Number and Subject: ~~1.12 Electron beam/plasma interactions.~~

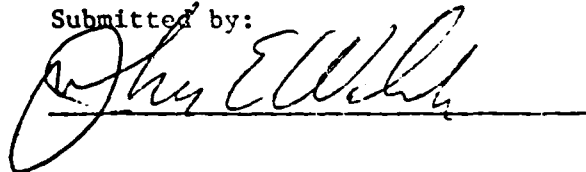
Experimental

A Two-Stage Cerenkov Oscillator, J.E. WALSH, S. VON LAVEN, R.W. LAYMAN, E. GARATE and R. COOK, Dartmouth College*--Recently¹, 100 KW levels of output power have been obtained in Cerenkov oscillator experiments. The device, which has been described in more detail elsewhere, consists of a pulse transformer-generated, 100-200 KV, 10-20 A, 1 μ sec beam pulse, a dielectric-loaded guide, and a variety of output coupling structures. The output power levels indicate that the beam is nearly 100% modulated during its passage through a 10 cm-long resonator. This in turn suggests that enhancement of the output power could be obtained if the now bunched beam is passed through a second resonator which is weakly coupled to the first, and whose phase velocity is lower than that of the first resonator. Such a device is similar to a multi-cavity klystron or a velocity-tapered traveling wave tube. A theoretical analysis and results of experimental investigation of this concept will be presented.

1. A High Power Cerenkov Maser Oscillator, S. Von Laven, J. Branscum, J. Golub, R. Layman and J. Walsh, Appl. Phys. Lett., Sept. 1, 1982, to be published.

Supported in part by AFOSR Contract # 82-0168 and ARO Contract # DAAG-29-79-C-0203-A01.

Submitted by:



John Walsh

No preference for
Session

Dartmouth College, Hanover, N.H. 03755

III. Technical Reports

- a) Stimulated Cerenkov Radiation, John Walsh, in Advances in Electronics and Electron Physics, V58, Edited by C. Marton (Academic Press, 1982)
- b) Tunable Cerenkov Lasers, John Walsh and James Murphy, J. Quant. Elect. QE18, 1259 (1982).
- c) Characterization of a Cerenkov Maser, S. Von Laven.
- d) Cerenkov Radiation in Dielectric Lined Waveguides, K. Felch, K. Busby, R. Layman, D. Kapilow and J. Walsh, Appl. Phys. Lett. 38(8), 601 (1981).

STIMULATED ČERENKOV RADIATION

JOHN E. WALSH

Department of Physics and Astronomy,
Dartmouth College

* * *

	Page:
I. Introduction	
A. Čerenkov Radiation	1
B. Čerenkov Masers	5
II. Theory	8
A. Čerenkov Gain on a Strongly Magnetized Beam	
A. 1. Current Modulation	9
A. 2. The Wave Equation	10
A. 3. The Dispersion Relation	12
A. 4. Čerenkov Gain	13
B. Gain from an Unmagnetized Beam	20
C. Bounded Structures	24
C. 1. Cylindrical Guide with a Beam Channel	25
C. 2. Coupling of a Beam to a Bounded Resonator	30
C. 3. The Beam-Guide Dispersion for a Bounded Structure	30
C. 4. Finite Gap Between the Beam and Resonator	35
D. The Effect of Beam Velocity Spread	37
D. 1. Beam Space Charge Waves	37
D. 2. Gain in the Warm Beam Limit	39
E. Comments on Nonlinear Behavior	46
E. 1. Nonlinear Scaling Arguments	47
III. Experiment	
A. The Electron Beam	49
B. A Millimeter Wave Experiment	55
C. Čerenkov Devices in the Short Wavelength Limit	58
IV. Conclusions	62
Table	63
Acknowledgments.....	64
References	65
Figure Captions	67

* * *

INTRODUCTION

I A. ČERENKOV RADIATION

The electromagnetic wave produced by a charged particle moving with greater than light velocity in a dielectric medium is known universally as Čerenkov¹ radiation. Čerenkov's experiments, which were performed independently during the 1930's, and the subsequent analysis of the phenomena by Frank and Tamm² did, however, have some precursors.

Heaviside,³ in 1889, analysed the problem of the radiation produced by a charged particle when it moved with uniform velocity. This work was done prior to the development of the special theory of relativity, and Heaviside assumed that it was possible for a particle to move with a velocity greater than that of light in a vacuum. When it was so assumed, radiation was produced. In a formal sense, his results were similar to those of Frank and Tamm. Sommerfeld,⁴ in 1904, without apparent knowledge of Heaviside's results, performed a similar analysis. There were also some experimental precursors to Čerenkov's work. M. Curie,⁵ in 1911, observed that radiation produced in the walls of glass containers holding radioactive material was probably due in part to the penetration of the glass by fast-charged particles. Some experiments performed by Mallet⁶ in

in 1926 were, in part, observations of Čerenkov radiation. None of this early work, however, lessens the importance of pioneering experiments of P.A. Čerenkov.

Following the initial experiments of Čerenkov and theory of Frank and Tamm, an extremely large number of both theoretical and experimental contributions have appeared. General discussions, with hundreds of additional references, may be found in Jelley,⁷ in Zrelov⁸ and in the review article by Bolotovskii.⁹ The interest of many contributors has been the potential use of the Čerenkov process as a practical radiation source. Notable among these contributions were the papers of Ginzburg,¹⁰ in which he considered a number of ways in which electrons could be coupled to dielectrics and be made to produce radiation in the millimeter and submillimeter regions of the electromagnetic spectrum.

Much of the early work dealt with the radiation produced by single electrons. As we shall see, however, this spontaneous radiation is a relatively weak process for all wavelengths longer than that of the blue ultra-violet regions of the spectrum. Hence, in order to produce useful amounts of radiation, it was natural to consider the radiation produced by a bunched electron beam. At wavelengths long compared to the length of the bunch, the radiated power is proportional to the square of the number of electrons involved, and hence the power emitted rises dramatically. A number of experiments were designed to explore the properties of the

Čerenkov radiation produced by prebunched electron beams moving in close proximity to a dielectric surface. Important contributions were made by Coleman,¹¹ by Danos,¹² by Lashinsky,¹³ and by Ulrich.¹⁴ In these experiments, no provision was made for feeding back the emitted radiation on subsequent bunches and hence they could be categorized as observation of enhanced spontaneous emission.

Suggestions have also been made that Čerenkov radiation could be used as the basis of a microwave tube.^{15,16,17} In these, a dielectric tube was used as a slow wave structure. The general configuration suggested was similar to that used in traveling wave tubes. When electron beams in the energy and current range found in conventional microwave tubes are used, however, the resulting devices are unsatisfactory for several reasons. We will develop this line of argument carefully in subsequent sections, since these difficulties must be surmounted in constructing a useful Čerenkov source.

A major difficulty in constructing a Čerenkov source that is capable of producing useful amounts of radiated power is the coupling of the electron beam to the dielectric. In elementary discussions, it is usually assumed that the electron is passing right through the dielectric. This can actually be done for the limiting case of very high energy particles and gaseous or liquid dielectrics. In this regime, Čerenkov radiation actually finds wide practical

application as a diagnostic tool.⁷ There have also been serious attempts^{18,19,20} to observe stimulated Čerenkov radiation in the visible and ultra-violet region from a high-energy beam/gaseous dielectric combination. In these latter experiments, momentum modulation^{18,19} by an applied electromagnetic has been observed, but as yet there is no clear-cut evidence of true stimulated emission. An alternative to passing an electron beam directly through a dielectric is to let a beam propagate along a channel. Recent experiments^{21,22,23} in which millimeter-wavelength stimulated Čerenkov radiation has been observed have been of this type.

A primary purpose of the present paper is to explore the potential of the latter option. We will establish criteria necessary for producing usable levels of stimulated Čerenkov radiation at wavelengths which are short compared to the characteristic scale length of both the transverse and longitudinal dimensions of a dielectric resonator.

I B. CERENKOV MASERS

The goal of the general area of research pertaining to devices now often called free-electron lasers is to produce coherent, tunable, moderate, and high-power radiation in parts of the electromagnetic spectrum where such a source is not now available. All of the devices suggested to date have much in common with microwave tubes, and hence the designation "maser" or "laser" could be the subject of debate. It is possible, but not necessary, to formulate the equations of motion quantum-mechanically. The electron transitions are between continuum states. The recoil due to single-photon emission is negligible, and thus Planck's constant does not appear in any final working formula. A classical analysis based on either fluid or kinetic equations will lead to the same expressions. Therefore, much of what is known about microwave tubes will apply also to free-electron lasers. Microwave tubes, however, operate at wavelengths comparable to or greater than the device, while the opposite will be the case for any free-electron laser or maser. This difference, although minor from some viewpoints, accounts for many of the difficulties encountered in attempting to build short wavelength, beam-driven radiation sources.

II. THEORY

A series of calculations aimed at establishing the beam energy, current, and velocity spread, which are required in order to obtain growth of stimulated Čerenkov radiation, will be presented in this section. The analysis will proceed along classical lines similar to those used in traveling wave tube and beam plasma theory. In Sections II A and B we will examine the exponential gain of stimulated Čerenkov radiation obtained when it is assumed that either a strongly magnetized or a completely unmagnetized monoenergetic electron beam passes directly through a dielectric medium. The limit implied by the assumption that the beam is monoenergetic will be examined in Section II C, and modified gain formulas will be derived. Section II D will then be devoted to some resonator configurations which are more practical for the present application. Emphasis will be on the slab geometry, since in this case it is possible to present a reasonably compact analytic result. The results obtained from other geometries will be similar. A few brief comments and calculations related to nonlinear effects will be outlined in Section II E.

II A. CERENKOV GAIN ON A STRONGLY MAGNETIZED BEAM

We consider first the case of a plane wave propagating at an angle to strongly magnetized electron beam. The geometry is shown in Fig. 3.

II A. 1. Current Modulation

When the beam is strongly magnetized, the beam density and modulation are one-dimensional and lie along the beam and magnetic axis. In this limit, the linearized equation for the velocity modulation has only one component, v_z , where:

$$\frac{dv_z}{dt} = - \frac{e}{m\gamma^3} E_z \quad (1)$$

The solution of this equation for the assumed E_z is readily found:

$$v_z = - \frac{ie}{m\gamma^3} \frac{1}{\omega - k v_0} E_z \quad (2)$$

This result together with a linearized equation of continuity gives for the density modulation n ,

$$\begin{aligned}
 n &= \frac{n_o k_o v}{(\omega - kv)} \\
 &= - \frac{(in_o e)}{m \gamma^3} \frac{k E_z}{(\omega - k v_o)^2} \quad (3a)
 \end{aligned}$$

$$= - [in_o e / (m \gamma^3)] k E_z / (\omega - k v_o)^2 \quad (3b)$$

Thus the current produced by the wave is given by:

$$J_z = - n_o e v - n e v_o \quad (4a)$$

$$= + \frac{i \omega_p^2}{4 \pi \gamma^3} \frac{\omega E_z}{(\omega - k v_o)^2} \quad (4b)$$

where $\omega_p^2 = 4 \pi n_o e^2 / m$ is the beam plasma frequency.

II A. 2. The Wave Equation

The current given by eq. (4b) appears in Maxwell's equations as a source term. These are:

$$\nabla \times \underline{E} = - \frac{1}{c} \frac{\partial \underline{B}}{\partial t} \quad (5a)$$

and

$$\nabla \times \underline{B} = + \frac{4 \pi}{c} \underline{J} + \frac{1}{c} \frac{\partial \underline{D}}{\partial t} \quad (5b)$$

In writing the second of these, we assume that the wave and the beam are in a dielectric medium where:

$$\underline{D} = \epsilon \underline{E} \quad (6)$$

Taking the time derivative of the second of Maxwell's equations and substituting the first gives a single-wave equation:

$$\nabla \times \nabla \times \underline{E} + \frac{\epsilon}{c^2} \frac{\partial^2 \underline{E}}{\partial t^2} = - \frac{4}{c^2} \frac{\partial \underline{J}}{\partial t} \quad (7)$$

There is no current component in the direction perpendicular to the beam and, hence, the perpendicular component of eq. (7) may be used to express E_x in the terms of E_z . Doing this and substituting into the longitudinal component of eq. (7), and making use of the assumed time and z-dependence, we obtain a single wave equation for E_z :

$$\frac{\partial^2 E_z}{\partial x^2} + \frac{\frac{\omega^2 \epsilon}{c^2} - k^2}{c^2} E_z = \frac{4\pi i}{\omega \epsilon} \left(\frac{\frac{\omega^2 \epsilon}{c^2} - k^2}{c^2} \right) J \quad (8)$$

Since we have also assumed a plane wave dependence in the perpendicular as well as longitudinal direction, we also obtain immediately:

$$\left[\frac{\frac{\omega^2 \epsilon}{c^2} - k^2 - p^2}{c^2} - \frac{\omega p^2}{\epsilon \gamma^3} \frac{(\frac{\omega^2 \epsilon}{c^2} - k^2)}{(\omega - kv_0)^2} \right] E_z = 0 \quad (9)$$

where p is the perpendicular component of the wave number.

II A. 3. The Dispersion Relation

We are obviously interested in the case $E_z \neq 0$ and, hence, the coefficient of eq. (9) is the dispersion relation:

$$\frac{\omega^2 \epsilon}{c^2} - k^2 - p^2 - \frac{\omega_p^2}{\epsilon \gamma^3} \frac{\left(\frac{\omega^2 \epsilon}{c^2} - k^2 \right)}{(\omega - kv_0)^2} = 0 \quad (10)$$

for a plane wave propagating through a dielectric medium at an angle to a strongly magnetized electron beam.

Equation (10) is a quartic in both ω and k and hence it has four roots. When $v_0 < c/\sqrt{\epsilon}$, all four roots are real, while if $v_0 > c/\sqrt{\epsilon}$ it has two real roots and a complex conjugate pair. One of the real roots is related to a wave propagating in the direction opposite to that of the beam (in the negative, z -direction). The other three result from the coupling of an electromagnetic wave propagating in the positive z -direction and two beam space charge waves. The latter two, fast and slow space charge waves, would be normal modes of the free beam. In the presence of the dielectric, however, they become coupled to the electromagnetic wave. When the velocity threshold $v_0/c = 1/\sqrt{\epsilon}$ is exceeded, the beam-wave dielectric system becomes unstable.

II A. 4. Čerenkov Gain

The presence of the beam is obviously felt most strongly for waves near "synchronism", i.e. when

$$\omega \simeq kv_0 \quad (11a)$$

and

$$kv_0 \leq \omega_{ok} \quad (11b)$$

where we define ω_{ok}^2 as

$$\omega_k^2 = c^2(k^2 + p^2)/\epsilon \quad , \quad (11c)$$

the dispersion relation of the electromagnetic waves in the absence of the electron beam.

In the region where eqs. (11a) and (11b) are valid, the dispersion relation, eq. (10), becomes an approximate cubic:

$$(\omega - kv_0)^3 - \frac{\omega_p^2}{2\gamma^3 \epsilon} \omega (1 - 1/\beta^2 \epsilon) = 0 \quad (12)$$

Equation (12) follows from (10) when kv_0 is set equal to ω in those terms where the substitution does not give zero. This is a valid assumption provided ω_p^2 is small in a sense which we will define shortly.

When $\beta^2 \epsilon < 1$ eq. (12) has three real roots while in the reverse case, the roots are:

$$(\omega - kv_0) = \left[\frac{\omega_p^2}{2\epsilon\gamma^3} (1 - 1/\beta^2 \epsilon) \right]^{1/3} \quad (13a)$$

and

$$(\omega - kv_0) = \left(\frac{\omega_p^2}{2\gamma^3 \epsilon} \right)^{1/3} (1 - 1/\beta^2 \epsilon)^{1/3} \frac{(1 \pm i\sqrt{3})}{2} \quad (13b,c)$$

The root corresponding to eq. (13b) is an exponentially growing wave in either time, $\text{Im}\omega \neq 0$, or space, $\text{Im}k \neq 0$. The choice between these will be determined by initial and boundary conditions.

We will, for the moment, assume that the spatial growth is of interest and we will let $\text{Im}k = \alpha$, then:

$$\alpha = \frac{\sqrt{3}}{2} \left(\frac{\omega_p^2}{2\epsilon\gamma^3} \right)^{1/3} \frac{(1 - 1/\beta^2 \epsilon)^{1/3}}{c\beta} \quad (14)$$

Examination of eq. (14) shows that the spatial gain increases with the two-thirds power of the beam density and the one-third power of the frequency. It vanishes as the beam energy approaches the Čerenkov threshold and decreases as ϵ and γ become large.

Shown in Fig. 4 are sketches of free wave dispersion curves for two different perpendicular wave numbers, p_1 and p_2 . The curves leave the $k = 0$ axis at the point

$\omega/c = p/\sqrt{\epsilon}$, cross the speed of light at $\omega/c = p/\sqrt{\epsilon-1}$ and then asymptotically approach a wave propagating in the z-direction. Along this curve, the angle of propagation is varying from $\theta = \pi/2$ to $\theta = 0$. Also shown in Fig. 4 is a beam "velocity" line, $\omega = ck\beta$. The points at which this line intercepts the dispersion curves are points at which the beam velocity and the phase velocity of the free waves are the same; they are in "synchronism".

Consideration of eqs. (11a) and (11b) shows that, at this point, the angle of propagation is the same as the Čerenkov angle, $\theta_c = \cos^{-1}(1/\beta\sqrt{\epsilon})$. At this point, the dispersion is modified by the beam and the wave will grow at a rate given by eq. (14). If γ , ϵ , and the beam density are left unchanged, the rate of growth at the synchronous point on the p_1 curve will be greater than that on the p_2 curve by an amount equal to the frequency ratio to the one-third power. Thus the stimulated Čerenkov process is a potential short wavelength radiation source.

Growth will also occur at angles other than the Čerenkov angle. Shown in Fig. 5 is a numerical solution of the complete dispersion relation (eq. (10)). We see that there are three solutions in the positive ω , positive k quadrant of the $\omega - k$ plane. One is purely real, while the other two are a complex conjugate pair in the region below and near synchronism and real above this point. The gain peaks just below synchronism (the shift is equal to

the $\text{Re}(\omega - kv_0)$ given in eq. (13)) and goes identically to zero at the point $\omega = kv_0$. On the small k side the $\text{Im}(\omega/c)$ goes to zero more slowly. The exact shape of this curve will depend upon γ , ϵ and the beam density.

We have now established that by controlling the angle of propagation, ϵ , and the beam energy, the frequency at this maximum growth occurs increases as $\omega^{1/3}$. It will be instructive to consider the magnitude of the gain as these parameters are manipulated. In order to do this, we rewrite again eq. (14), now in this form:

$$\alpha = \left(\frac{\beta \omega^2 p}{2c^3} \right)^{1/3} G(\gamma_T) F(\gamma, \gamma_T) \frac{\gamma_T}{\gamma} \quad (15)$$

where

$$\gamma_T^2 = \frac{\epsilon}{\epsilon - 1} \quad (16a)$$

is the threshold energy ($\beta_T^2 = 1/\epsilon$),

$$G(\gamma_T) = \frac{(1 - 1/\gamma_T^2)^{1/3}}{\gamma_T^{5/3}} \quad (16b)$$

and

$$F(\gamma, \gamma_T) = \frac{(1 - \gamma_T^2)^{1/3}}{(1 - 1/\gamma^2)} \quad (16c)$$

One power of β has been inserted in front of ω_p^2 so that we may subsequently express it in terms of the beam current, a form which we will find convenient in our numerical evaluation of the gain. Before we do this evaluation, we will examine the functions G , F , and γ_T/γ .

The function G depends only upon the dielectric constant of the material. A sketch is shown in Fig. 6a. It shows a vertical rise at $\gamma_T = 1$, the point where the dielectric constant of the material approaches infinity, reaches a maximum at $\gamma_T^2 = 7/5$ ($\epsilon = 7/2$), and finally decreases as $\gamma_T^{-5/3}$ as γ_T becomes large ($\epsilon \rightarrow 1$). Thus, in considering a practical Čerenkov source, one cannot move profitably in the direction of low beam energy, optically-dense materials ($\gamma \rightarrow 1$, $\gamma_T \rightarrow 1$, $\epsilon \rightarrow \infty$) since the gain vanishes rapidly in this limit. As a practical matter, one could not propagate a beam in this type of material in any event. In the opposite limit, we would have gasses ($\epsilon \rightarrow 1$). In this region, the gain will also decrease, but conclusions as to the usefulness of this limit must also include consideration of the $\omega^{1/3}$ term. It is interesting, and perhaps important, for practical mm-submm wavelength devices that G peaks in the region of the dielectric constant of quartz.

The function F depends both upon the threshold energy, γ_T , and the beam energy of γ . It rises vertically from $\gamma = \gamma_T$ and asymptotically approaches unity from below.

Sketches of F , γ_T/γ and their product are shown in Fig. 6b. There is obviously a local maximum in the growth rate. The value of the product at this maximum is about .5 .

Before we consider some actual numerical values for the growth rate, it will be useful to consider one further scaling, which will be that of the beam density. We assume for the present that the beam is now a rectangular slab of thickness and that the variation of \underline{E} in the x-direction is still given by $\exp(ipx)$. The term

$$\frac{\beta \omega_p^2}{2c^3} = \frac{4\pi\beta n e^2}{2mc^2} \frac{\omega}{c} \quad (17a)$$

can be re-expressed as

$$\frac{\beta \omega_p^2}{2c^3} = \frac{2\pi I}{I} \cdot \frac{\omega a}{c} \cdot \frac{1}{a^3} \quad (17b)$$

where

$$r_0 = e^2/mc^2 \quad (18a)$$

$$I_0 = ec/r_0 \quad (18b)$$

and I is the electron beam current. When I is measured in amperes, I_0 has the value 17 kA. Hence, the factors preceding the energy and material form factors in the expression for gain, eq. (15), are given by:

$$\left(\frac{\beta \omega_p^2 \omega}{2c^3}\right)^{1/3} = \left(\frac{2\pi I}{I_0}\right)^{1/3} \left(\frac{\omega a}{c}\right)^{1/3} \frac{1}{a} \quad (19)$$

When I is approximately $3A$, the first of the three factors is approximately equal to 0.1, while if it $3ma$ it becomes 0.01. The second factor may, in principle, vary from zero to a moderately large number, and the characteristic scale length a may be anything from .01 to 1 centimeter. Hence, substantial gain is possible in principle. A discussion of ways in which this may be achieved in practical cases will be deferred until after we have made some mention of wave-guiding structures.

II B. GAIN FROM AN UNMAGNETIZED BEAM

The preceding analysis presumes that the current density modulation occurs only in the z-direction. As we will see in later discussion, one class of Čerenkov device will make use of mildly relativistic electron beams and will somewhat resemble microwave tubes. The beams in these devices will almost certainly propagate along a strong axial guide field, and, in this limit, the assumptions made in the last section be at least approximately valid.

Another class of device, however, might make use of a more relativistic beam such as that used in the injector of a linear accelerator, a linear accelerator itself, or perhaps some other type of accelerator. The beam in this case may very well not be magnetized. It will then have rapidly varying components in the transverse as well as the longitudinal direction, and the gain formulas will be modified.

When the beam is unmagnetized, the linearized equation for the perpendicular motion is:

$$\frac{dv_{\perp}}{dt} = \frac{e}{m\gamma} \left(\underline{E}_{\perp} + \frac{v_0}{c} \times \underline{B} \right) \quad (20)$$

while the longitudinal motion is still governed by eq. (1). Assuming the same geometry given in Fig. 1, the one non-vanishing component of this equation will lie in the x-direction.

$$\frac{dv_x}{dt} = -\frac{e}{m\gamma} \left(E_x - \frac{v_o B_y}{c} \right) \quad (21)$$

Equation (21), with the aid of Faraday's law, may be restated in the form:

$$\frac{dv_x}{dt} = -\frac{e}{m\gamma} \left[\left(\frac{\omega - kv_o}{\omega} \right) E_x + \frac{pv_o}{\omega} E_z \right] \quad (22)$$

The $\underline{v} \times \underline{B}$ term gives rise to an E_z as well as E_x dependence for v_z .

The solution to eq. (21), together with the linearized equation of continuity, may be used to construct expressions for the current density. These are:

$$J_x = \frac{i p^2}{4\pi\gamma} \frac{1}{\omega} \left(E_x + \frac{pv_o}{\omega - kv_o} E_z \right) \quad (23a)$$

and

$$J_z = \frac{i\omega p^2}{4\pi\gamma} \frac{1}{\omega} \left[\frac{pv_o}{\omega - kv_o} E_x + \left(\frac{\omega^2}{\gamma(\omega - kv_o)^2} + \frac{p^2 v_o^2}{(\omega - kv_o)^2} \right) E_z \right] \quad (23b)$$

The current terms can now be substituted in eq. (7). When this is done, we have as our new wave equation:

$$\begin{pmatrix} k^2 + \frac{\omega p^2}{c^2} - \frac{\omega^2 \epsilon}{c^2} & pk + \frac{pv_o}{\omega - kv_o} \frac{\omega p^2}{c^2} \\ pk + \frac{pv_o}{\omega - kv_o} \frac{\omega p^2}{\gamma c^2} & p^2 + \left(\frac{\omega p^2}{\gamma c^2} \frac{\omega^2 \gamma^2 + p^2 v_o^2}{\gamma^2 (\omega - kv_o)^2} \right) - \frac{\omega^2 \epsilon}{c^2} \end{pmatrix} \begin{pmatrix} E_x \\ E_z \end{pmatrix} = 0 \quad (24)$$

The determinational equation for eq. (24) is now the dispersion relation for the unmagnetized beam-dielectric combination. It is:

$$\left(k^2 + \frac{\omega^2 p^2}{\gamma^2 c^2} - \frac{\omega^2 \epsilon}{c^2}\right) \left(p^2 + \frac{\omega^2 p^2}{\gamma^3 c^2} \cdot \frac{\omega^2 \gamma^2 p^2 v_o^2}{(\omega - kv_o)^2} - \frac{\omega^2 \epsilon}{c^2}\right) - \left(pk + \frac{pv_o}{\omega - kv_o} \frac{\omega^2 p^2}{\gamma^2 c^2}\right)^2 = 0 \quad (25)$$

Equation (25), which appears quite cumbersome in comparison with eq. (9), is still a quartic in either ω , k or both. All qualitative comments made about the strongly magnetized case apply here as well. However, the results are quantitatively somewhat different. Again, the strongest coupling region of the beam to the wave is in the velocity synchronism ($\omega/ck = \beta$).

If terms proportional to $1/(\omega - kv_o)^2$ are collected separately, we obtain for the dispersion relation:

$$\begin{aligned} & \frac{\omega^2 \epsilon}{c^2} \left(\frac{\omega^2 \epsilon}{c^2} - k^2 - p^2 - \frac{\omega^2 p^2}{c^2} \right) \\ & - \frac{\omega^2 p^2}{\gamma^2 c^2} \frac{1}{(\omega - kv_o)^2} \left[\left(\frac{\omega^2 \epsilon}{c^2} - k^2 - p^2 \frac{\omega^2 p^2}{c^2} \right) p^2 v_o^2 \right. \\ & \left. + \frac{\omega^2}{\gamma^2} \left(\frac{\omega^2 \epsilon}{c^2} - k^2 \right) - p^2 (\omega^2 - v_o^2 p^2 - v_o^2 k^2) \right] = 0 \end{aligned} \quad (26)$$

Near synchronism, this reduces to:

$$\left(\frac{\omega^2 \epsilon}{c^2} - k^2 - p^2 - \frac{\omega^2 p^2}{\gamma^2 c^2} \right) - \frac{\omega^2 p^2}{\gamma^2 c^2} \frac{\omega^2 (\epsilon - 1) (\beta^2 \epsilon - 1)}{(\omega - kv_o)^2} \quad (27a)$$

or

$$\left(\frac{\omega - kv_o}{v_o} \right)^3 = \frac{\omega^2 p_\omega}{2\gamma c^3} \frac{(1 - 1/\beta^2 \epsilon)}{\beta^3 \gamma_T^2} \quad (27b)$$

Once again, the dispersion relation is cubic and the frequency and the dependence upon the size of the Čerenkov angle ($\theta = \sin^{-1}(1 - 1/\beta^2 \epsilon)$) are the same. However, the beam energy and ϵ dependence are different. If we use the functions defined earlier, we have for the spatial growth rate:

$$\alpha = \left(\frac{\beta \omega^2 p_\omega}{c^3} \right)^{1/3} G(\gamma) F(\gamma, \gamma_T) \left(\frac{\gamma_T}{\gamma} \right)^{1/3} \quad (28)$$

The energy dependence is now $\gamma^{-1/3}$ in the high energy limit, as opposed to the more constrictive γ^{-1} dependence in the strongly magnetized limit. If all other factors are the same, the gain in the unmagnetized limit will be greater than that for the strongly magnetized beam. This is because the electrons in the beam can now do work on the wave in both the transverse and longitudinal direction.

II C. BOUNDED STRUCTURES

Excepting the possibly interesting limit of extremely relativistic beams and gaseous dielectrics, it is not practical to have the beam penetrating the dielectric. Hence, in assessing the practicality of Čerenkov sources, it is important to consider dielectric wave guides and resonators which have channels for the beam propagation. This complicates the analysis. Thus, before we take up the cases quantitatively, it will be useful to consider, at this point, the regime where the results of the preceding section are qualitatively useful.

First, we note that with minor changes, the results of the last section will apply exactly to a metal-bounded, cylindrical, dielectric waveguide through which an electron beam propagates. The perpendicular wave number, p , is now a root of zero order Bessel function and is no longer completely free. The only other change is that the factor π in the current term no longer appears, because the beam is now also cylindrical. The field symmetry is now transversely magnetic.

II C. 1. Cylindrical Guide with a Beam Channel

When the beam propagates in a hole in the dielectric, we have a situation such as that sketched in Fig. 7. If the diameter of the hole is sufficiently small, a concept which, shortly, will be quantitatively specified, the results of the preceding section might be expected to apply more or less exactly.

It is obviously the relative size of the hole which is the fundamental difference. Fortunately, it is possible to attain considerable insight into its effect with little analysis. We consider, for the moment, a metal-lined guide partially filled with dielectric. The dispersion curves sketched in Fig. 7 are similar to those shown in Fig. 4. The main difference is the shape near the light line, $\omega = ck$. The point where the curve crosses this line is now controlled by the relative filling factor, d/b , as well as the dielectric constant of the material. As d/b and ϵ become small, the point where the partially-filled guide becomes a slow wave structure, $\omega/ck < 1$, can thus still be made to occur at an arbitrarily high frequency.

When $\omega/ck > 1$, outside the light line, the field in the hole is proportional to $J_0(pr)$, an ordinary Bessel function. In this regime it peaks in the center of the hole. However, we must operate in the regime $\omega/ck < 1$, and in this case, the radial dependence is proportional to a modified Bessel function, $I_0(qr)$. The field is now

a minimum at $r = 0$, and the beam wave coupling is obviously decreased.

A sketch of the field dependence in the two regimes is shown in Fig. 8. The wave number in the dielectric, p , is still given by:

$$p^2 = \frac{\omega^2}{c^2} - k^2 \quad (29)$$

while the wave number in the hole, when $\omega/ck < 1$, is now given by

$$q^2 = k^2 - \frac{\omega^2}{c^2} \quad (30)$$

The latter is obviously one measure of the field depression in the hole. Since we operate near synchronism, $\omega = ck\beta$, we have for q :

$$q = k/\gamma \quad (31a)$$

$$q = \omega/c\beta\gamma \quad (31b)$$

or

$$q = 2\pi/\lambda\beta\gamma \quad (31c)$$

Hence, when non-relativistic beams are used $\beta\gamma \approx v/c$, the field drops off away from the dielectric in a distance small compared to a wavelength. If, however, the beam is at least mildly relativistic, $\beta\gamma \gtrsim 1$, the opposite limit

applies and we can operate with wavelengths that are small compared to the hole.

The latter considerations actually apply to any structure supporting a wave for which $\omega/ck < 1$. One might then ask about the relative advantages of a dielectric tube since, if $\beta\gamma \geq 1$, then coupling would be improved at short wavelengths for only slow wave structure.

The advantages of the dielectric tube also lie in the short wavelength range. In a conventional slow wave structure, the periodicity must also be comparable to the wavelength. Structures of reasonable length are, therefore, a great many wavelengths long and they become very difficult to fabricate at relatively long wavelengths (a few millimeters). It is possible, but not easy, to build conventional structures with a fundamental period smaller than a few millimeters. The dielectric is, however, a smooth structure and easy to fabricate. When the beam is relativistic, the coupling impedance becomes comparable to that of other structures. Modifications of this basic structure, such as a dielectric tube with no metal boundary and multiple coupled tubes, may also be of practical use. Another basic structure, a dielectric slab bounded on one side by a conductor, also shows promise for application in the shorter wavelength region. This follows from the fact that a greater mode separation at small wavelengths can be obtained from this more open structure. Hence, it may well

be easier to make single-mode devices with this type of structure, and for this reason we will analyze it in some detail.

The basic geometry is shown in Fig. 9. Assuming, for the moment, that no beam is present, we have for the TM modes of the guide:

$$\underline{E} = (0, E_y, E_z) \quad (32a)$$

where

$$\left[\frac{d^2}{dy^2} + \left(\frac{\omega^2 \epsilon}{c^2} - k^2 \right) \right] E_z = 0 \quad (32b)$$

and

$$E_y = \frac{ik}{\frac{\omega^2 \epsilon - k^2}{c^2}} \frac{\partial E_z}{\partial x} \quad (32c)$$

In the region $0 \leq y \leq d$, the dielectric constant ϵ appears while in the region $y \geq d, \epsilon = \infty$ is set equal to unity.

Anticipating the fact that we are concerned only with slow waves bound to the surface guide, we have for the electric fields:

$$E_z = A \sin py \quad (33a)$$

where

$$p^2 = \frac{\omega^2 \epsilon}{c^2} - k^2 \quad (33b)$$

in the region $0 \leq y \leq d$. Outside the dielectric, the field is:

$$E_z = B e^{-qy} \quad (34a)$$

$$q^2 = k^2 \omega^2 / c^2 \quad (34b)$$

Matching the tangential electric and magnetic fields can be used to eliminate the constants A and B. Thus we have for the dispersion relation of the dielectric slab wave guide:

$$\epsilon q \cot pd = p \quad (35)$$

A plot of the roots of this function is given in Fig. 10. The lowest order mode has no cutoff. It comes up along the light line, $\omega = ck$, until pd gets somewhat closer to the neighborhood of $\pi/2$. Thereafter, as ω becomes larger, it asymptotically approaches the speed of light in the dielectric. In the region $\pi/2 \leq pd \leq \pi$ there are no solutions to q . (45), while, when $\pi \leq pd < 3\pi/2$, a second mode which has a finite ω cutoff frequency can also propagate. At successively higher frequencies, more of these modes appear. Several are shown in Fig. 10.

II C. 2. Coupling of Beam to Bounded Resonator

Also shown in Fig. 10 is a beam speed line, $\omega = ck\beta$. It is obvious that if the beam velocity satisfies the Čerenkov conditions, $\beta > 1/\sqrt{\epsilon}$, phase synchronization between an electron beam and a wave can be maintained. When the beam is added, the wave equation in the vacuum region becomes:

$$\left[\frac{d^2}{dy^2} + \left(\frac{\omega^2}{c^2} - k^2 \right) \epsilon_{||} \right] E_z = 0 \quad (36a)$$

where

$$\epsilon_{||} = 1 - \frac{\omega_p^2 / \gamma^3}{(\omega - kv_0)^2} \quad (36b)$$

In arriving at eqs. (36a) and (36b), it has been presumed that beam density modulation occurs only in the z-direction, that the left edge of the beam is close to the dielectric, and that the beam extends indefinitely in the region $y > d$. The size of the actual gap between the beam and the dielectric will be an important parameter in a short wavelength device and its role will be discussed separately.

II C. 3. The Beam-Guide Dispersion for a Bounded Structure

When a bounded structure is used to support the wave, as it must in almost any practical source, the dispersion relation becomes a transcendental as opposed to an algebraic

function. It will be more or less straightforward to obtain values for the roots by numerical means, but it is not immediately obvious how to obtain a good qualitative understanding of the roots.

One method which is appropriate for relatively weak beams is the following. Assume a relation of the form:

$$D(\omega, k, \omega_p^2) = 0 \quad (37)$$

where the presence of ω_p^2 in eq. (37) indicates the presence of the beam. If the beam is weak, we can write:

$$D(\omega, k, \omega_p^2) = D^{(0)}(\omega, k) + \omega_p^2 \frac{\partial D}{\partial \omega_p^2} \quad (38a)$$

where

$$D^{(0)}(\omega, k) = D(k, \omega, 0) \quad (38b)$$

is the dispersion relation for the waves supported by the structure when no beam is present. This function can, in a region near to the solution $D^{(0)}(\omega, k) = 0$ be written as

$$D^{(0)}(\omega, k) = (\omega - \omega_k) \partial D^{(0)} / \partial \omega \quad (39)$$

where ω_k are the roots of eq. (35).

The second term in eq. (38a) can also be further reduced. The dependence of the dispersion relation upon ω_p^2 always enters through ϵ and hence the second term of

Equation (38a) will also have the form:

$$\omega_p^2 \frac{\partial D}{\partial \omega_p^2} = \frac{\omega_p^2 C(\omega, k)}{\gamma^3 (\omega - kv_0)^3} \quad (40)$$

where $C(\omega, k)$ is a function which will depend upon the detail of the structure. It may, for example, have zeros, but it will not have any poles near either $\omega = kv$, or $\omega = \omega_k$.

Thus, near synchronism, $\omega_k = kv_0$, and for beams which are not too strong, $I/I_0 \ll 1$, we again have a cubic dispersion relation:

$$0 = (\omega - \omega_k) \frac{\partial D^0}{\partial \omega} + \frac{\omega_p^2}{\gamma^3 (\omega - kv_0)^2} C(\omega_k, k) \quad (41a)$$

or

$$(\omega - kv_0)^3 = \frac{\omega_p^2}{\gamma^3} \frac{C(\omega_k, k)}{\partial D^0(\omega_k, k) / \partial \omega} \quad (41b)$$

Thus, the qualitative nature of the roots is rather independent of the exact geometry of the wave-supporting structure.

When the wave-supporting structure is a dielectric slab and the assumptions made earlier apply, the dispersion relation becomes:

$$q \cot pd = \frac{p}{\epsilon} \sqrt{\epsilon_{\parallel}} \quad (42)$$

The expansion procedure outlined in the preceding subsection then gives for eq. (41b):

$$\left(\frac{\omega - kv_o}{v_o}\right)^3 = \left(\frac{\beta \omega_p^2}{c^3}\right) \frac{(1 - 1/\beta^2 \epsilon)}{\epsilon \beta^4 \gamma^3} \cdot \frac{\sin^2 pd}{\frac{kd}{\gamma} + \frac{\gamma^2}{2\epsilon \gamma_T} \sin^2 pd} \quad (43)$$

The first two groups of factors on the right-hand side of eq. (43) are identical to the results obtained when it was assumed that the beam propagated in the dielectric, and much of the discussion presented at that point applies here as well. The last group of factors contains the dependence on the geometry. It can be seen that, in addition to the Čerenkov threshold dependence, the coupling also goes to zero as the thickness of the slab goes to zero, and is a result that could easily be anticipated.

The other trends in the gain can be understood as follows: On the fundamental mode, the value of pd varies from 0 at $\omega = 0$ up to $\pi/2$ as $\omega, k \rightarrow \infty$. On the higher branches, it varies from $n\pi$ at cutoff ($\omega = ck$) to $(2n + 1)\pi/2$ as the curve asymptotically approaches the speed of light in the dielectric. The value of $\sin^2 pd$ thus varies monotonically from zero to one. Assuming that the velocity synchronism is maintained along the dispersion curve, the gain will vanish at $\omega = ck$, because in this limit, $\gamma \rightarrow \infty$, and it becomes increasingly difficult to modulate the beam. Furthermore, as $\beta \rightarrow 1/\sqrt{\epsilon}$, the gain also vanishes due to the factor $(1 - 1/\beta^2 \epsilon)$ in the coefficient.

The gain thus vanishes at both ends of the dispersion curve and peaks in between. A sketch of the general behavior is shown in Fig. 11.

The maximum value that the gain can achieve is similar to that of the filled guide case. Some typical results for a thin, quartz slab waveguide are shown in Figs. 12a and 12b. In these plots, the factor $(\beta\omega_p^2/c^2)^{1/3}$ has been omitted for convenience. The remaining factors contain all the relevant frequency and energy dependencies. Maximum values somewhat greater than unity are obtain for this particular set of parameters. The omitted term $(\beta\omega_p^2/c^2)^{1/3}$ is actually the beam current density in A/cm² divided by I_0 ($= 17$ kA) all to the one-third power. It is relatively easy to obtain values of 0.1 for this number, hence the plots shown in Figs. 12a and 12b demonstrate that with a quartz slab guide, it is possible in principle to have relatively large gain ($\alpha = .233$) gives (1db/cm) well into the submillimeter part of the spectrum.

The gain plot in Fig. 12 also indicates that the gain is a bit higher on the higher order modes. This trend is a reflection of the $\omega^{1/3}$ factor in the gain. It is real, but it depends upon two assumptions whose validity are also frequency dependent. These are: first, that the beam is infinitesimally close to the dielectric and second, that the beam is monoenergetic. The first of these will be discussed now and the second point will be covered in a later section.

II C. 4. Finite Gap Between Beam and Resonator

If we assume that there is a small gap between the beam and the dielectric surface, we would have a situation such as that shown in Fig. 13. The analysis proceeds as before, but the resulting dispersion relation

$$\frac{\omega_p^2 e^{-q d_2}}{2(\omega - k v_0)^2} = \frac{q \epsilon \cot p d - p}{p} \quad (44)$$

is, at first sight, much more complicated. However, if we again assume that the roots at synchronism lie along the dispersion curve for the free modes, the situation simplifies considerably and the end result is that the gain is modified by an exponential factor which depends upon the size of the gap:

$$\alpha = \alpha(d) e^{-k d_2 / \gamma^3} \quad (45)$$

As long as $k d_2 / \gamma$ is small, the gain on the higher order modes will be comparable to or greater than the gain on the fundamental mode. Values of d_2 of about 1 millimeter would be conservative and fractions of this are easily obtained. Hence, provided that one uses $\beta \gamma \geq 1$, the quart guide system discussed above will still be viable well into the submillimeter region of the spectrum.

We have been assuming that the beam extends indefinitely in the positive y -direction. As long as the beam is

at least a few e-foldings thick, this assumption does not affect the gain. Since we are primarily interested in high frequencies, this assumption will normally be valid.

The fall-off of the field in the transverse direction may also be useful in obtaining some mode selection. If a relatively thin beam is used, the fields for the lower order modes may penetrate through to the other side. If a lossy material is placed above the beam, it may be possible to further reduce the gain on the lower order mode.

In the fall-off of the electric field, operation at arbitrarily short wavelengths could be obtained if γ is allowed to become large, i.e. kd_2/γ will remain small. This will involve a penalty in the maximum value of gain obtainable, but since it is relatively large to begin with, the resulting system will still be potentially useful. In this way, with more relativistic e-beams, it might be possible to operate well into the infrared portion of the spectrum. This will be discussed further in a later section.

II D. THE EFFECT OF BEAM VELOCITY SPREAD

Prior to this point in our discussion, we have assumed that the electron beam was perfectly monoenergetic. It is intuitively plausible that this is a wavelength-dependent assumption, and we will now examine its consequences. The discussion will be divided into three parts. First, we will determine wavelength limit for a simple beam space charge wave. Then, this result will be compared with a similar criterion for a Čerenkov instability. Finally, having set the limiting wavelength for treating the beam as monoenergetic we will derive gain expressions valid in the region where the assumption is violated.

II D. 1. Beam Space Charge Waves

The linearized equation of motion for a strongly-magnetized electron beam is given by eq. (1). If this is taken along with the equation of continuity eq. (3a), Poisson's equation, and assumptions similar to those of that section, the dispersion relation for space charge waves

$$\omega = kv_0 \pm \omega_p/\gamma^{3/2} \quad (46)$$

may be easily derived.

The upper (lower) sign in eq. (46) corresponds to a fast (slow) space charge wave. See Fig. 14a.

We will concern ourselves with a slow space charge wave. Shown in Fig. 14b is a sketch which illustrates the meaning of the statement: "the wave is resolved from the beam". The wave is clearly resolved when the beam may be regarded as a delta function in frequency space, (the arrows located at ω and kv_0). If, on the other hand, the velocity spread of the beam, Δv , is such that the self-consistent frequency separation, $\Delta\omega = \omega - kv_0$ (derived under the assumption that the beam was monoenergetic) is less than $k\Delta v$, the assumption is violated. A quantitative criterion for this critical k is:

$$k_c \Delta v = \frac{\omega_p}{\gamma^{3/2}} \quad (47)$$

Equation (47) may be re-expressed in terms of physically more intuitive variables if we write: $k_c = \omega/c\beta = 2\pi/\lambda_c \beta$, Δv in terms of $\Delta\gamma$ and β , and ω_p in terms of the beam current density J_b . Then we have:

$$\lambda_c = \pi \frac{\Delta\gamma}{\gamma} \left(\frac{I_0}{\beta\gamma J_b} \right)^{1/2} \quad (48)$$

where I_0 is still $ec/r_0 = 17$ kA. If $\beta\gamma$ is of order unity, $\Delta\gamma/\gamma$ is of order 10^{-2} and J_b is a reasonable fraction of an ampere/millimeter² then λ_c is a fraction of a millimeter. These are relatively modest requirements, and thus we predict that it should be possible to make effectively cold beams well into the submillimeter part of the spectrum.

The critical wavelengths given by eqs. (47) and (48) are dependent upon the assumption of a simple space charge wave. When we are considering a Čerenkov instability, however, $\Delta\omega = \omega - kv_0$ is actually larger than $\omega_p/\gamma^{3/2}$, and hence the beam can be effectively colder at a given wavelength. The criterion for resolution is:

$$k_c \Delta v = \frac{\omega_I}{2} \quad (49)$$

where the right-hand side of eq. (49) is the real part of the detuning (eq. 13b). Substitution of the expressions for ω_I can be made for the appropriate case.

When the beam propagates through the dielectric, eq. (13b) applies directly and we have:

$$\lambda_c = \sqrt{2\pi} \left(\frac{\Delta\gamma}{\beta\gamma} \right)^{3/2} \left(\frac{I_0}{\beta\gamma J_b} \right)^{1/2} \cdot \frac{1}{\sqrt{1-1/\gamma}} \cdot \frac{1}{\sqrt{\gamma^2/\gamma_T^2 - 1}} \quad (50)$$

The current density dependence is similar to that of eq. (48), but provided the beam is at least mildly relativistic ($\beta\gamma \geq 1$), the energy dependence is more favorable. Overall, presuming that γ_T and γ/γ_T are not excessively large, the value λ_c , given by eq. (50), will be at least as small as that given by eq. (48). The addition of the form factor associated with a more practical resonator will not alter this essential conclusion.

II D. 2. Gain in the Warm Beam Limit

When the criteria given in the preceding paragraphs are violated, the beam is to be regarded as "warm" at the wavelength in question. The gain does not vanish in this limit, but it does begin to drop as ω^{-1} , as opposed to the general $\omega^{1/3}$ trend in the cold beam limit. This trend means that oscillators can probably be built in the warm beam limit, but amplifiers will be impractical.

In calculating the gain, we will use the Vlasov equation as the basic equation of motion and we will retain the assumption that the beam is strongly magnetized. In this case, the Vlasov equation is:

$$\frac{\partial f}{\partial t} + v_z \frac{\partial f}{\partial z} + p_z \frac{\partial f}{\partial p_z} = 0 \quad (51)$$

If this is linearized, $f = f_0 + \delta f$, and is Fourier-transformed, we have for the perturbed component distribution:

$$\delta f = -ie E_z \frac{\partial f_0 / \partial p_z}{\omega - kv_z} \quad (52)$$

The current is now given by:

$$J_z = \int v_z \delta f \partial p \quad (53a)$$

$$= ie E_z \int v_z \frac{(\partial f_0 / \partial p_z)}{\omega - kv_0} dv_z \quad (53b)$$

Substitution of this into eq. (8) will then lead to a dispersion relation. If the beam distribution is a delta function, then the integral can be performed immediately and the current given by eq. (4b) is recovered. However, we are now interested in the limit where the beam velocity spread is finite.

An exact solution of a dispersion relation containing a integral kernel, such as that of eq. (54), can be found using numerical techniques. The results of such a procedure will be discussed below. However, some insight into the general behavior can be obtained in the limit where k times the width of the beam distribution is broad in comparison with the gain which would be obtained from a calculation in which it were assumed that the beam were cold (monoenergetic).

The dispersion relation obtained from the above procedure is:

$$\frac{\omega^2 \epsilon}{c^2} - k^2 - p^2 + \frac{\omega_p^2}{\omega \epsilon} (\omega^2 \epsilon / c^2 - k^2) \int_{-\infty}^{\infty} \frac{mv \partial f / \partial p dp}{\omega - kv} = 0 \quad (54)$$

In its present form, the integral which appears in eq. (54) is to be performed along the real momentum line, and hence the procedure for handling the singularity at synchronism is not yet defined. Borrowing from the theory of plasma physics, we handle it by formally extending the integral into the complex plane. First, we re-express eq. (54) as a

velocity integral. Then:

$$\frac{\omega^2 \epsilon}{c^2} - k^2 - p^2 + \omega_p^2 \frac{(\omega^2 \epsilon / c^2 - k^2)}{\omega \epsilon} \int \frac{v \partial F / \partial v dv}{\gamma^3 (\omega - kv)} = 0 \quad (55)$$

we now let

$$\frac{1}{\omega - kv} = P \frac{1}{\omega - kv} - i\pi \delta(\omega - kv) \quad (56)$$

where P stands for the principal part of the integral. Multiplying through by c^2/ϵ and using the condition $v = \omega/k\omega\epsilon$, we find for the imaginary part of the dispersion relation:

$$D'' = - \frac{\pi \omega_p^2 \beta^2 (1 - 1/\beta^2 \epsilon)}{\epsilon \gamma^3} \frac{\partial F(\omega/k)}{\partial(\omega/k)} \quad (57)$$

It is sufficient for the purpose of the present discussion to ignore the small correction to the real part of the dispersion represented by the principle part of the integral. In the limit, the real part of the dispersion is:

$$D' = \omega^2 - \omega_k^2 \quad (58a)$$

and providing the growth is small, the imaginary part of the frequency is adequately represented by:

$$\omega_I = \frac{D''}{\partial D' / \partial \omega} \Big|_{\omega = \omega_k} \quad (58b)$$

or

$$\omega_I = \pi \omega_p^2 \frac{\beta^2 (1 - 1/\beta^2 \epsilon)}{2 \epsilon \omega_k \gamma^3} \frac{\partial F(\omega_k/k)}{\partial \omega_k/k} \quad (58c)$$

Obviously, there will be wave growth (inverse Landau damping) in the region of velocity space where $\omega_k/k < v_0$. Sketches of the unperturbed dispersion relation, $\omega = \omega_k$ and ω_I are shown in Fig. 15. The region of positive ω_I lies on the larger k side of the synchronous wave number, $k_s = \omega/v_0$, and peaks at a velocity which is below v_0 by an amount approximately equal to the half width of the velocity distribution.

Thus, the wave growth in the warm beam limit has a shape which is complimentary to that obtained in the cold beam limit. This result may seem to imply that the growth due to inverse Landau damping is fundamentally different from the growth obtained in the warm beam limit. However, this is not the case. If the roots of eq. (55) are followed as the beam width is varied from a value of zero up to $k \Delta v \omega_I$ (cold), we find that one regime passes smoothly into the other. The peak absorption shown in Fig. 15 is always somewhat less than the gain. It is a composite of the long wavelength, cold beam gain and Landau damping caused by that part of the beam which has $\partial F/\partial v < 0$. The peak gain obtainable in the warm beam limit will always be less than ω_I (cold). This occurs because, as the beam distribution becomes arbitrarily sharp, the self-consistent beam density

dependent frequency shift will move the phase velocity of the wave downward relative to the position of maximum $\partial F/\partial v$.

In spite of this, the warm beam limit may very well be of interest. An assessment of this requires that we estimate eq. (58c) which, in general, depends upon the detailed shape of the beam distribution. We can, however, proceed without undue complication if we recognize that if $\sim 1/\Delta v$, and thus $\partial F/\gamma v$ at its maximum is $\sim 1/\Delta v^2$. Then, in terms of $\Delta \gamma$, an approximate expression for ω_I becomes:

$$\omega_I \approx \frac{\pi \omega^2 p}{2\epsilon} \cdot \frac{\gamma}{\omega} \cdot \left(\frac{\beta \gamma^2}{\Delta \gamma} \right) (1 - 1/\beta^2 \epsilon) \quad (59a)$$

or

$$\alpha \approx \frac{\lambda}{\epsilon} \cdot \frac{J_b}{I_0} \cdot \left(\frac{\gamma^2}{\Delta \gamma} \right) \cdot \frac{(\gamma^2/\gamma_T^2 - 1)}{\beta^2 \gamma} \quad (59b)$$

It is interesting to evaluate the possible gain in the 10 μ range. In this case, $\lambda = 10^{-3}$ centimeters. If we can achieve $J_b/I_0 \sim 10^{-3}$ and $\Delta \gamma/\gamma > 10^{-2}$, it appears that $\alpha \sim .1 \text{ cm.}^{-1}$ are within the realm of possibility. Thus, it might be possible to construct Čerenkov lasers down to wavelengths comparable to those achieved in stimulated Compton devices.

It is also interesting to evaluate eq. (59b), when λ is equal to λ_c . Upon substitution, we obtain:

$$\alpha = \sqrt{2\pi} \left(\frac{\gamma}{\Delta\gamma} \right)^{\frac{1}{2}} \left(\frac{J_b}{\gamma I_0} \right)^{\frac{1}{2}} (\gamma^2/\gamma_T^2 - 1)^{\frac{1}{2}} \quad (60)$$

Examination of eq. (60) supports the conjecture that $\alpha \geq .1\text{cm.}^{-1}$ are attainable in cold to warm crossover region ($\lambda \lesssim \lambda_c$).

II E. COMMENTS ON NONLINEAR BEHAVIOR

It would be possible at this point to develop a reasonably complete nonlinear theory for single-mode Cerenkov devices. This would, in part, follow lines of argument originally established to explain microwave tubes, beam plasma interactions, and more recently, free-electron lasers. In the wavelength regime which is of primary interest, however, the ratio L/λ is large and there will be, at the very least, a few axial modes within the half-width of the gain curve. There may also be a mixture of transverse modes, although if the device can be made to operate on a single transverse mode, it will be advantageous to do so. Relatively less is known about electron beam devices in the multimode region, and the development of a complete nonlinear theory, analogous to that developed by Lamb²⁴ for the gas laser, should take account of multimode operations. This would be a substantial undertaking. It could be productive, however, since we generally expect that Čerenkov devices will exhibit many phenomena intrinsic to all multimode oscillators, and that some of these may be useful in applications (e.g., mode locking). Hence, because the development would at this point omit some of the most interesting parts of the problem (on account of its length and because the motivation for experimental development rests primarily on the prediction of the linear gain which would be expected in specific wavelength regions) we will restrict discussion of nonlinear problems to a few simple scaling arguments.

II E. 1. Nonlinear Scaling Arguments

In the operating regime where the beam velocity distribution can be regarded as cold and the motion one-dimensional, the relative density modulation is given by:

$$\frac{\delta n}{n_0} = \frac{kv}{\omega - kv_0} \quad (61)$$

Now the change from electron orbits, which move progressively forward compared to the phase of the wave (untrapped) to orbits which are winding up (trapped), occurs in the vicinity of $|\delta n/n_0| \simeq 1$. Thus it occurs where

$$k\delta v \simeq |\omega - kv_0| \quad (62a)$$

or

$$k\delta v \simeq \omega_I \quad (62b)$$

This can be converted to a prediction of the magnitude of the axial component of the electric field at which saturation of the linear growth is in progress. We find from eq. (1) and eqs. (61a) and (61b):

$$|E_z| \simeq \frac{m\gamma^3}{e} \frac{\omega_I^2}{k} \quad (63)$$

The Poynting's flux, and hence also the total power carried to the wave, will be proportional to E_z^2 and thus up to ω_I^4 . The latter will in turn be proportional to $(I/I_0)^{4/3}$.

Hence, up to form factors (which can vary between small numbers and unity) the overall power at the separatrix crossing value of E_z (eq. (62)) will be:

$$P_{\text{wave}} \sim \left(\frac{I}{I_0} \right)^{1/3} P_{\text{beam}} \quad (64)$$

This is a conversion factor which can be expected in any traveling wave device. Enhanced conversion could be obtained by tapering the phase velocity and thus "deepening" the trapping well. Still more energy could be recovered if the beam were collected at high potential (depressed collector operation). An estimate of the overall efficiency obtainable from a Čerenkov device is thus a subtle and complex matter. In the final analysis, however, tube-like efficiencies of perhaps fifty percent could be attainable.

III. A. THE ELECTRON BEAM

The single most important component of an electron beam-driven radiation source is the beam itself. Its parameters will, in large part, determine the performance of the system. In order to examine the potential of Cerenkov sources in the millimeter and submillimeter parts of the spectrum, it will be useful to examine the parameters of some typical electron beam generators which may be used in this application.

A few general types of electron beam generators and their parameters are listed in Table 1. All of the beams are at least mildly relativistic; a choice is dictated by coupling considerations developed in earlier sections. However, the values of the beam current and the modes of operation vary widely. We will begin our discussion of the entries in the table by considering the role of the beam energy.

The beam energy helps to determine the operating wavelength in several interrelated ways: first, by synchronism; second, by the magnitude of the gap between the beam and the resonator, which must be present in any real system; and third, by its entry into the equations which determine the beam modulation. The first of these alone does not place any stringent limit on the attainable wavelength. This is

because the design of dielectric resonators which will support a wave of any reasonable phase velocity does not present a problem. The second and third aspects of the energy dependence will therefore be more important in setting the short wavelength limit to a device. The rate at which the electric field decreases as the distance from the resonator increases is given by $q = 2\pi/\lambda\beta\gamma$. The gain, however, increases with frequency and hence we would expect it to peak somewhere in the vicinity of $qa \approx 1$, where a is a characteristic distance between the beam and resonator. A modest value for a would be approximately one millimeter, and a more difficult but attainable value would be about one-tenth of this. Taking this range and assuming $qa \approx 1$, we can determine the limiting wavelength for good beam-to-resonator coupling. The range of this wavelength is shown in the table. Examination of the table and the figure will show that relatively compact machines could ultimately be expected to work well into the submillimeter region of the spectrum, while if one extends the range of beam generator complexity, operation in the infrared could be possible.

While the beam-to-resonator coupling decreases away from the resonator due to the fall-off of the electric field with distance, an arbitrary increase in beam energy will lower the minimum wavelength by a corresponding amount. However, the

beam energy also enters into consideration through the equations of motion for the electrons, and increasing γ furthers the difficulty of attaining good beam modulation. Hence, these two effects must be traded against each other. When the beam is strongly magnetized, the energy-dependence of the growth is approximately $\alpha \sim \gamma^{-1}$, and when it is not magnetized, $\alpha \sim \gamma^{-1/3}$. Since the criterion for strong magnetization becomes more difficult to meet as λ decreases, short wavelength operation will probably require unmagnetized, or at least weakly magnetized, electron beams.

The current available from the variety of generators listed in Table 1 also covers a wide range. When the beam is cold, the gain will scale as $(J_b/I_0)^{1/3}$, and thus a beam with 17_0 A/cm^2 will make this parameter 0.1. We have seen earlier that if this is used with reasonable values of the other parameters, the gain will be in the $.1 - .5 \text{ cm.}^{-1}$ range. The first and third entries in the table can probably achieve values in this vicinity, while the second and fourth entries could do so without question. The greater current available from the second and fourth type of generator might also make up for deficiencies in another parameter.

Field emission diode generators produce very large currents. Hence, they are in principle capable of producing a lot of gain. It was partly for this reason that a generator of this type was used in early experiments designed to demonstrate the utility of stimulated Čerenkov radiation. They also have the ability to produce beams

whose energy is sufficient to couple well into the sub-millimeter region. Their drawback for short wavelength operation may, ironically, be the fact that the current is large. This is because the self-fields, which have been neglected in our analysis of gain, may lead to larger $\Delta\gamma/\gamma$, and hence to a limit of the usable range of wavelength.

The accelerators listed in the table will also be capable of operating at current densities which give usable gain. The peak current will be low, but the focussing could be better. The current in a linear accelerator will also have a complicated time structure (the typical value of I is the peak in the micropulse), and this will complicate the gain calculations. If used, however, such a generator will be designed to work at short wavelengths and the microstructure may be a minor feature. Both this complication and the role of self-fields are worth further analysis.

The pulse length and peak power entries in the table are largely self-explanatory, although one consequence of the pulse versus continuous operation is worthy of comment. We will see below that when the Q of a cavity is reasonable, the current density required to initiate oscillation will be quite modest. Thus, systems with relatively low gain, $\alpha - 0.01$ to 0.1 , may be very usable as oscillators well into the infrared, whereas the same beam generator would not be a suitable source for an amplifier. Overall, it is to be expected that the pulsed beam generators, due primarily to

the larger current densities available, could be used as both oscillators and amplifiers while the steady-state generators would be largely restricted to application as oscillators.

In addition to its relation to the gain of the device, the current density plays a role in determining the wavelength of which the beam may no longer be regarded as "cold". Clearly, if all parameters other than current remain fixed, increasing the current decreases the wavelength for which the beam must be regarded as warm. The current density, the energy and the energy spread are not truly independent, but we will, for the purpose of discussion, treat them as though they were.

Restating the expression $k\Delta v = \omega_I/2$ in terms of the spatial gain, $\alpha(\text{cm.}^{-1})$, and a beam energy spread $\Delta\gamma$, we have for the wavelength at which the cold/warm transition occurs:

$$\lambda_c = \left(\frac{4\pi}{(\beta\gamma)^2} \right) \left(\frac{\Delta\gamma}{\beta\gamma} \right) \frac{1}{\alpha} \quad (65)$$

It is clear that the beam generator in the lower energy end of the range considered must achieve relatively better energy collimation if it is to operate in the "cold" regime at any given wavelength. The lower energy, pulsed electrostatic devices with their larger currents can be expected to operate in this mode for wavelengths in the upper submillimeter to one-millimeter range. As the beam energy rises,

the crossover wavelength becomes smaller, and hence with accelerator-produced beams, one would be encouraged to attempt to experiment with infrared Čerenkov sources. is quite an extrapolation from any present stimulated Čerenkov experiment. But other modes of e-beam use have achieved success in this range. Beam dependent limitations are largely dependent on the particular interaction, however, and thus comparisons of Čerenkov and, for example, stimulated Compton sources will depend primarily upon the gain. In the former device we must couple to a suitable resonator, but in the latter a relatively large transverse velocity modulation must be induced on the beam. Thus the two methods of e-beam use may produce at least comparable results.

III B. A MILLIMETER WAVELENGTH EXPERIMENT

Shown in Fig. 16a is the schematic diagram of an apparatus which has been constructed in order to test a number of the concepts discussed in Section II. It consists of a high-voltage pulse transformer, a thermionic cathode, a single-gap accelerating stage, a static magnetic field to guide the beam, and a tubular quartz - dielectric resonator. The beam is guided along the axis of the resonator and is collected on the surface of a plane mirror placed at a 45-degree angle to the end of the copper tube which supports the quartz. The output is then focussed into a plane-parallel Fabry-Pérot resonator.

The transformer has a peak capacity of 400kv at 200A for 10μ seconds at a 300hz repetition rate. However, typical operating conditions for the present work are 100-300kv at 0.5-20A for approximately 1μ second. At the present time, the pulse repetition frequency is a few hz. The primary of the transformer is driven by a hydrogen-thyratron triggered, single-stage, pulse-forming network. A characteristic high-voltage trace and an accompanying millimeter-wavelength radiation pulse is shown in Fig. 16b. The voltage range of the generator, which provides adequate power for stimulated χ Cerenkov radiation experiments, is such that millimeter-submillimeter operation can be expected.

Coherent output radiation has been obtained at wavelengths extending from about 1 centimeter to below 1.5 millimeters. The wavelength of the radiation depends upon the guide radius, the relative amount of dielectric and its dielectric constant, and the beam voltage. Configurations which should work in the fundamental mode over the 1 centimeter - 3 millimeter range have been studied, and reasonable agreement with the theory of Section II is found. The diameter of the copper guide which supports the quartz tube is approximately 1.5 centimeter, and tubes with 1-3 millimeter wall thicknesses have been used most recently. Thus output wavelengths which are less than the transverse dimension of the waveguide have already been obtained.

At the longer wavelengths, the frequency has been determined with the Fabry-Pérot interferometer, and some typical data illustrating the behavior is shown in Fig. 17. In Fig. 17a, a calibration trace made with a 35 hz Gunn diode source is displayed, and in Fig. 17b, experimental data with approximately the same wavelength is shown. The trace shown in Fig. 17b consists of many repetitions of the e-beam pulser, and it shows that the average spectral width, which is itself quite narrow (.1-1 percent), is primarily due to shot-to-shot reproducibility. The output of a single pulse is apparently very coherent. An interferometer for shorter wavelengths is under construction. The shorter wavelengths have been measured with cutoff filters.

The output is monitored by ordinary microwave diodes, either IN23's, IN26's, or IN53's, with the latter being used down to wavelengths below 1.5 millimeters. Attenuation levels of 30-60 db are required in order to insure that the output levels are below the burnout levels of the diodes. The absolute output power levels are not yet precisely determined except within an experimental uncertainty which becomes greater at shorter wavelengths and varies between .1 and 5 percent of the beam power. All of the factors which control this conversion efficiency are not yet well understood. The loaded Q of the resonator is modest, and the system is probably operating as a super-radiant oscillator. If this is so the previously-stated conversion efficiencies are plausible, but as is the case with the theory, nonlinear behavior of the experimental device is practically unexplored.

The experiment described above is in a relatively early stage of development. It does appear, though, that millimeter-submillimeter Čerenkov devices are a realistic possibility.

III C. ČERENKOV DEVICES IN THE SHORT WAVELENGTH LIMIT

The bulk of the analysis presented in the preceding sections was devoted to systems which would work in a way similar to microwave devices of the traveling wave type. We emphasized the region which was collective where there was an interaction of fields with the beam. Recently,²⁵ however, radiation with a wavelength of about 3μ was obtained from an electron beam produced by a linear accelerator and a coupler, which was a helical, static, magnetic field. This device operated in the so-called single-particle limit:

$$\omega_p L / c\beta\gamma^{3/2} \ll 1 \quad (66)$$

In this expression, L is the length of the interaction region, and the other quantities are defined in earlier sections.

The interaction in this free-electron laser depends upon the coupling between the transverse velocity modulation imparted to the beam by the helical pump, and the magnetic field component of the wave in question. The beat wave produced, which is sometimes called a ponderomotive wave, travels at a phase velocity. Hence it, too, is a slow wave interaction.

There is no reason why the slow wave supported by a thin film dielectric wave guide could not also be used in the l_μ range. Furthermore, the beam quality requirements

are the same if

$$kb/\gamma \approx 1 \quad (67)$$

where b is the beam thickness. The electric field associated with the slow wave structure can be greater than that of the ponderomotive wave. A detailed comparison of the two modes of interaction (dielectric versus static B pump) would be too lengthy to present here, but in view of the above comment, it follows that there are beam-resonator combinations for which the Čerenkov device gain will exceed the gain of the ponderomotive wave-based free-electron laser (FEL). In this case, the behavior of a Čerenkov device will be more "forgiving" than the FEL. An example of this is the relaxation of the energy collimation required if a beam in the single-particle limit is to be considered monoenergetic. Simple consideration of the phase shift accumulated in a length L leads to the requirement:

$$ck \Delta\beta L/v < \pi \quad (68a)$$

or

$$\frac{\lambda}{L} > \frac{2\delta\gamma}{(\beta\gamma)^3} \quad (68b)$$

Higher gain would allow a shorter length, and hence a system which was in the "cold" region at a shorter wavelength. Due to this and to other considerations, it is of

interest to make a detailed comparison of these two systems. We will conclude this section with a brief discussion of two possible configurations which might be used in the μ range. The first is shown in Fig. 18.

Shown in the figure is a thin dielectric guide with tapered ends. An electron beam passes over the guide and couples to the evanescent field. When the beam has a high enough energy, the coupling will be good. The tapered ends face mirrors which, together with the guide, form an optical resonator.

It might also be useful to taper the thickness of the guide near its ends. By doing this, the field energy in the guide can be increased at the expense of that stored above the guide. If the taper is adiabatic on the scale of k^{-1} , the dispersion relation will vary smoothly as will the field distribution. Shown in Fig. 19 are the results of one possible experimental configuration including a taper. As the guide thickens, the field distribution is pulled down into the guide and formed into a half-sinusoid. The latter form, which is closed to the normal mode distribution of a guide which is covered top and bottom, should give better control of the input-output coupling.

Another possible version of a short wavelength system is shown in Fig. 20. In this system, the output optics are placed below the beam. Incident radiation comes through the end face of the guide and normal to the face, but the angle formed with the top surface is greater than that required for total internal reflection. This guide is also

tapered. As it thins out, the field is pushed out to increase the coupling. It is then pulled in again and passed to a second mirror.

The two configurations just discussed are highly schematic. The beam-to-field coupling will be a straightforward matter, but the overall optical system may be quite complex. Self-reproducing patterns of the general type discussed should exist, however, and well-collimated relativistic beams, together with the resonator, could form the basis of far-infrared Čerenkov devices.

IV. CONCLUSION

The theme of the preceding three sections is the use of the combination of the electron beam and the dielectric resonator to generate coherent radiation in the millimeter through infrared portions of the electromagnetic spectrum. At the present time, there is experimental confirmation of some of the basic theoretical assumptions in the 10-millimeter to 1-millimeter region. The theoretical advantages of smooth-bore, slow wave structures at shorter wavelengths indicate that submillimeter-infrared operation is also a realistic possibility. Beams with the monoenergeticity and current sufficient to achieve oscillation for moderate Q resonators ($(\omega_I Q / \omega) > 1$) currently exist. The long-term interest in these sources will not depend upon whether they work at all, but how they might compare to other possible sources.

TYPE:	ENERGY (Mev):	CURRENT (A):	PULSE LENGTH:	PEAK POWER:	"GOOD" COUPLING WAVELENGTH:
1-stage Thermonic	.1 - .2	.1 - .2	∞	10-50KW	1mm
1-stage Thermonic	.04 - 5	10-100	μ sec	1-100MW	1mm
n-stage Thermonic	.1 - 1	.1	∞	10-100KW	.3mm
n-stage Thermonic	1	KA	μ sec	1GW	.5mm
Field Emission Diode	.5-5	multi KA	.01 - .1 sec	multi GW	.5mm
Linac	2-100	.01 - 1	10 ps	50MW	1 μ

TABLE 1
Electron Beam Generators of Potential Use
in Cerenkov Sources.

ACKNOWLEDGMENTS

This is a report of work in progress. It owes debts to those who have already contributed and to those who are currently engaged in the research. I would most especially thank Robert Layman for continuing to carry a major portion of the burden of the experimental work, of which only a small portion has been reported herein. In addition, Kenneth Busby and Kevin Felch have helped build the first apparatus and took the first measurements. John Bagger and Geoffrey Crew performed calculations during the early stages of the work. Portions of their senior theses appear in Section II. To be thanked also are John Branscum, John Golub, David Kapilow, James Murphy, David Speer, and Douglas Wise, who currently bear a major part of the responsibility for the experimental and theoretical program. Finally, thanks to Desiree Rastrom for research and administrative assistance.

Support for this work has been provided by Dartmouth College, by the Air Force Office of Scientific Research, by the Army Research Office, and by the Office of Naval Research.

REFERENCES

1. Cerenkov, P.A. (1934). Dokl. Akad. Nauk. SSSR 2,451.
2. Frank, I.M., and Tamm, I (1937). Dokl. Akad. Nauk. SSSR 14,109.
3. Heaviside, O. (1888). Phil. Mag. Feb. p.130, Mar. p.202, May. p.379, Oct. p.360, Nov. p.434, Dec. p.488.
4. Sommerfeld, A. (1904). Götting, Nachricht 99,363.
5. Curie, E. (1941). "Madame Curie." Heinemann, London.
6. Mallett, L. (1926). C.R. Acad. Sci. a) 183,274. b) 187,222. c) 188,445. Paris.
7. Jelly, J.V. (1958). "Čerenkov Radiation and its Applications." Pergamon, London.
8. Zrelov, Z.P. (1970). "Čerenkov Radiation in High Energy Physics." Israeli Program for Scientific Translations.
9. Bolotovskii, B.M. (1961). Usp. Fiz. Nauk. 75,295. (1962) Soviet Physics Uspekhi 4,781.
10. Ginzburg, V.L. (1947). Dokl. Akad. Nauk. SSSR 3,253.
11. Coleman, P., and Enderby, C. (1960). J. Appl. Phys. 31, 1695.
12. Danos, M. (1953). J. Appl. Phys. 26,2.
13. Lashinsky, H. (1956). J. Appl. Phys. 27,631.

14. Ulrich, R. (1967). Zeitschrift für Physik 199,171.
15. Ahiezer, A. (1956). Nuovo Cimento, Series 10 3,591.
Abele, M. (1952). Nuovo Cimento, Series 9 207.
16. Mourier, G. (1958). In "Microwave Tubes", Vol. 2, p. 132.
Elsevier, Amsterdam.
17. Glinhart, G. (1958). In "Microwave Tubes", Vol. 2,
p. 136. Elsevier, Amsterdam.
18. Piestrup, M.A., Powell, R.A., Rothbart, G.B., Chen, C.K.,
and Pantell, R.H. (1976). Appl. Phys. Lett. 28,92.
19. Chu, A.N., Piestrup, M.A. Barbee, T.W., and Pantell,
R.H. (1978). Proc. Int. Conf. on Lasers, p. 744-749.
20. Stockton, M., and Walsh, J.E. (1978). J. Opt. Soc. Am.
68,1629.
21. Walsh, J.E., Marshall, T.C. and Schlesinger, S.P. (1977).
Phys. Fluids 20,709.
22. Felch, K.L., Busby, K.O., Layman, R.W., Kapilow, D.,
and Walsh, J.E. (1980). "Free Electron Generators of
Coherent Radiation," Physics of Quantum Electronics,
(S. Jacobs, H. Pilloff, M. Sargent, M. Scully, and
R. Spitzer, eds.), Vol. 7. Addison-Wesley.
23. Felch, K.L., Busby, K.O., Layman, R.W., Kapilow, D.,
and Walsh, J.E. (1981). Appl. Phys. Lett. 38,60.
24. Lamb, W. (1964). Phys. Rev. A134,1429.
25. Deacon, D.A., Elias, L.R., Madey, J. Ramian, G.,
Schwettman, H., and Smith, T. (1977). Phys. Rev.
Lett. 38,892.

FIGURE CAPTIONS

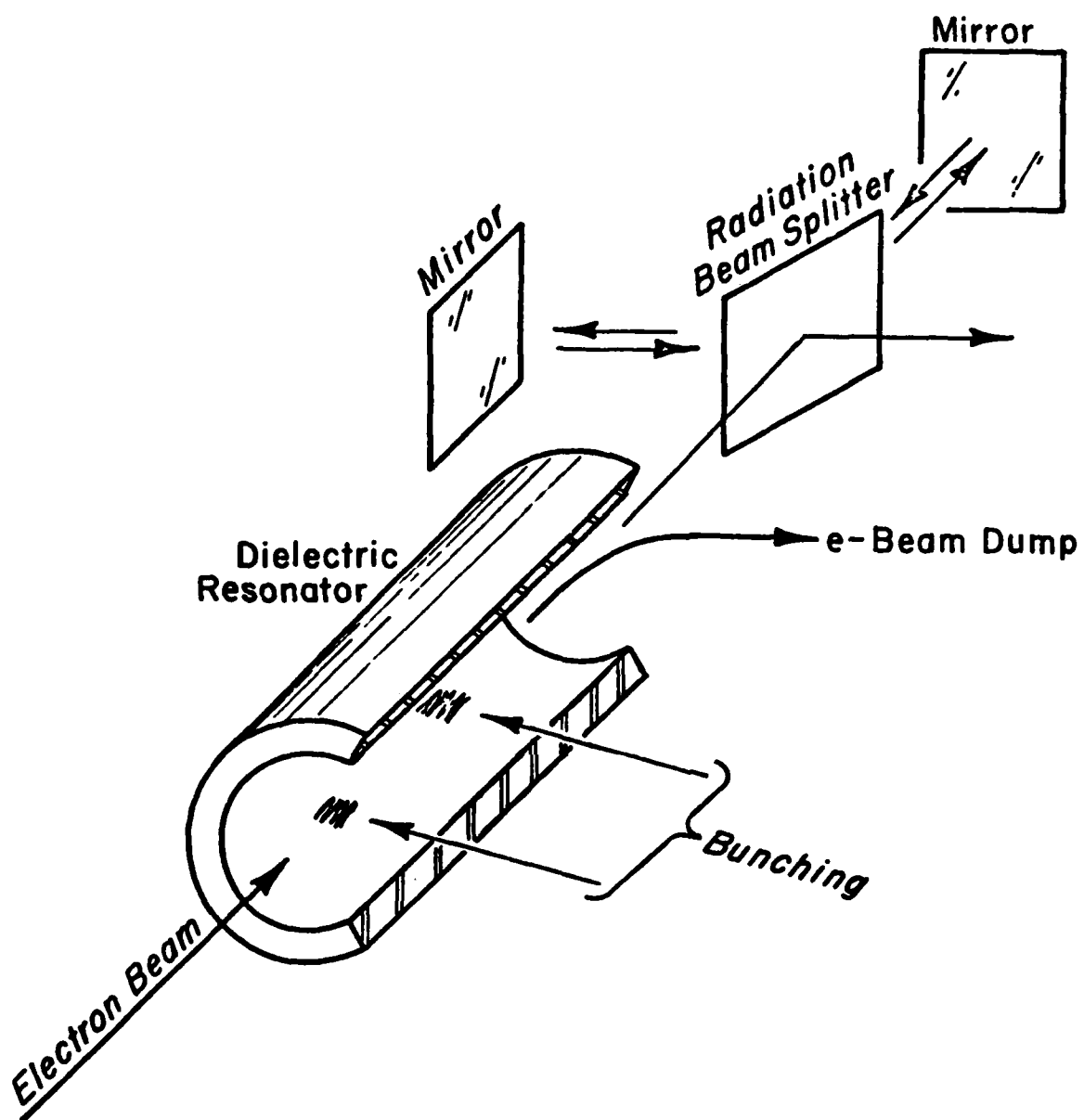
- Figure 1: Cerenkov maser components.
- Figure 2: Alternate configurations of the basic device. a) slab waveguide; b) possible Čerenkov gas laser.
- Figure 3: Geometry for the plane-wave - e-beam interaction in a dielectric medium.
- Figure 4: The relations ω vs k for two different perpendicular components of wavenumber ($P_1 > P_2$).
- Figure 5: The complete dispersion relation for the e-beam dielectric system. The region of instability.
- Figure 6: The components of growth rate. a) the dielectric contribution; b) the beam threshold function F .
- Figure 7: Dispersion relation for the free waves of a partially-filled guide.
- Figure 8: The radial dependent of the axial electric field. a) the fast wave region; b) the slow wave region.

- Figure 9: The basic slab guide geometry and axial field dependence.
- Figure 10: The dispersion relation for the slab guide.
- Figure 11: Gain curve shape vs. beam velocity for the beam-slab guide system.
- Figure 12: Numerical values of dispersion (a) and spatial gain (b) vs. beam velocity for a .025 cm. thick quartz guide.
- Figure 13: Geometry of slab guide/beam system when there is a finite gap between the beam and the guide.
- Figure 14: The relative positions of the phase velocity and the beam velocity distribution function ($F\beta$) when the beam is "cold" and when it is "warm".
- Figure 15: Qualitative shape of the dispersion and gain in the "warm" beam limit.
- Figure 16: The configuration of an experimental device designed to produce mm-wavelength stimulated Čerenkov radiation. a) the device; b) typical voltage and radiation pulse.
- Figure 17: Fabry-Perot interferometer output. a) calibration (35 GHz source); b) stimulated Čerenkov radiation.

Figure 18: Slab guide resonator configuration for a possible far-infrared device.

Figure 19: The effect of tapering the slab guide thickness. a) the guide; b) the field distribution.

Figure 20: Another possible configuration for short wavelength operation.



CERENKOV MASER

Figure 1.

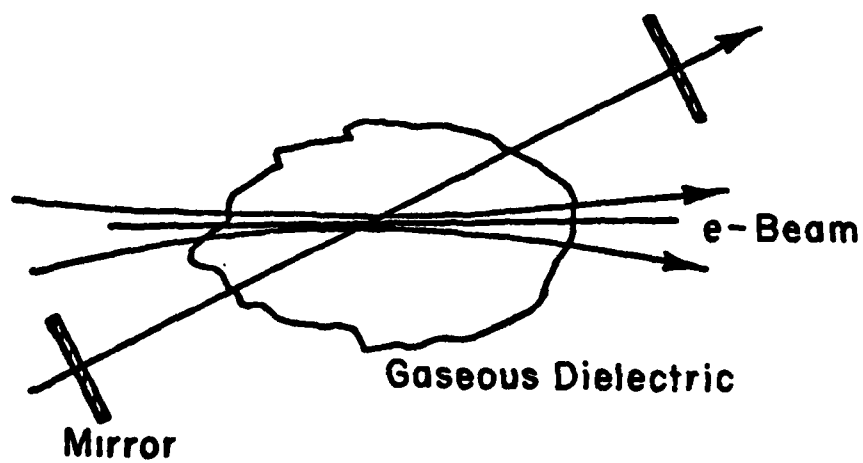
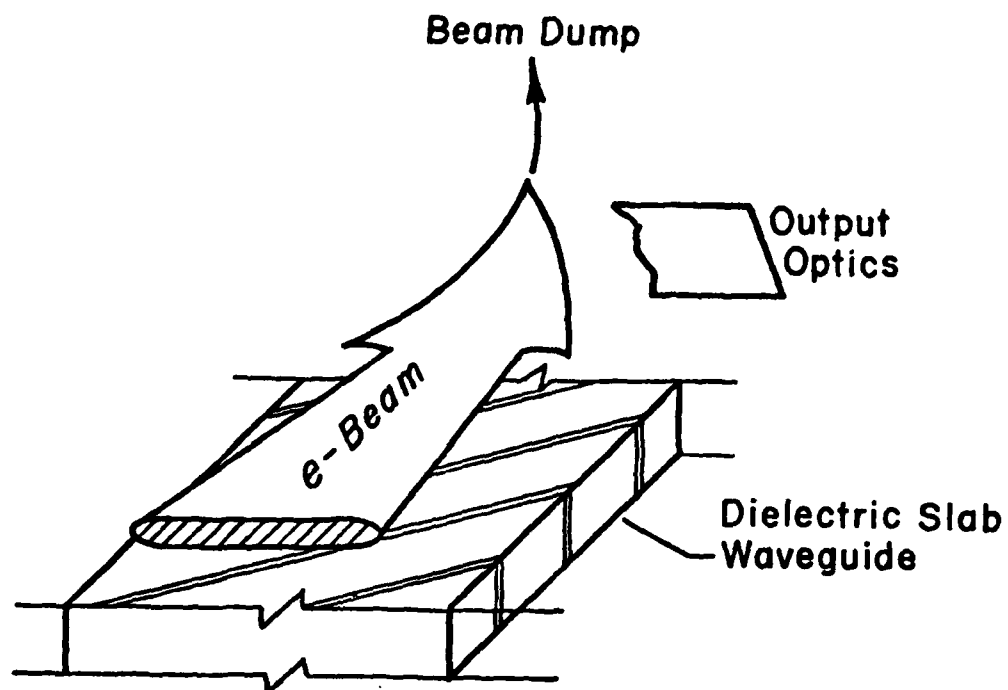


Figure 2. a), b)

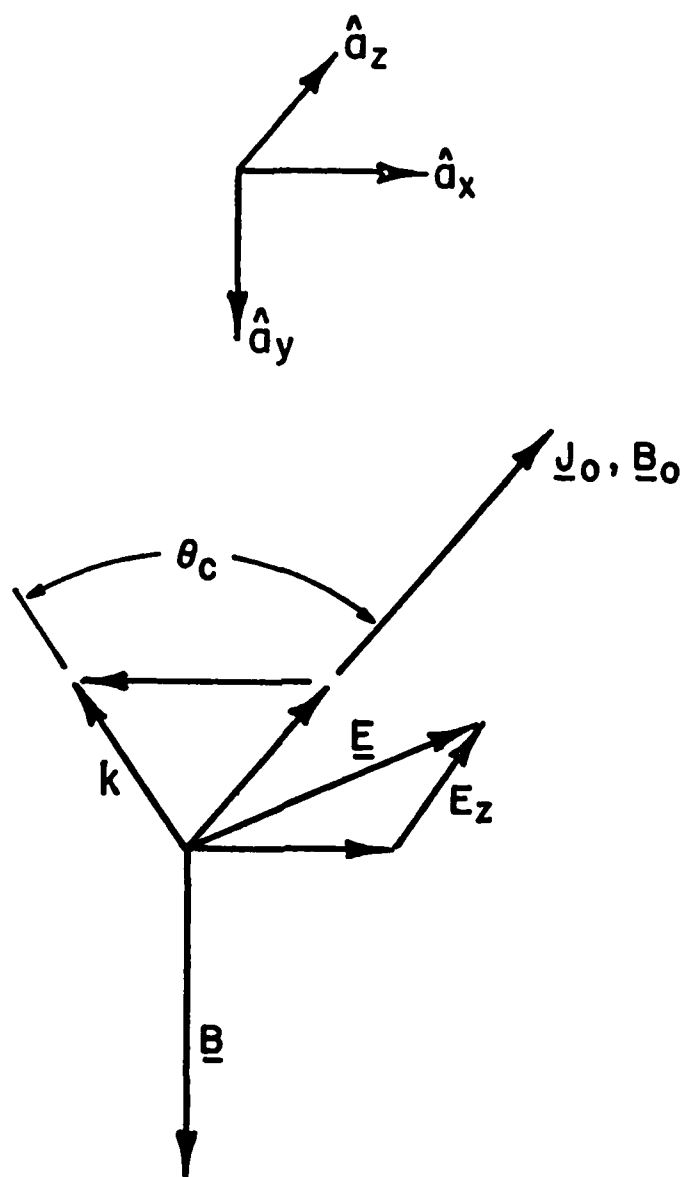


Figure 3.

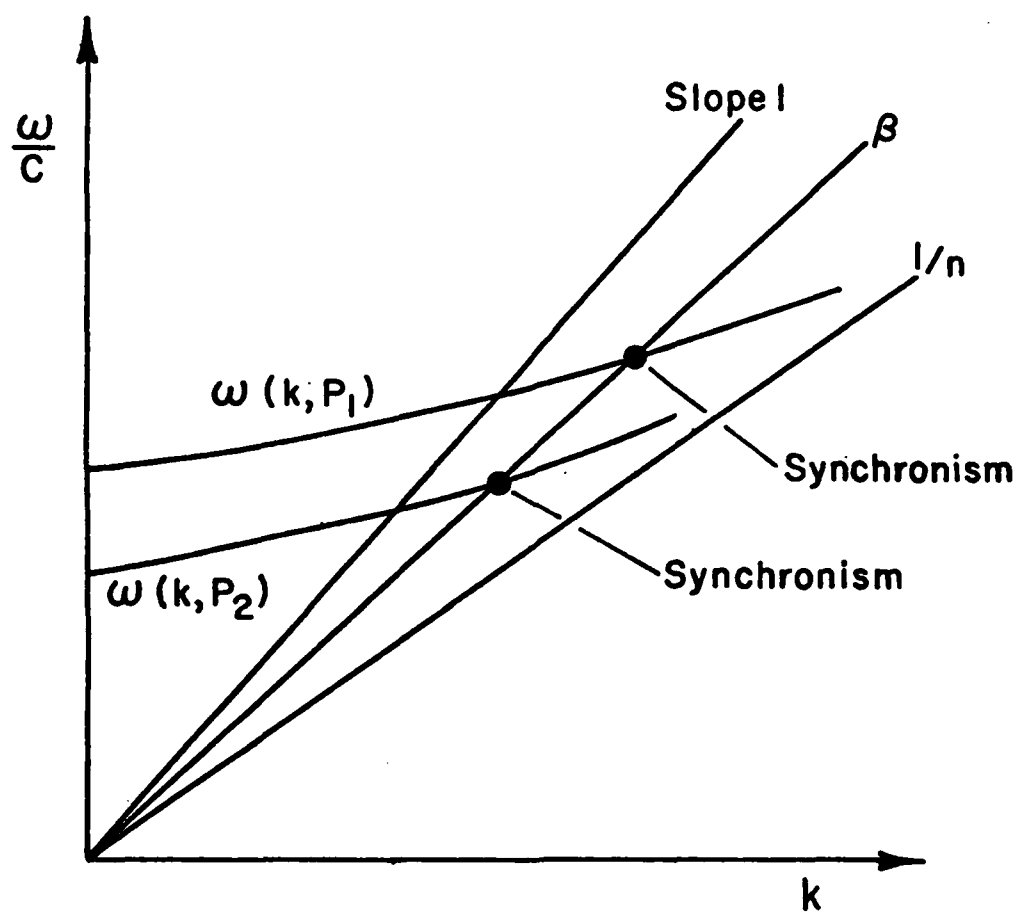


Figure 4.

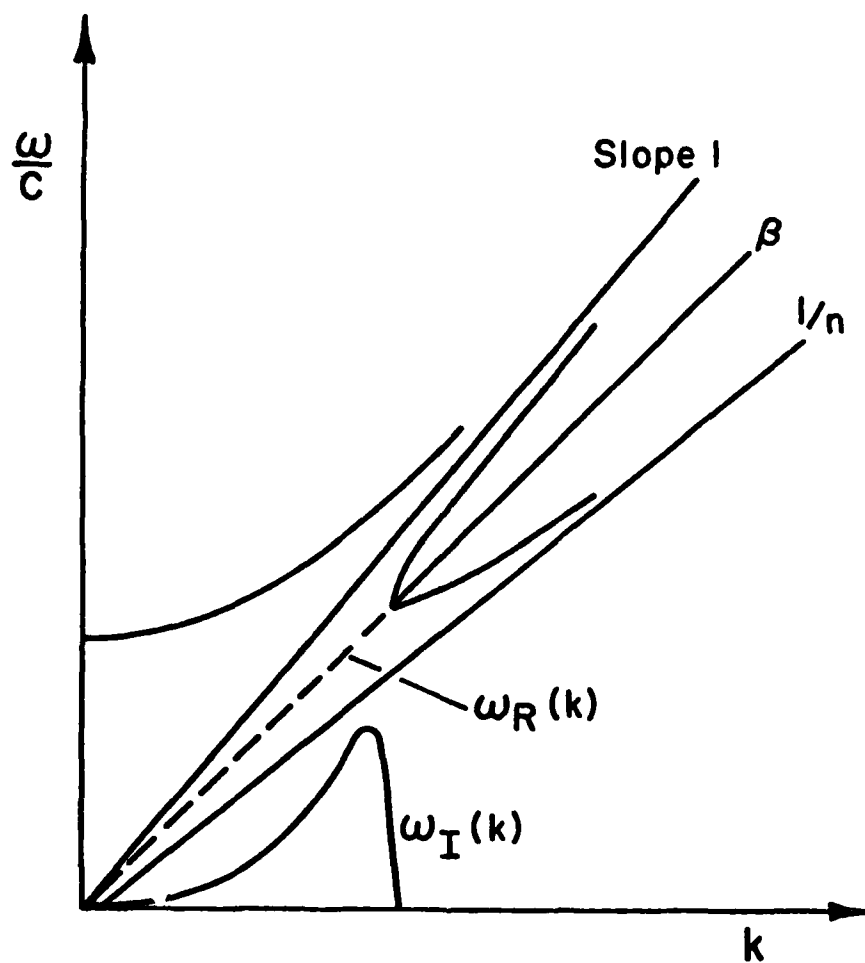


Figure 5.

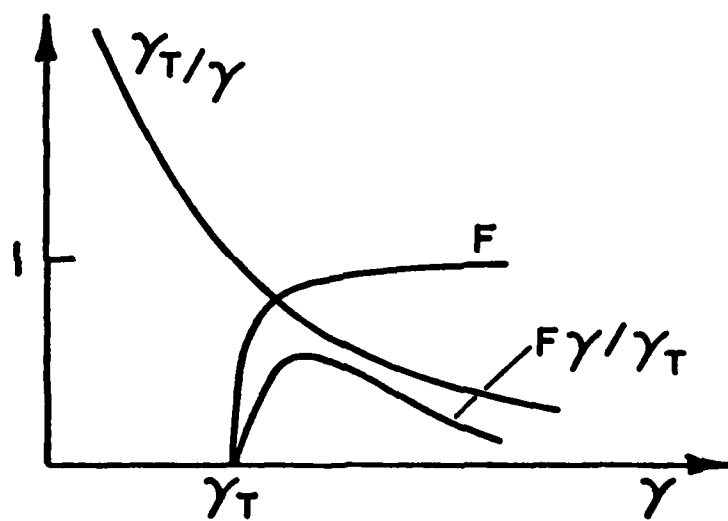
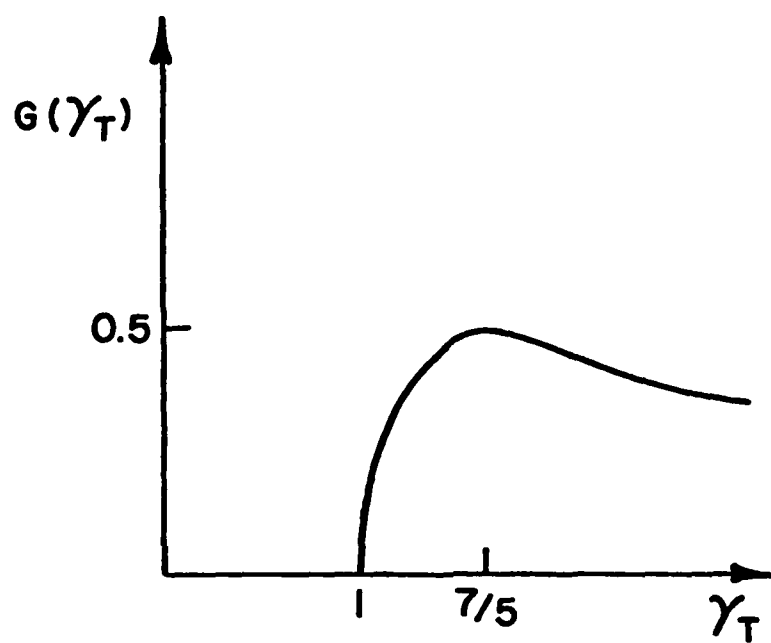


Figure 6. a), b).

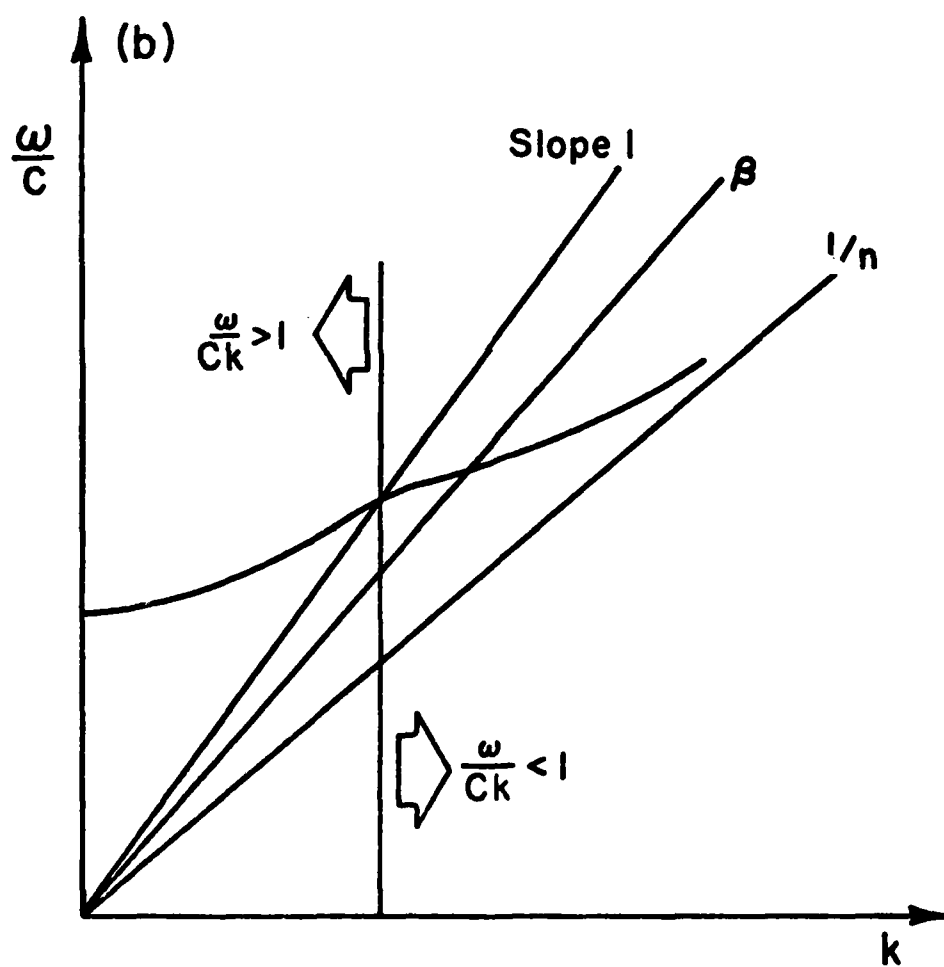
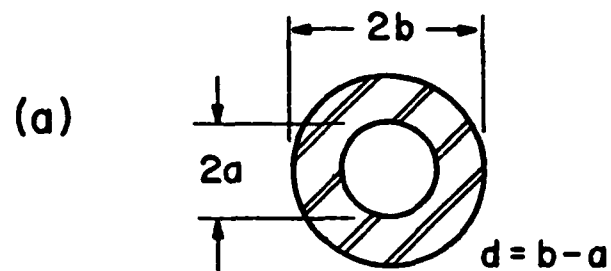


Figure 7.

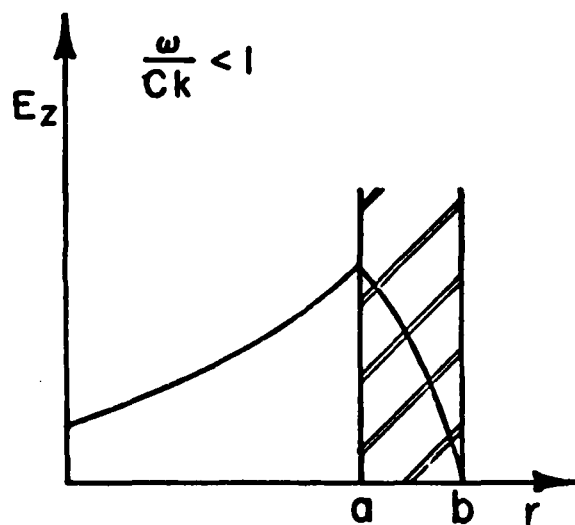
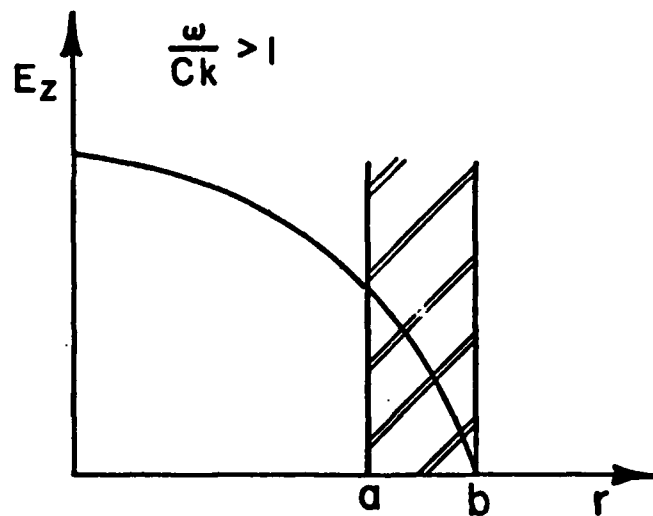


Figure 8. a), b).

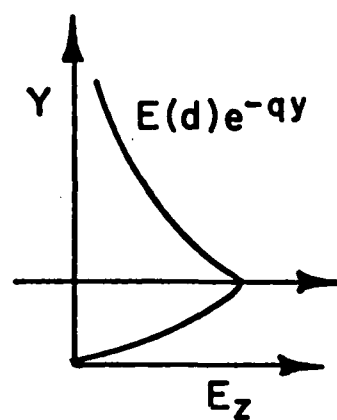
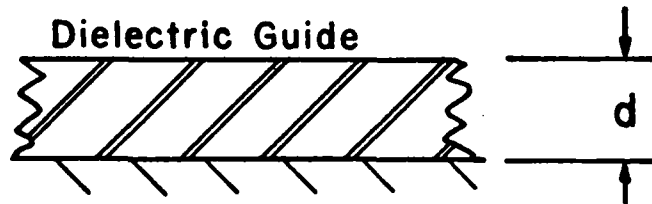


Figure 9.

AD-A122 683

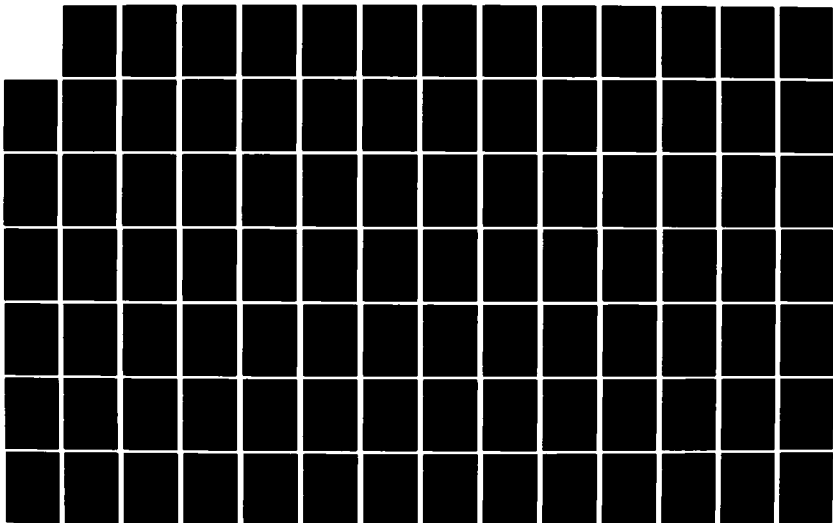
CERENKOV MASER AND CERENKOV LASER DEVICES(U) DARTMOUTH
COLL HANOVER N H DEPT OF PHYSICS AND ASTRONOMY
J E WALSH DEC 82 ARO-16572.3-PH DAAG29-79-C-0203

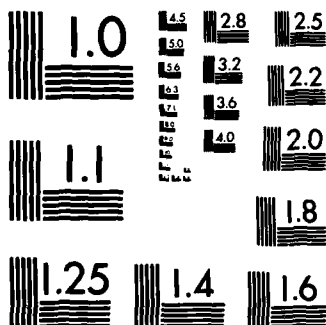
2/3

UNCLASSIFIED

.F/G 20/5

NL





MICROCOPY RESOLUTION TEST CHART
NATIONAL BUREAU OF STANDARDS-1963-A

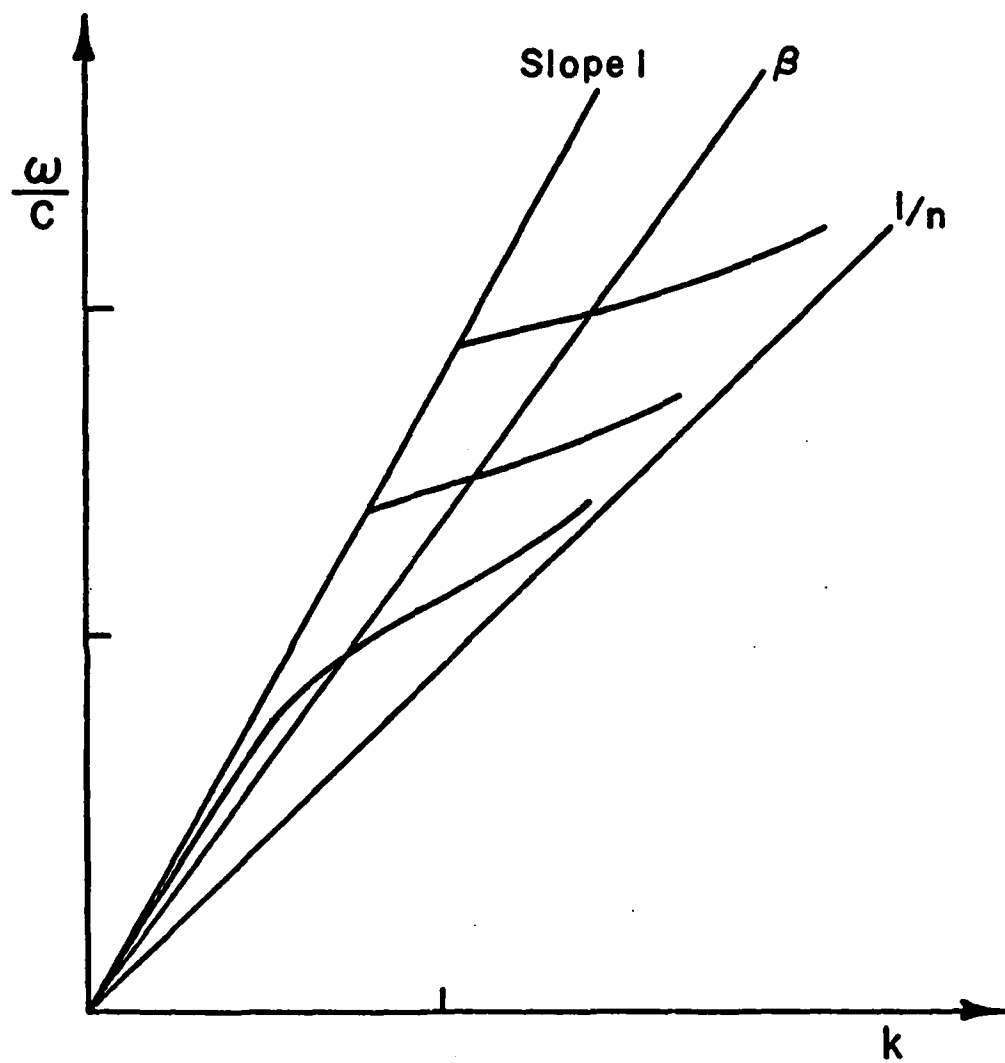


Figure 10.

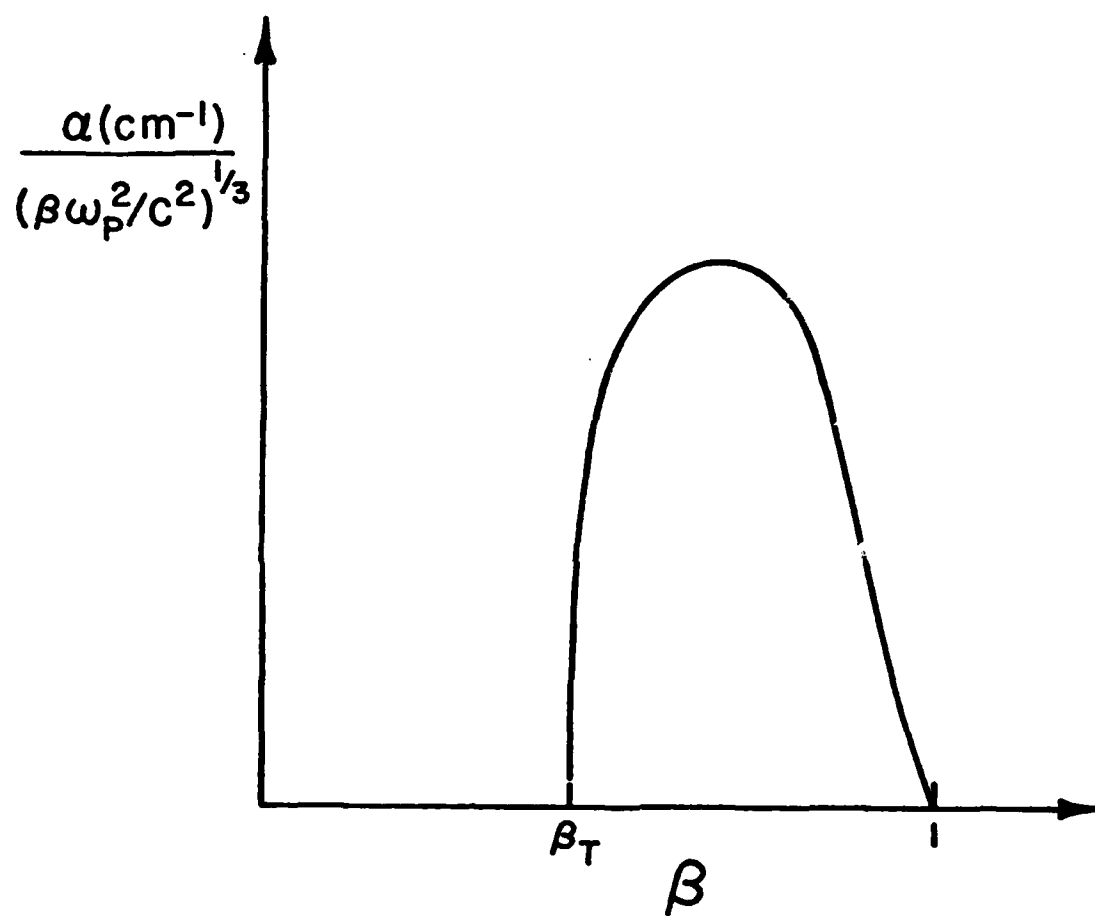


Figure 11.

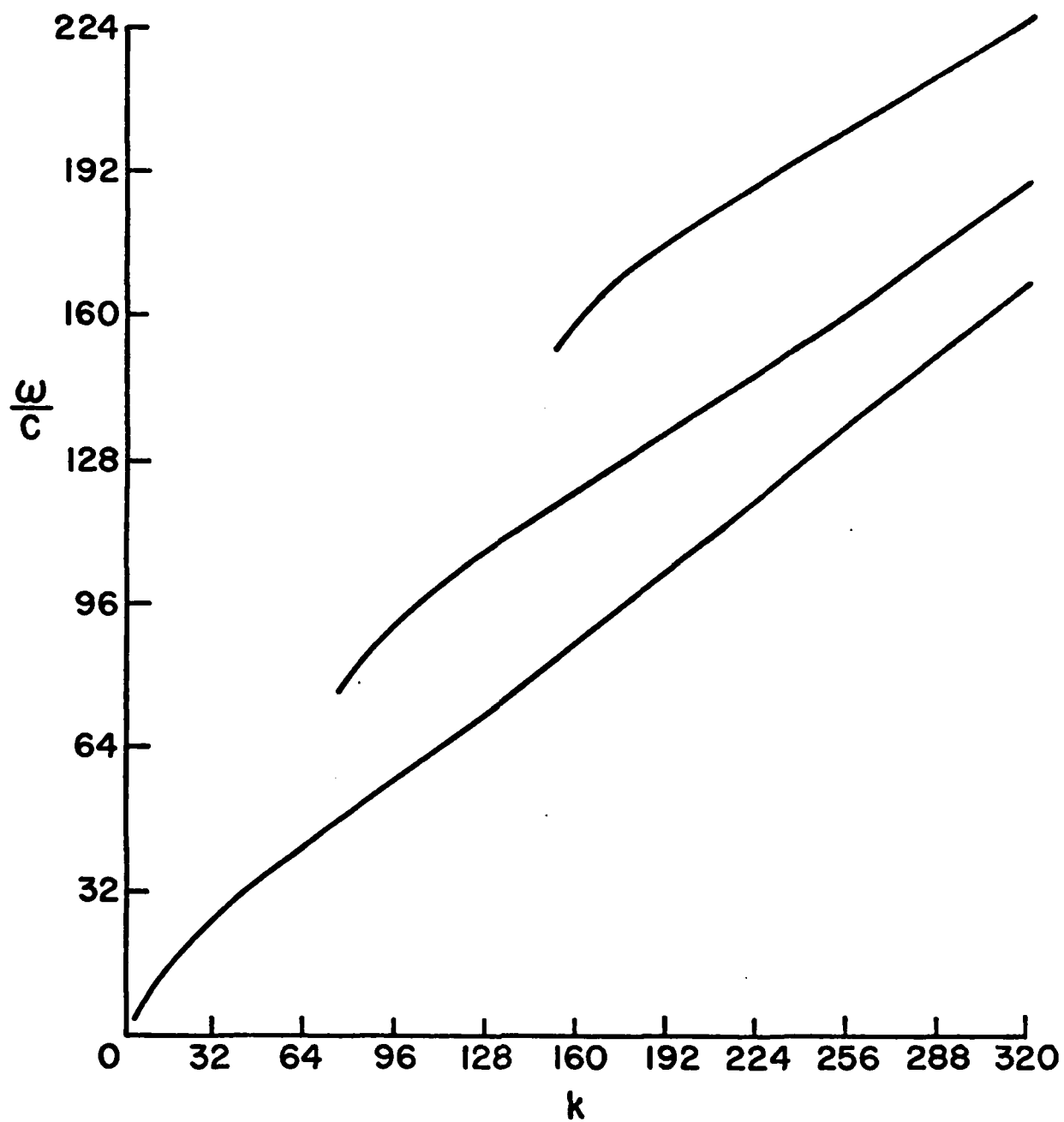


Figure 12. a)

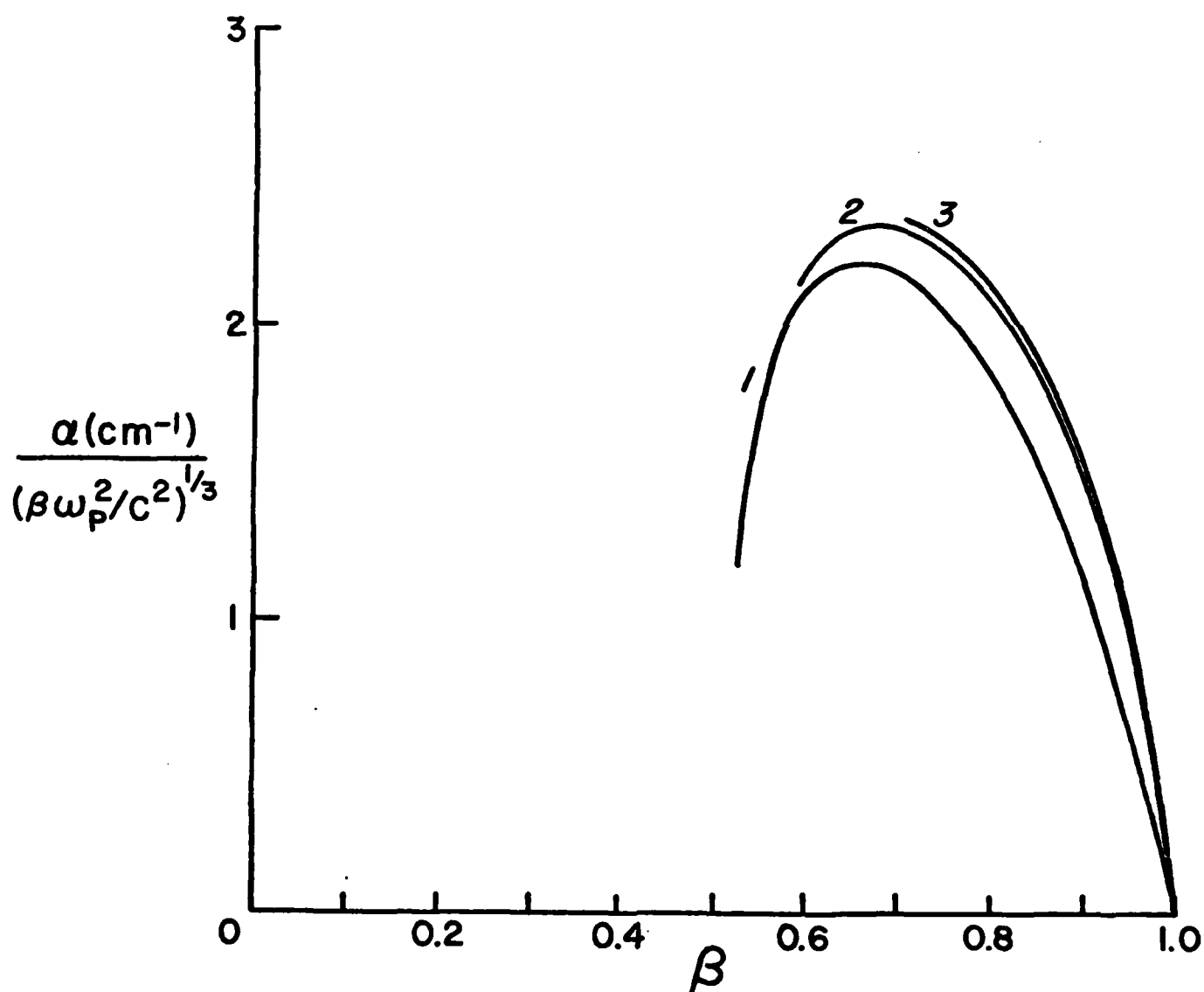


Figure 12. b)

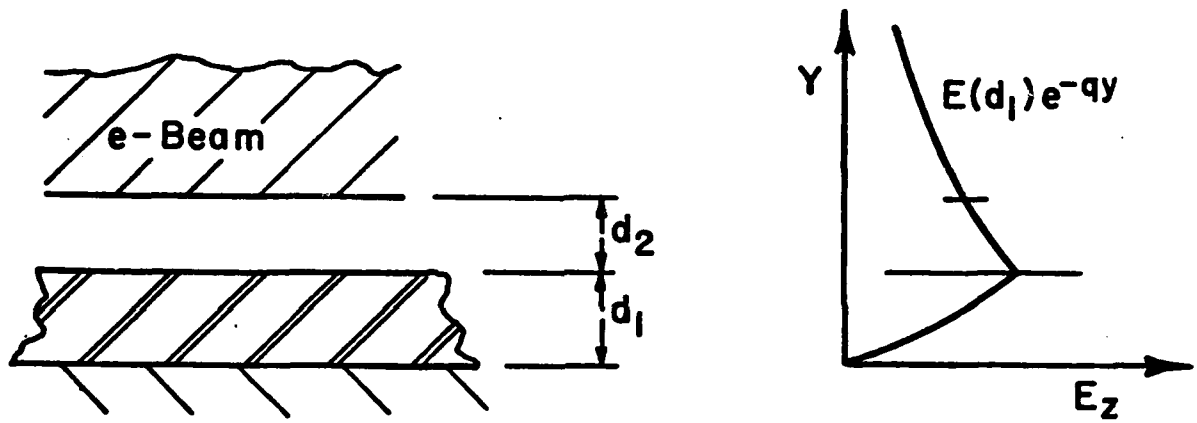


Figure 13.

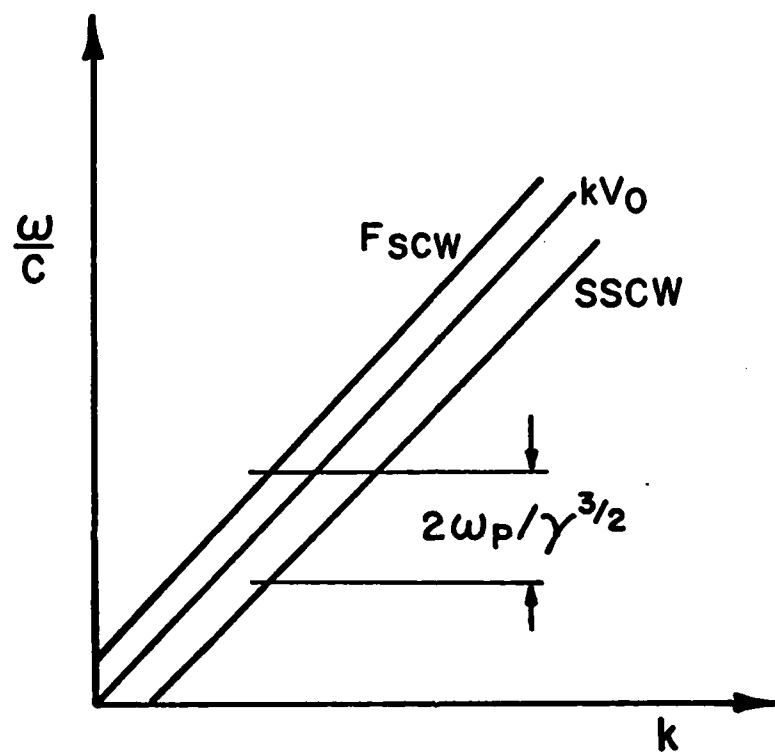


Figure 14. a)

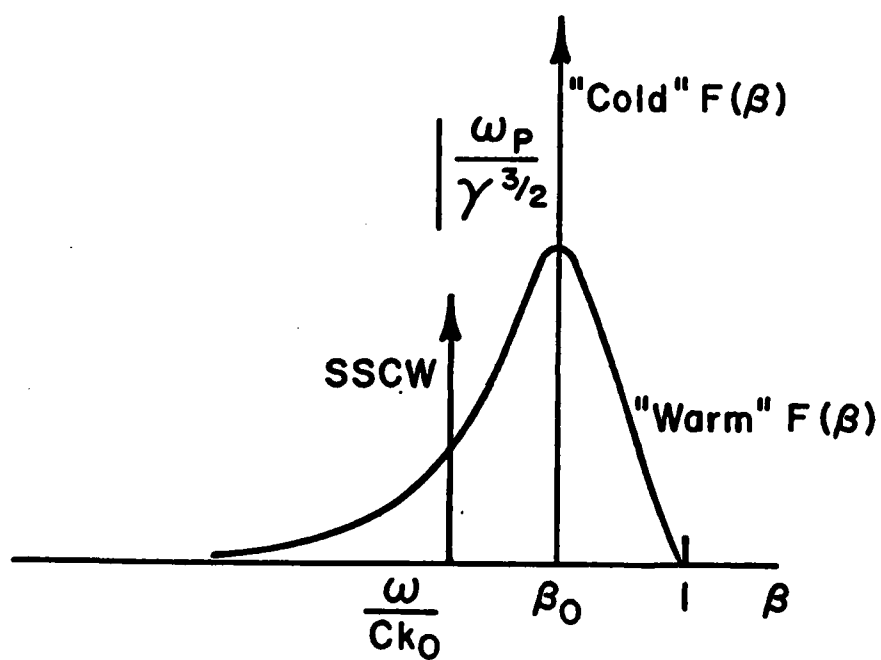


Figure 14. b)

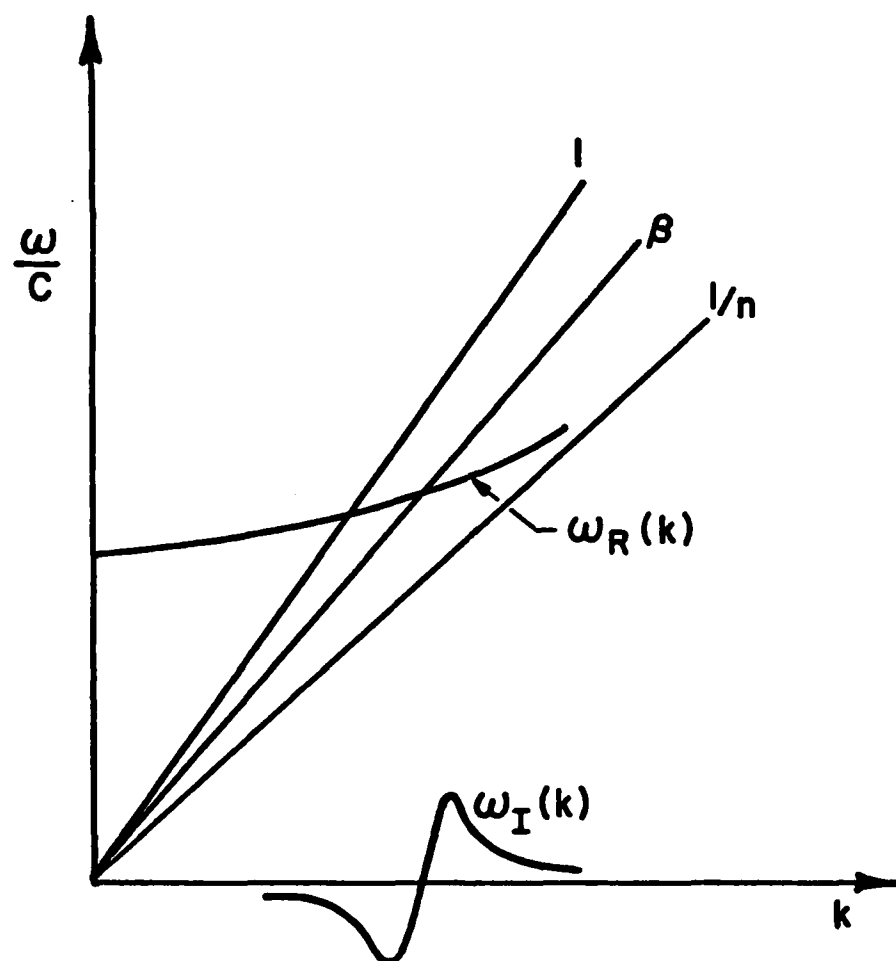


Figure 15.

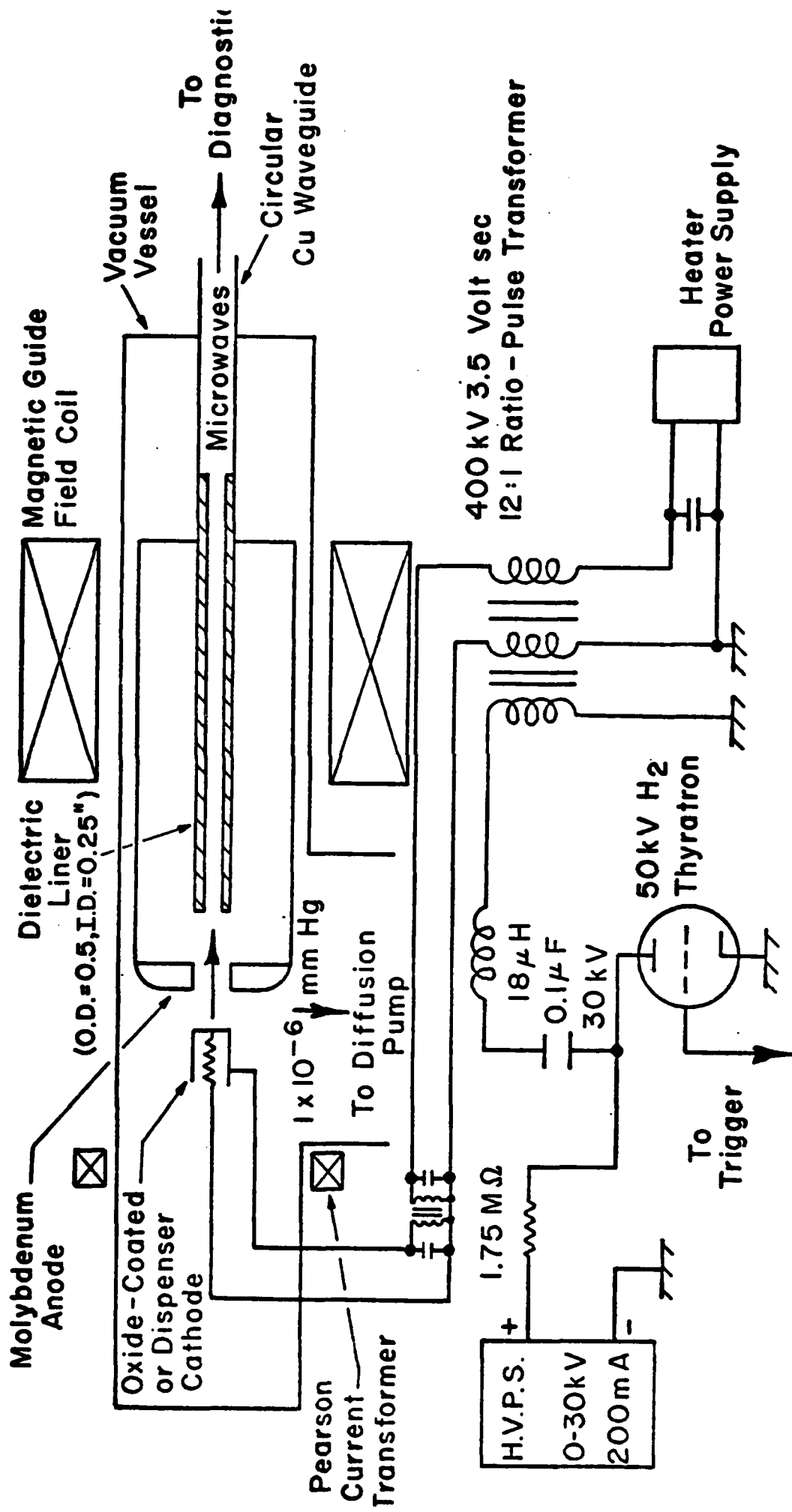


Figure 16. a)

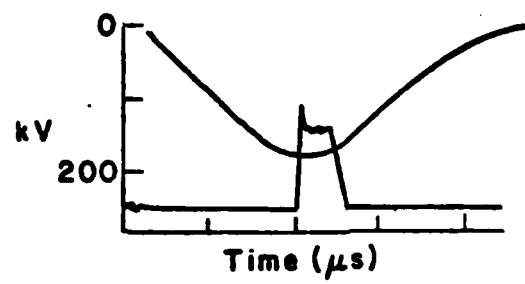
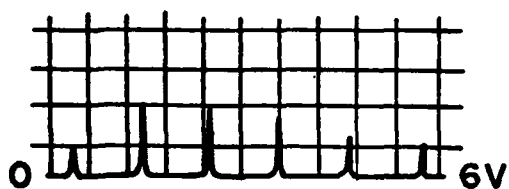


Figure 16. b)

T555 - .2V/cm
k155 μ V Meter - 100mV Range
15 x 18 Mesh
1N53 Detector



0720 30 Aug. 80
35 GHz
.65" ϵ /S DX
1.46" E-S DX
1.38" D-S DX



#5
22 Aug.

#7

Figure 17.

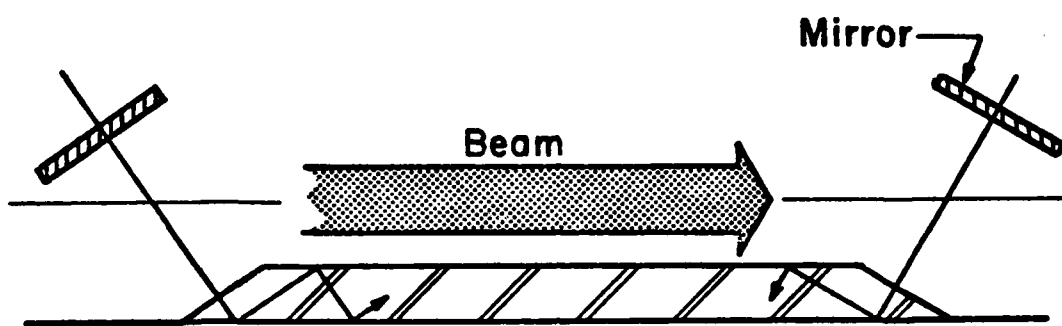


Figure 18.

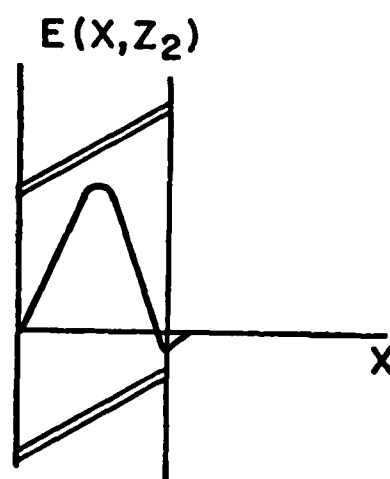
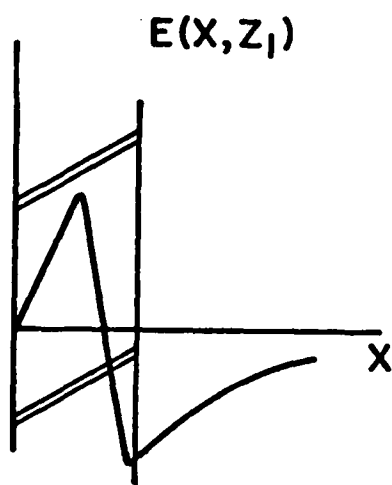
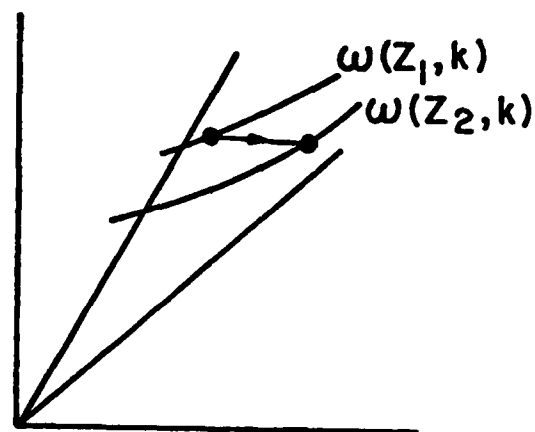
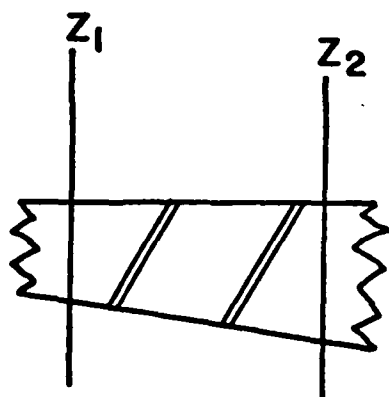


Figure 19.

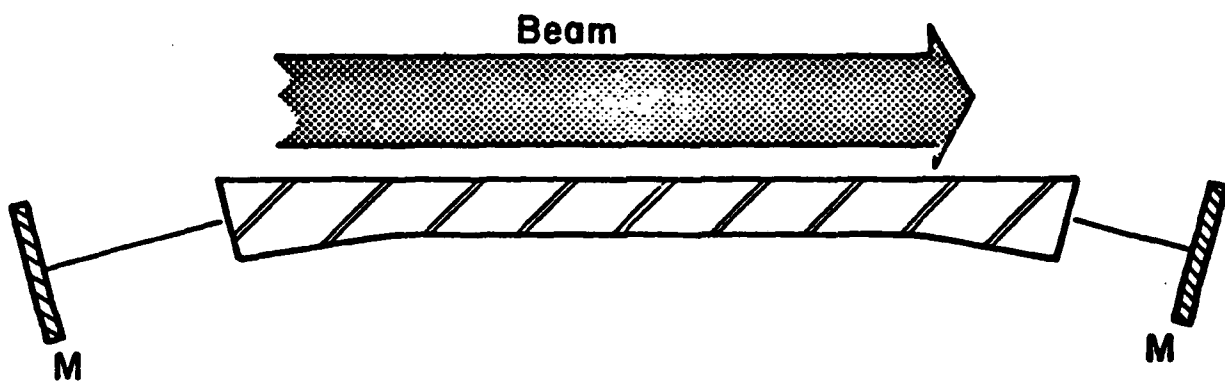


Figure 20.

TUNABLE CERENKOV LASERS*

J.E. Walsh and J.B. Murphy

Department of Physics and Astronomy
Dartmouth College
Hanover, N.H. 03755

Abstract

The concept of a tunable Cerenkov laser is introduced and expressions for the operating wavelength and stimulated emission rate are developed. Emphasis is on the development of criteria which must be met if tunable, far-infrared device operation is to be achieved.

I. INTRODUCTION

A Cerenkov laser consist of a mildly to moderately relativistic electron beam, a dielectric resonator, and output coupling components. One possible configuration of such a device, which is based in part on concepts [1] which have been experimentally demonstrated [2],[3],[4] in the middle- to lower-mm portion of the spectrum, is shown in Fig. 1. In Fig. 1, an electron beam passes over a thin dielectric guide and interacts (primarily) with the axial component of the TM modes of the structure. A bunching of the beam will occur and hence stimulated emission will be produced in those modes which have a phase velocity slightly less than the velocity of the beam. In the example chosen, waves are launched from the slab waveguide by a taper. The cavity is then completed by mirrors. Other configurations would also be potentially useful.

A general result of the analysis given in subsequent sections is that a typical transverse scale length d , wavelength λ and relative beam energy, $\gamma = \epsilon/mc^2$, are related by $\lambda\gamma \sim 2\pi d$. When the scale length is some fraction of a mm, γ in the 2 to 10 range implies device operation in the far-infrared portion of the spectrum. Other devices [5]-[8], particularly those which use a periodic magnetic field pump to couple an electron beam with a radiation field are possible

tunable infra-red sources. In a certain fundamental sense, all electron beam-driven sources are similar, and some very brief comparison of Cerenkov and other coupling schemes will be included in the last section.

Finally, before proceeding to the detailed analysis, it should be pointed out that the notion that Cerenkov radiation could be used as the basis of a practical radiation source is not new [9]. Several groups [10],[11],[12] have studied spontaneous Cerenkov emission and some have used prebunched beams to enhance the otherwise weak spontaneous emission level. In addition, the general idea that stimulated Cerenkov radiation could be used to obtain laser action has been mentioned [13],[14],[15] as a theoretical possibility. The first clear-cut demonstration of the stimulated Cerenkov radiation process does seem to be the work reported in Refs. [2],[3], and [4].

The remainder of this paper is divided into four sections. These deal with: the development of an expression for the linearized gain, a summary of those features of the dielectric slab guide behavior which would be important in Cerenkov laser operation, a discussion of the implications of the results of the preceding two sections for far-infrared device performance, and finally a few brief concluding remarks.

II. THE STIMULATED CERENKOV EMISSION RATE

In this section, an expression for the gain of a Cerenkov Maser will be deduced. The calculation is facilitated by making a number of simplifying assumptions: 1) that the beam is monoenergetic; 2) that the beam density is low enough so that space charge waves may be neglected; and 3) that the gain in a single pass of the resonator is small. Numerical criteria for these will be established and the way in which they limit possible device performance will be discussed in Section IV.

The energy gained ($d\mathcal{E}/dt$) by the fields as the electron beam traverses the resonator may be expressed as:

$$\frac{d\mathcal{E}}{dt} = - \frac{R_e}{2} \int_{\text{beam}} \underline{j} \cdot \underline{E}^* dV \quad (1)$$

where \underline{j} is the modulated current produced on the beam by the fields and the integration covers the volume of the beam. It is most convenient to compute the current with the aid of the linearized Vlasov equation. This may be written in the form:

$$\frac{d\delta f}{dt} = - \underline{\dot{p}} \cdot \nabla_p f_0(p) \quad (2)$$

Appearing in Eq. (2) are δf and f_0 , the perturbed and average components of the beam momentum distribution function. The term \underline{p} is the momentum of an electron. The expression

d/dt on the LHS of Eq. (2) is the total derivative with respect to time, along a zero order orbit (one unperturbed by the fields). If we now assume further that the coupling is in the axial direction and with a traveling wave moving in the positive z direction

$$\underline{E} = \hat{a}_z E_z(x,y) e^{i(kz-\omega t)} \quad (3)$$

we have

$$\delta f = + e E_z \frac{\partial f_o}{\partial p_z} \frac{(1 - e^{i(kv-\omega)z/v})}{i(kv-\omega)} e^{i(kz-\omega t)} \quad (4)$$

This form of the solution of Eq. (2) satisfies the boundary condition $\delta f(z,p,t) \Big|_{z=0} = 0$, i.e., the beam enters the resonator region unmodulated. The current is given by:

$$j = - ne \int v_z \delta f dp \quad (5)$$

where n is the beam density.

The results of Eqs. (4) and (5) may be substituted into Eq. (1) and an expression for the rate at which energy is added to the resonator obtained. It is also convenient at this point to perform the axial portion of the spatial integral. When this is done, Eq. (1) becomes:

$$\frac{d\epsilon}{dt} = \frac{e^2}{4} \int_{\text{beam}} dA \ n |E_z|^2 L^2 \int dp_z \frac{\partial f_o}{\partial p_z} \frac{\sin^2}{\theta^2} \quad (6)$$

where

$$\theta = (kv - \omega) L/2v \quad (7)$$

is the relative phase change "seen" by a beam electron traversing a resonator of length L . Equation (6) may be further reduced by re-writing the momentum integral with the aid of the transformation:

$$\frac{\partial}{\partial p_z} = \frac{dv_z}{dp_z} \frac{d\theta}{dv_z} \frac{\partial}{\partial \theta} \quad (8)$$

Introducing the beam distribution in phase coordinates $F(\theta)$ and performing an integration by parts. Eq. (6) becomes:

$$\frac{d\mathcal{E}}{dt} = -\frac{e^2}{8m} \int_{\text{beam}} dA \, n |E_z|^2 L^3 \omega \left[\frac{d\theta F(\theta)}{\gamma^3(\theta) \beta^2(\theta)} \frac{\partial}{\partial \theta} \frac{\sin^2 \theta}{\theta^2} \right] \quad (9)$$

We can now make use of our assumption that the beam distribution is monoenergetic and perform the phase integral. Before making this straightforward substitution, however, it will also be useful to introduce some further definitions.

Let

$$\bar{n} |E_z|^2 A_b = \int dA \, n |E_z|^2 \quad (10)$$

where A_b is the beam area and \bar{n} is an effective, wavelength-dependent, density. The normalizing field strength $|E_z|^2$ is chosen as some convenient point (e.g., the surface of the dielectric in the present case).

Now expressing the gain in terms of a reciprocal quality factor Q_b^{-1} defined by:

$$\frac{1}{Q_b} \equiv - \frac{1}{\omega \mathcal{E}} \frac{d\mathcal{E}}{dt} , \quad (11)$$

we have

$$\frac{1}{Q_b} = \frac{1}{(\beta_o \gamma_o)^3} \cdot \frac{I_b}{I_o} \cdot \frac{\bar{n}}{n_o} \cdot \frac{L^3 |E_z|^2}{8 \pi \mathcal{E}} G'(\theta) \quad (12a)$$

where

$$G'(\theta) = \frac{\partial}{\partial \theta} \frac{\sin^2 \theta}{\theta^2} \quad (12b)$$

is the derivative of the diffraction lineshape. In writing Eq. (12) we have also identified the total beam current,

$I_b = -n_o e c \beta_o A_b$, and an effective current, $I_o = e c / r_o$ ($r_o = e^2 / m c^2$) which appears naturally in the problem.

A sketch of Q_b^{-1} vs θ is shown in Fig. 2. Since $Q_b^{-1} < 0$ when $0 < \theta < \pi$, the system will have gain in this region. When $|Q_b|$ becomes less than the Q of the resonator, oscillation threshold is reached. Also shown in Fig. 2 is the electron beam velocity distribution which has been plotted as a function of the relative phase. A beam with relative phase spread

$$(\Delta \theta)_b < \pi \quad (13)$$

may be regarded as monoenergetic. All the electrons in such a

beam can contribute to gain. This is the condition illustrated in Fig. 2. An alternative and more useful expression for this condition may be obtained when Eq. (7) is used together with Eq. (13) to relate the beam energy spread $\delta\gamma$ to the wavelength for which inequality (13) is just satisfied. This is:

$$\lambda > L \frac{\delta\gamma}{(\beta\gamma)^3} \quad (14)$$

Discussion of the magnitude of Ω_b^{-1} and the limiting wavelength will be given after a particular resonator is introduced.

III. THE SLAB WAVEGUIDE RESONATOR.

The dielectric slab waveguide [16] is one possible choice of the wave-supporting structure for a Cerenkov laser. This choice may not offer the highest possible gain, but it would allow relatively straightforward independent adjustment of the beam and resonator axes. Thus it is an experimentally interesting choice, and we will consider it in some detail.

The basic geometry, shown in Fig. 3, consists of a beam of thickness b , at a distance d above the surface of the guide. We assume that propagation occurs in the z direction and that all quantities are uniform in y , the direction perpendicular to both the normal-to-the-guide surface and the direction of propagation. Later, in order to facilitate numerical evaluation, we will assume that the beam and mode widths in the y direction are approximately b and a_m respectively.

The electric fields associated with the TM modes of the structure shown in Fig. 3 are:

$$E_z = E_{z0} e^{-qx} e^{i(kz - \omega t)} \quad (15a)$$

$$E_x = -\frac{ik}{q^2} \frac{\partial E_z}{\partial x} \quad (15b)$$

in the region $x > a$. In the region $x < a$

$$E_z = E_{z1} \sin px \quad (16a)$$

and

$$E_x = \frac{ik}{p^2} \frac{\partial E_z}{\partial x} \quad (16b)$$

The terms:

$$p^2 = \frac{\omega^2 \epsilon}{c^2} - k^2, \quad (17a)$$

and

$$q^2 = k^2 - \frac{\omega^2}{c^2} \quad (17b)$$

are the squares of the transverse wavenumber in the dielectric and in the vacuum regions respectively. The relative dielectric constant of the guide materials is denoted by ϵ .

The fields, together with the boundary conditions, can be used to obtain a dispersion function:

$$D(k, \omega) = p \frac{\tan pa}{\epsilon} - q \quad (18)$$

whose roots $D = 0$ determine the relation between ω and k for the TM modes of the structure. Typical results, plotted in units of $a/\lambda = \omega a/2\pi c$ vs $a/\lambda_g = ka/2\pi$ are shown in Fig. 4. The lowest mode, TM_{01} , has no lower frequency cutoff while all higher order modes have a long wavelength cutoff given by:

$$\lambda_{co} = 2a \sqrt{\epsilon - 1} \quad (19)$$

The trajectories a/λ vs a/λ_g lie in the region of the plane bounded by the light line (slope 1) and the light line in the dielectric material, the line of slope $1/\epsilon$ ($\epsilon = n$) on Fig. 4. Also shown on Fig. 4 is a line whose slope is equal to β , the velocity of a beam electron relative to the speed of light. When $\beta > 1/n$ the beam satisfies the Cerenkov threshold condition:

$$\gamma > \gamma_T \quad (20a)$$

where

$$\gamma_T^2 = \epsilon/(1-\epsilon) \quad (20b)$$

$$= 1/(1 - \beta_T^2) \quad (20c)$$

and

$$\beta_T^2 = 1/\epsilon \quad (20d)$$

Velocity synchronism is defined as that point where the phase velocity of one of the guide modes is equal to β .

Examination of Eq. (18) indicates that, for a given ϵ , the location of the dispersion curves is a function of the guide thickness alone. Thus we arrive at a basic scaling of a Cerenkov device of this type: $\lambda \sim a$. As the guide thickness is decreased, the wavelength at which phase velocity synchronism occurs decreases as well.

We can now also obtain an expression for \bar{n}/n_0 , the effective beam density defined in Section II. If we imagine

that we vary the beam velocity from $\beta = 1$ down to $\beta = \beta_T$ we sweep the synchronous point along the dispersion curve. Thus the output is voltage tunable. However, at the synchronous point the transverse wavenumber in the vacuum becomes:

$$q = k/\gamma \quad (21a)$$

or, since $\omega = ck\beta$ at synchronism,

$$q = 2\pi/\lambda\beta\gamma \quad (21b)$$

The field decreases more rapidly in the x direction as the beam velocity decreases. The coupling becomes weaker. The effective beam density for the flat slab resonator is thus given by:

$$\frac{\bar{n}}{n_0} = e^{-2qd} \frac{(1-e^{-2qb})}{2qb} \quad (22)$$

We have assumed in deriving Eq. (22) that the actual density distribution of the beam is approximately rectangular in the x direction. The first factor in Eq. (22) is a decoupling, and the second factor represents the fraction of the beam seen by the field.

The fields given by Eqs. (15) and (16) may, together with the usual definition of energy, be used to obtain an expression for the energy stored, \mathcal{E} , and hence also for $|E_{z0}|^2$ in terms of \mathcal{E} . Straightforward calculation leads to:

$$\frac{L^3 |E_{zo}|^2}{8\pi \xi} = \frac{L^2}{aa_m} \frac{(1-\gamma_T^2/\gamma^2)}{(\beta\gamma)^2} \frac{ka/\gamma}{1 + \frac{ka}{\gamma}(1+\frac{\epsilon}{\gamma^2})} \quad (23)$$

We now have in hand all the expressions needed in order to estimate the gain for a specific choice of experimental parameters.

IV. DISCUSSION

The results of the two preceding sections may be used to infer some general features of the gain of a Cerenkov laser and hence also to make estimates of the parameters required to achieve oscillation threshold at a given wavelength. The full expression for the relative gain of a slab guide Cerenkov device is:

$$\frac{1}{Q_b} = \frac{1}{(\beta\gamma)^5} \frac{L^2}{aa_m} \frac{I}{I_0} \frac{\bar{n}}{n_0} \frac{(1-\gamma_T^2/\gamma^2)ka/\gamma}{1 + \frac{ka}{\gamma}(\frac{\epsilon}{\gamma^2}+1)} G'(\theta) \quad (24)$$

Shown in Fig. 5 is a sketch of the TM_{02} dispersion curve together with a sketch of the general behavior of $Q_b^{-1}(\pi/2)$. The latter is plotted vs γ^{-1} and is displayed in a way that emphasizes how the gain behaves as the beam velocity is varied between $\beta = 1$ and $\beta = \beta_T$. Near the light line the gain is small and the behavior is dominated by the $(\beta\gamma)^{-5}$ term. As β moves away from the light line the gain increases until it reaches a maximum determined by the exponential factors in \bar{n}/n_0 . Further decreases in β results in a rapid decreases of Q_b as $\beta \rightarrow \beta_T$. Because of the $(\beta\gamma)^{-5}$ term the gain will peak when the arguments of the exponentials which appear in \bar{n}/n_0 are somewhat greater than unity.

It is also convenient at this point to mention the effect of finite energy spread in the electron beam. The gain expression displayed in Eq. (24) holds when the beam energy spread is small enough to allow the bulk of the beam distribution to fall within one loop of $G'(\theta)$. When this is

not the case some beam electrons hinder wave growth. In order to understand the effect of this on the gain it is easiest to consider the gain expression when the integration by parts on P (or θ) is not performed, and $G(\theta)$ can be regarded as narrow compared to $F(\theta)$. The gain is now proportional to $F'(\theta)$ (or $F'(P)$). Furthermore, the Jacobian ($dP/d\theta$) will no longer appear and hence we lose a factor of ω . Thus in the warm beam limit:

$$Q_b^{-1} \sim \omega^{-1} \quad (25)$$

and gain will decrease with decreasing wavelength.

Holding all factors save $\beta\gamma$ constant, a relative maximum in Eq. (24) occurs when

$$\lambda \approx \frac{2\pi d}{3\beta\gamma} \quad (26)$$

We anticipate the use of modest $\beta\gamma$ and thus we expect the cold-warm transition wavelength defined by Eq. (14) will be longer than λ determined by Eq. (26). If this is the case, the gain will reach a maximum at a wavelength longer than that at the maximum for a cold beam. When this condition applies, the general behavior is shown by the wavy line on Q_b^{-1} in Fig. 5.

In order to make a quantitative estimate of the magnitude of Q_b^{-1} we make further specific choices. We assume that the warm-cold transition wavelength is about twice the wavelength given by Eq. (26) and that we will examine the possibility of operating at the still longer wavelength:

$$\lambda = \frac{2\pi b}{\beta\gamma} \quad (27)$$

This last choice is equivalent to setting $2qb = 2$ and hence to assuming that a transverse scale length adequate for the maintenance of good coupling is assured. An expression for the size of Q_b^{-1} at any point then takes the following much simpler form:

$$\left. \frac{1}{Q_b} \right|_{\beta\gamma = \frac{2\pi b}{\lambda}} = .54 \left(\frac{\lambda}{2\pi b} \right)^5 \frac{L^2}{a_m^2} \frac{I}{I_0} \frac{(1-e^{-2})}{2} e^{-d/b} \quad (28)$$

The factor, .54, arises from setting $G'(\theta) = G'(\theta)_{\max}$. In addition to the desired operating wavelength, variables remaining in Eq. (28) are those pertaining to the production, focussing and guiding of the electron beam. Before addressing these, however, it will be convenient to briefly examine cavity and output coupling losses. We will thereby establish the approximate magnitude of Q_b^{-1} needed for threshold.

We assume that two losses predominate; the first is absorption in the guide material, and the second is the output coupling loss. The latter, expresses as a loading Q_L , is given approximately by:

$$\frac{1}{Q_L} = \frac{\lambda}{2\pi L} \frac{(1-\rho)}{\rho} \quad (29)$$

where ρ is a reflection coefficient. If we assume that we have no interest in cavities with L less than 10 cm, nor in

wavelengths greater than 1 mm, relatively modest ρ will place (Q_L^{-1}) in the 10^{-4} range.

The general expression for the energy lost in the dielectric takes the form:

$$\frac{d\mathcal{E}_D}{dt} = \frac{\omega \epsilon''}{8\pi} \int_{\text{diel.}} |E|^2 dv \quad (30)$$

The integral can be performed with the aid of expressions developed in Section II. Completing this and defining a dielectric quality factor Q_D we have:

$$\frac{1}{Q_D} = \frac{2\alpha b}{\sqrt{\epsilon}} \left(\frac{\lambda}{2\pi b} \right)^3 \gamma_T^2 \quad (31)$$

In expressing Q_D^{-1} we have also substituted for $\beta\gamma$ where appropriate, and denoted the dielectric absorption coefficient as $\alpha(\text{cm}^{-1})$.

Since losses in the submm and FIR regions are not necessarily small, we will use Eq. (31) to establish a condition for threshold:

$$\frac{.54\sqrt{\epsilon}}{\alpha a_m \gamma_T^2} \left(\frac{\lambda L}{2\pi b^2} \right)^2 \cdot \frac{I}{I_0} \frac{(1-e^{-2})}{2} e^{-d/b} > 1 \quad (32)$$

The factors involving $(\lambda L/\pi b^2)^2$ and I/I_0 will show the largest variation and hence they will be singled out for scrutiny. We assume, somewhat arbitrarily, that we will be most concerned with devices which are based on beam sources with

an available current between 1.75 ma and 17.5 A, and in the wavelength range 100μ to 1 mm. In the range of the former variable the ratio I/I_0 varies from 10^{-7} to 10^{-3} .

The magnitude of the term $(\lambda L/2\pi b^2)^2$ can be easily inferred if we re-express it in terms of the value of $\beta\gamma$ required by coupling. It is:

$$\left(\frac{\lambda L}{2\pi b^2}\right)^2 = \frac{L}{\beta\gamma b}$$

Electron beam focussing such that $b \sim 1\text{--}1.5$ mm is typical for beams associated with microwave tubes, and hence values of $L/\beta\gamma b$ in the $10^2\text{--}10^3$ range are quite realistic. This is in itself sufficient to achieve threshold within our chosen current range. Some further help in attaining threshold will be contributed by the terms in Eq. (32) which have a smaller variation. The value of a_m will be generally larger than, but comparable to, b and $\alpha \lesssim 1$ at a wavelength of 100μ can be obtained in several relatively low index materials [17]. At longer wavelengths ($\lambda \sim 1$ mm) values of α as low as 2×10^{-2} are realistic and the overall contribution to threshold by the material-related terms in Eq. (32) could be as large as 10^2 .

The beam energy collimation required if the beam is to be regarded as cold was given first in Section II. Returning now to Eq. (14) we see that $\lambda = 100\mu$ and $L = 10$ cm would require $\delta\gamma/\beta\gamma \lesssim 10^{-3}$ if $\beta\gamma \lesssim 1$. If $\beta\gamma$ rises to about three, the requirement drops to $\delta\gamma/\beta\gamma \lesssim 10^{-2}$. The first is an excellent but achievable value and the second is quite

straightforward. Beam velocity spread will not be a major obstacle to operation in the $100\mu - 1$ mm wavelength range.

Finally, it is possible to make a rough estimate of the efficiency. Since a change of the beam energy, which is sufficient to move the centroid out of the gain region in Fig. 2, represents an approximate non-linear limit, we have

$$\frac{\delta\gamma}{\gamma-1} \approx \frac{(\beta\gamma)^3}{\gamma-1} \frac{\lambda}{L} \quad (33)$$

or
$$\approx (\gamma + 1) (\beta\gamma)^2 \frac{\lambda}{L}$$

as the approximate efficiency.

V. CONCLUSIONS

The general conclusion which can be drawn from the preceding analysis is that it should be possible to construct tunable Cerenkov lasers in the far-infrared portion of the spectrum. These devices are beam-voltage-tunable and they could in principle have a reasonable efficiency. Moderate- to high-power output can probably be obtained. Like other free-electron lasers, decrease of the operating wavelength is achieved by increasing beam energy. However, the energy wavelength scaling $\lambda\beta\gamma \sim \text{const.}$ is such that the energy required to obtain far-infrared operation will be less than that required in a magnetic wiggler-coupled device. Hence Cerenkov devices may be relatively compact.

ACKNOWLEDGMENTS

The authors wish to acknowledge the support of the Army Research Office, Contract # DAAG-20-79-C-0203.

REFERENCES

- [1] J.E. Walsh, "Cerenkov and Cerenkov-Raman radiation sources", in Free Electron Generators of Coherent Radiation (Physics of Quantum Electronics), edited by S. Jacobs, H. Pilloff, M. Sargent, M. Scully and R. Spitzer (Addison-Wesley, Reading, MA 1980), vol. 5, pp. 255-322.
- [2] J.E. Walsh, T.C. Marshall, and S.P. Schlesinger, "Generation of coherent Cerenkov radiation with an intense relativistic electron beam", *Phys. Fluids*, vol. 20, pp. 709-710, 1977.
- [3] J.E. Walsh, T.C. Marshall, M.R. Mross, and S.P. Schlesinger, "Relativistic electron-beam-generated coherent submillimeter-wavelength Cerenkov radiation", *I.E.E.E. Trans. MTT-25*, pp. 561-563, 1977.
- [4] K.L. Felch, K.O. Busby, R.W. Layman, D. Kapilow, and J.E. Walsh, "Cerenkov radiation in dielectric-lined waveguides", *Appl. Phys. Lett.*, vol. 38, pp. 601-603, 1981.
- [5] R.M. Gilgenbach, T.C. Marshall, and S.P. Schlesinger, "Spectral properties of stimulated Raman radiation from an intense relativistic electron beam", *Phys. Fluids*, vol. 22, pp. 971-977, 1979.
- [6] D.A.G. Deacon, L.R. Elias, J.M.J. Madey, G.J. Ramian, H.A. Schwettman, and T.I. Smith, "First operation of a free electron laser", *Phys. Rev. Lett.*, vol. 38, pp. 892-894, 1977.
- [7] G. Providakes and J. Nation, "Excitation of the slow cyclotron and space charge waves in a relativistic electron beam", *J. Appl. Phys.*, vol. 50, pp. 3026-3030, 1979.
- [8] P. Sprangle, Cha-Mei Tang, and W.M. Manheimer, "Nonlinear analysis of a free electron laser", *Phys. Rev.*, vol. A21, pp. 302-311, 1980.
- [9] Many early references are contained in ref. [1].
- [10] P. Coleman and C. Enderby, "Megavolt electronics Cerenkov coupler for the production of millimeter and submillimeter waves", *J. Appl. Phys.*, vol. 31, pp. 1695-1696, 1960.
- [11] H. Lashinsky, "Cerenkov radiation from an extended electron beam", *J. Appl. Phys.*, vol. 27, pp. 631-635, 1956.
- [12] R. Ulrich, "Submillimeter Cerenkov radiation from a DC electron beam", *Z. Phys.*, vol. 199, pp. 171-185, 1967.
- [13] M.A. Piestrup, R.A. Powell, G.B. Rothbart, C.K. Chen, and R.H. Pantell, "Cerenkov Radiation as a light source for the 2000-600 Å spectral range", *Appl. Phys. Lett.*, vol. 28, pp. 92-98, 1976.

- [14] H. Dekker, "Cerenkov laser theory", Phys. Lett, vol. 59A, pp. 369-370, 1976.
- [15] J.E. Walsh, "Stimulated Cerenkov radiation", in Free Electron Generators of Coherent Radiation (Physics of Quantum Electronics), edited by S. Jacobs, M. Sargent, M. Scully, and R. Spitzer, (Addison-Wesley, Reading, MA 1978), vol. 7, pp. 357-380.
- [16] R. Collin, Foundations for Microwave Engineering. New York: McGraw-Hill, 1966, pp. 113-117.
- [18] E. Loewenstein, D. Smith, and R. Morgan, "Optical constants of far-infrared materials; 2 crystalline solids", Appl. Optics vol. 12, pp. 398-406, 1973.

FIGURE CAPTIONS

1. Possible Cerenkov laser configuration, showing a dielectric slab guide, a beam, and mirrors.
2. The relation between an approximately monoenergetic beam distribution function, measured in relative phase coordinates, $F(\theta)$, and the derivative of the diffraction line shape, $G'(\theta)$.
3. Geometric details of a) the beam, the guide and the gap;; b) the relation between the x dependence of the field and the preceding quantities.
4. The free space wavelength vs the guide wavelength, both measured in units of the guide thickness.
5. The relation between dispersion-related and beam-bunching quantities.

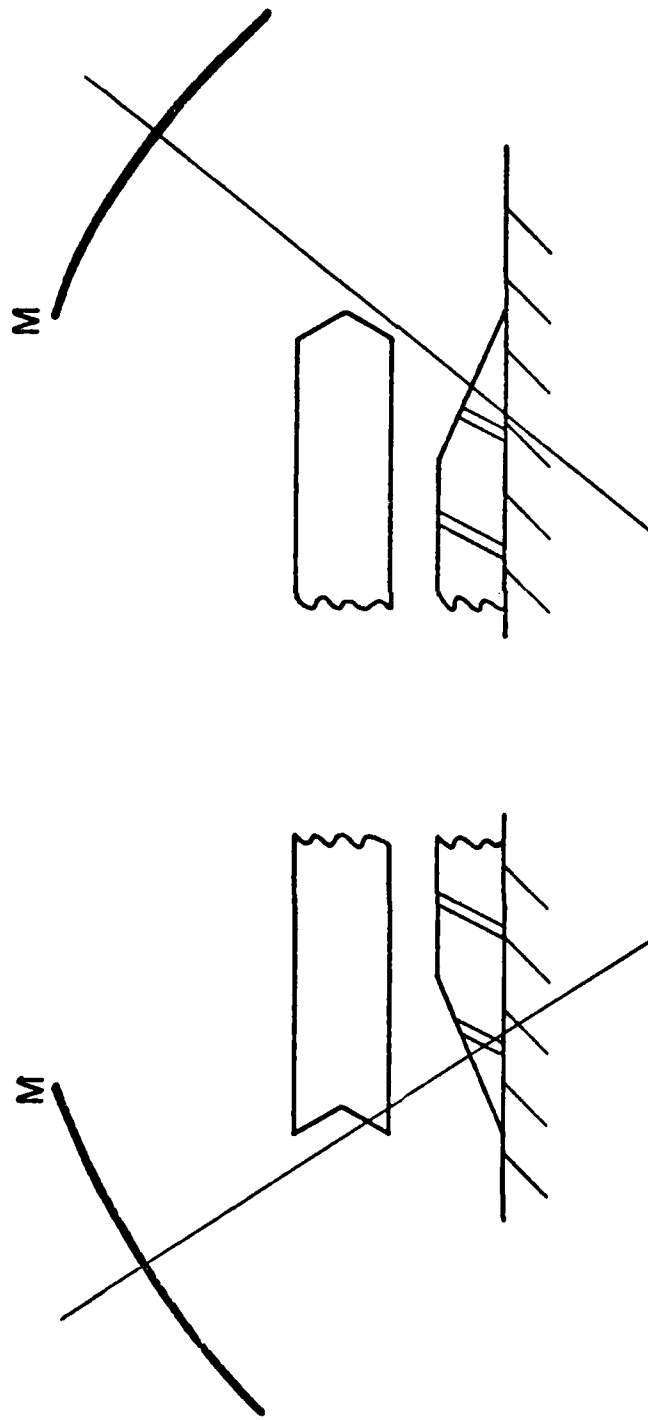


Fig. 1

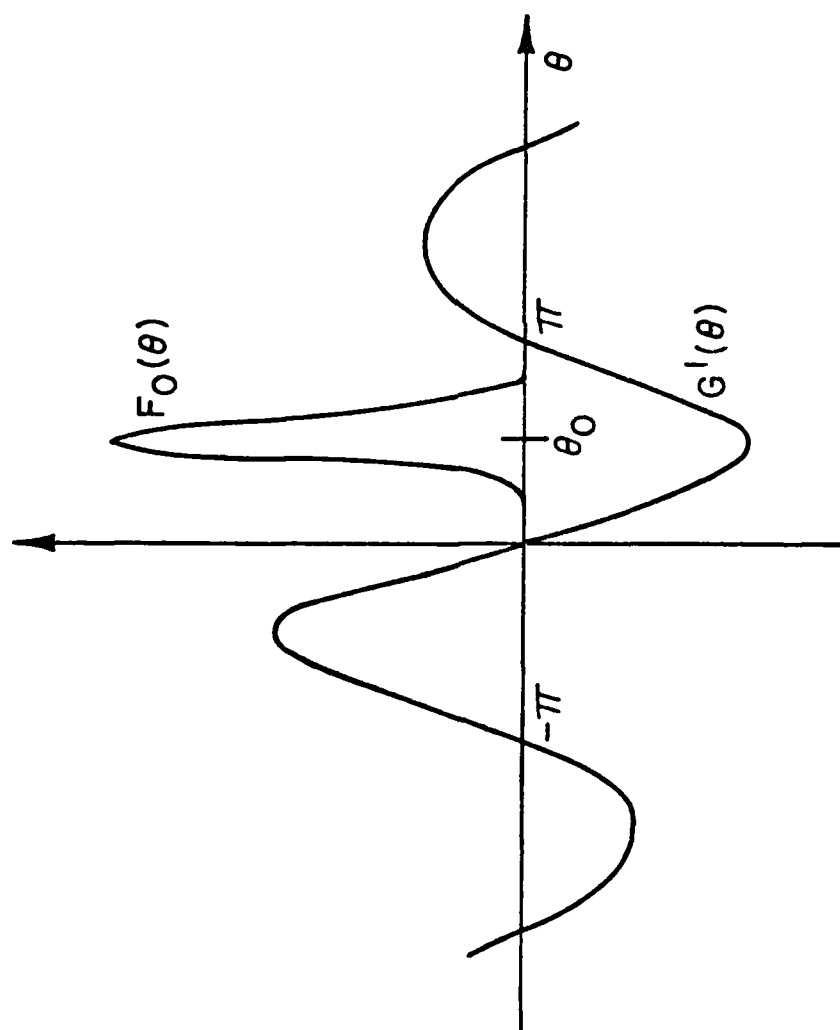


Fig. 2

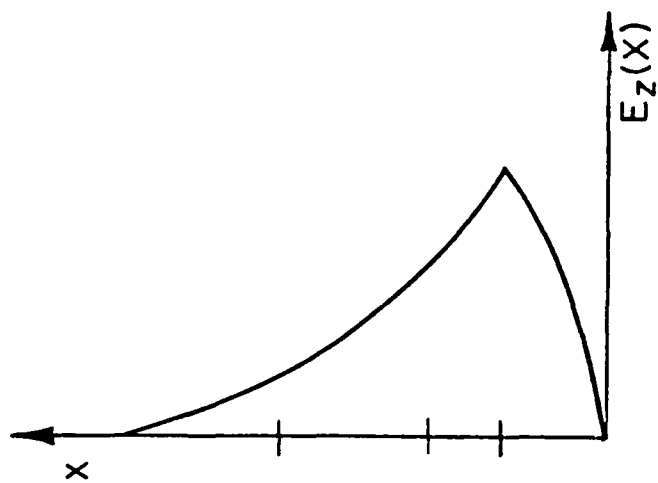


Fig. 3 b)

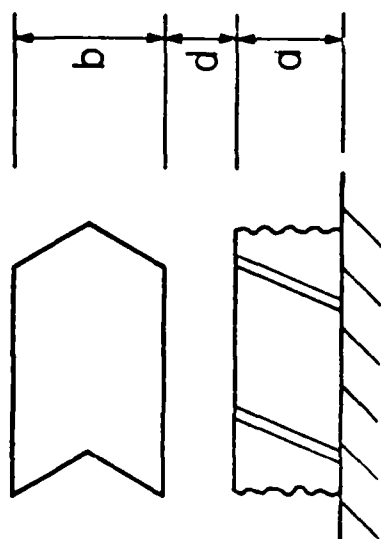


Fig. 3 a)

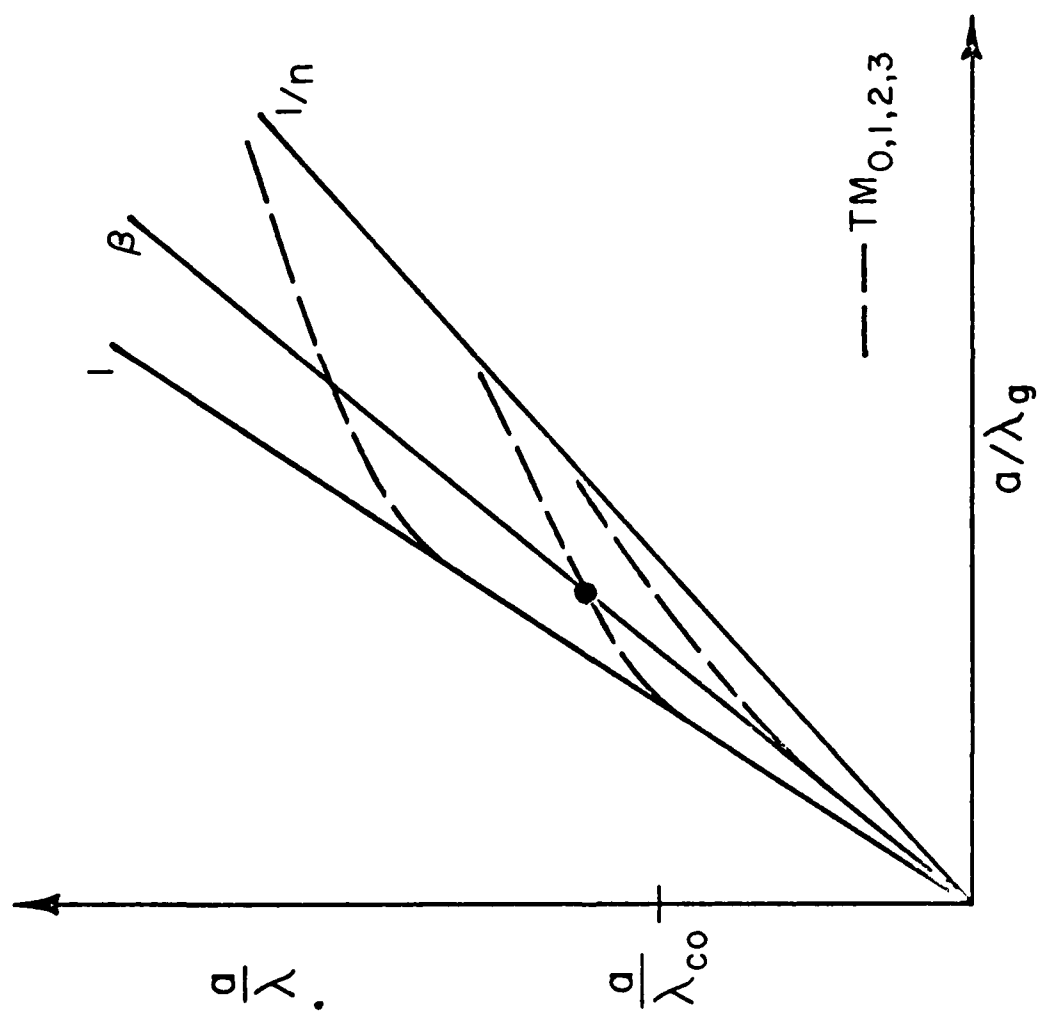


Fig. 4

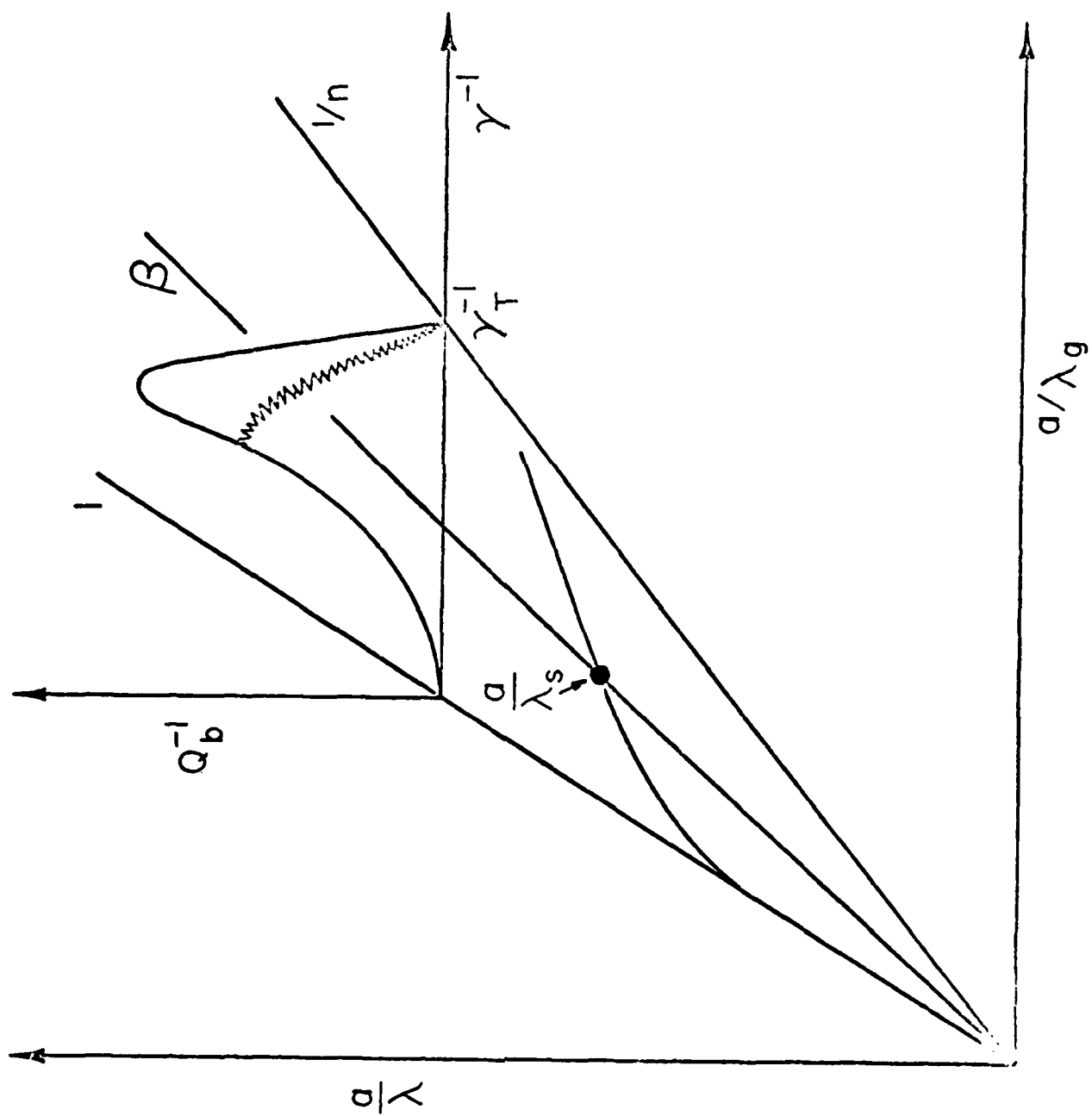


Fig. 5

CHARACTERIZATION OF A CERENKOV MASER

Scott A. Von Laven
Dartmouth College
Hanover, N.H. 03755
April, 1982

Support of U.S. Army Research Office Grant
DAAG-29-79-C-0203 is acknowledged.

Characterization of a Cerenkov Maser

* * *

Submitted in partial fulfillment of
the requirements for the degree
of Doctor of Philosophy

* * *

Dartmouth College
Hanover, N.H. 03755
April, 1982

ABSTRACT

The interaction of a magnetized electron beam with a slow guided electromagnetic wave has been studied experimentally. An electron beam driven, dielectric-lined, cylindrical waveguide has produced 30-100 kilowatts of coherent radiation over an octave band on the TM_{01} mode of the waveguide. Operation on the TM_{02} mode has been realized as well. Impedance mismatches at the ends of the liner section provide a reflected signal, which undergoes amplification during successive passes.

The growth rate of the interaction is calculated, taking into account the cylindrical geometry of the experiment, for the collective regime and for the single particle regime. An estimate of the saturating field amplitude leads to predicted powers for comparison with experiments.

ACKNOWLEDGEMENTS

A large number of people have participated in the Cerenkov maser project at Dartmouth. This thesis, in particular, draws heavily on the work of my advisor, John Walsh, and my predecessor, Kevin Felch. John Branscum, Dave Speer, and their technical crews took much of the data, using hardware built by Bob Layman, Kevin Felch, Ken Busby, Doug Wise, and others. John Walsh and Jim Murphy patiently answered my numerous questions. Bill Case and Bill Doyle also contributed ideas. Ken Jacobs, at M.I.T., provided a working version of the electron trajectory code. I deeply appreciate all of this help.

I would also like to thank my committee and other readers of preliminary drafts for their time and comments and the Physics Department staff for their technical and administrative help.

Special thanks goes to my family for their patience and support during all the years of school.

TABLE OF CONTENTS

CHAPTER I

1.1 INTRODUCTION	1
----------------------------	---

CHAPTER II

2.1 FREQUENCY DETERMINATION	6
2.2 DISPERSION RELATIONS	8
2.3 LIMITING CASES	12
2.4 FREQUENCY MEASUREMENTS	15

CHAPTER III

3.1 POYNTING FLUX, STORED ENERGY, AND THE DISPERSION FUNCTION	25
3.2 COLLECTIVE VS. SINGLE ELECTRON GROWTH RATE	28
3.3 GROWTH RATES FOR THE CYLINDER	39

CHAPTER IV

4.1 FEEDBACK	53
4.2 OUTPUT POWER	64
4.3 POWER MEASUREMENTS	72

CHAPTER V

5.1 CONCLUSION	77
--------------------------	----

APPENDIX I

A1.1 RADIAL TRIGONOMETRIC FUNCTIONS 79

APPENDIX II

A2.1 ANISOTROPIC DIELECTRIC LINERS 81

APPENDIX III

A3.1 SOFTWARE 84

REFERENCES 88

LIST OF ILLUSTRATIONS

DISPERSION CURVES	7
GEOMETRIES	9
EXPERIMENTAL GEOMETRY	16
INTERFEROMETER	17
FREQUENCY DATA	18-20,23
SINGLE PARTICLE GROWTH RATE LINESHAPE	30
PARTICLE SIMULATION RESULTS	36-38
GROWTH RATES, MODE DEPENDENCE	41,43
GROWTH RATES, DEPENDENCE ON VELOCITY AND DIELECTRIC CONSTANT	44,45,50
GROWTH RATES, DEPENDENCE ON LINER THICKNESS	51,52
TAPERED VS. SQUARE END LINER	56
INTERFEROGRAMS	58,60
OUTPUT PULSE BEHAVIOR	62,63
THEORETICAL POWER AND EFFICIENCY CURVES	66-71
POWER DATA	74-76
ANISOTROPIC DISPERSION CURVE	83

CHAPTER I

1.1 INTRODUCTION

The search for new sources of electromagnetic radiation has led to the construction of many novel devices. In the visible spectrum, dye lasers have achieved tunability while multi-stage CO_2 and neodymium lasers have achieved high power. In attempts to combine the virtues of tunability and high power, excited states have been stimulated to emit one photon at a widely tunable wavelength, while emission in one case of another photon,¹ and in another case a phonon,² completes the transition between states.

At millimeter and submillimeter wavelengths a similar but more hopeful situation exists. Tunable devices are typically low power. However, the free electron laser possesses both tunability and high power. It has so far been an experimental device, but a 12 kilowatt user facility is now under development at UCSB.^{3,4}

The Cerenkov maser, considered here, is another tunable, high power, millimeter source, which may have advantages over the free electron laser in certain situations. The tunability and power capability have been tested experimentally and are

found to confirm predictions. Significant power at three millimeters has been observed.

The Cerenkov maser is one of a class of schemes for extracting electromagnetic energy from electron beams. In the Cerenkov scheme, a dielectric, combined with a guiding structure, is used to support a slow electromagnetic wave in the vicinity of a beam. The longitudinal bunching of the beam and the amplitude of the electromagnetic wave drive each other to large amplitude.

A variety of other schemes exist in this class. The free electron laser employs a spatially modulated transverse magnetic field, which couples the beam to a radiation field.

The gyrotron uses a carefully designed electron gun and guiding magnetic field configuration to define helical orbits for the electrons in the beam. Bunching of the beam occurs along the helix rather than along the longitudinal axis, driving the amplitude of the beam's own cyclotron radiation. An annular beam with relatively large transverse energy is required.

The klystron, the magnetron, and the traveling wave tube depend on resonant cavity structures in different configurations to bunch the beam. Variations of these devices have been scaled to millimeter wavelengths at the expense of power and efficiency⁵ and scaled to high power at the expense of frequency.⁶ The frequency is ultimately limited by the ability to construct small resonant cavity structures.

One gyrotron has produced 1.1 megawatts at three millimeters in a 100 microsecond pulse.⁷ Another gyrotron, which will generate five millimeter, high power, cw radiation, is currently under development by Varian Associates.⁸ Gyrotron wavelengths are ultimately limited by the attainable magnetic field, since output is at the electron cyclotron frequency. The field, B, required to operate at wavelength, λ , is given by

$$B = (\gamma mc^2/e)/\lambda, \quad (1.1)$$

thus scaling inversely as the wavelength. The quantities m, e, c, and γ are the mass and charge of an electron, the speed of light, and $(1-(v/c)^2)^{-1/2}$, respectively, and v is the beam velocity.

One free electron laser has operated at a wavelength of 3.4 microns by employing a highly relativistic beam.⁹ The output wavelength is given by

$$\lambda = \lambda_p / (\beta(1+\beta)\gamma^2), \quad (1.2)$$

$$\beta = v/c,$$

where λ_p is the period of the transverse magnetic field modulation.¹⁰ The pump wavelength, λ_p was 3.2 cm for the above experiment; thus $\gamma=90$ was required. The lower limit on λ_p is approximately one centimeter. A beam energy of 79 keV is

required to give $\lambda = \lambda_p$, and 175 keV gives $\lambda = \lambda_p/2$. Thus relatively modest beam energies can be used to operate a free electron laser at millimeter wavelengths. More complete discussions of the operation and history of millimeter devices are available and contain further references.¹¹⁻¹⁷

The Cerenkov scheme imposes less severe requirements on structure complexity, magnetic field intensity, and electron beam energy than the above schemes. The original suggestion that coherent Cerenkov radiation might be obtained from a bunched beam came from Ginzburg.¹⁸ Other early contributions came from Lashinsky^{19,20} and Pierce.²¹ Bolotovskii has considered the spectrum of incoherent Cerenkov radiation in guiding structures.²²

The availability of relativistic electron beams with respectable current densities made possible the recent experimental effort. At Columbia a .5 MeV, 10 kA beam has been used to drive a lucite lined waveguide.²³ At Dartmouth a 100-250 keV, 1-40 amp, pulsed beam has driven a quartz lined waveguide. The dependence of output frequency on beam energy was measured in the quartz experiment and was found to be roughly as predicted.^{12,24}

Further experiments at Dartmouth, presented here, have confirmed the predicted frequency dependence on liner dimensions, dielectric constant, waveguide mode selection, and beam energy. Power measurements have been made as well.²⁵

These results are presented in this paper along with supporting calculations.

In Chapter II the electromagnetic field components which couple to the beam, and the dispersion relations governing their propagation, are discussed. Three possible geometries, including the experimental geometry, are considered in order to illustrate their similarities and differences. The predicted coupling frequencies are compared to measurements.

In Chapter III the results of Chapter II are used to write expressions for the growth rate of the Cerenkov instability in both the collective and single particle regimes. The criteria for choosing a regime as well as for overall validity of either analysis are explained and evaluated for the experimental parameters.

In Chapter IV the role of feedback is discussed. An estimate of the possible output power is compared to measurements.

CHAPTER II

2.1 FREQUENCY DETERMINATION

Several considerations restrict the set of frequencies to which the beam may couple in a dielectric-lined waveguide. Both beam and guide are assumed to be uniform in the longitudinal (z) direction and in one transverse (y or θ) direction. The electric and magnetic fields must satisfy Maxwell's equations and the boundary conditions imposed by the transverse geometry. These define all the possible modes of the passive guide.

The longitudinal component of electric field, E_z , must be as large as possible in the volume of space occupied by the beam in order to drive the axial bunching. Thus TE modes are eliminated. Uniformity in one transverse direction assigns the value of zero to the corresponding mode index. Thus only TM_{0n} modes need be considered.

Coupling is so far restricted to a family of continuous spectra as shown in Fig. 2.1. Angular frequency, ω , is a function of wavenumber, k , but k is a free parameter. Requiring the phase velocity, ω/k , of the radiation to be equal to the beam velocity fixes the frequency and wavenumber for a given TM_{0n} mode. The resulting discrete frequencies are

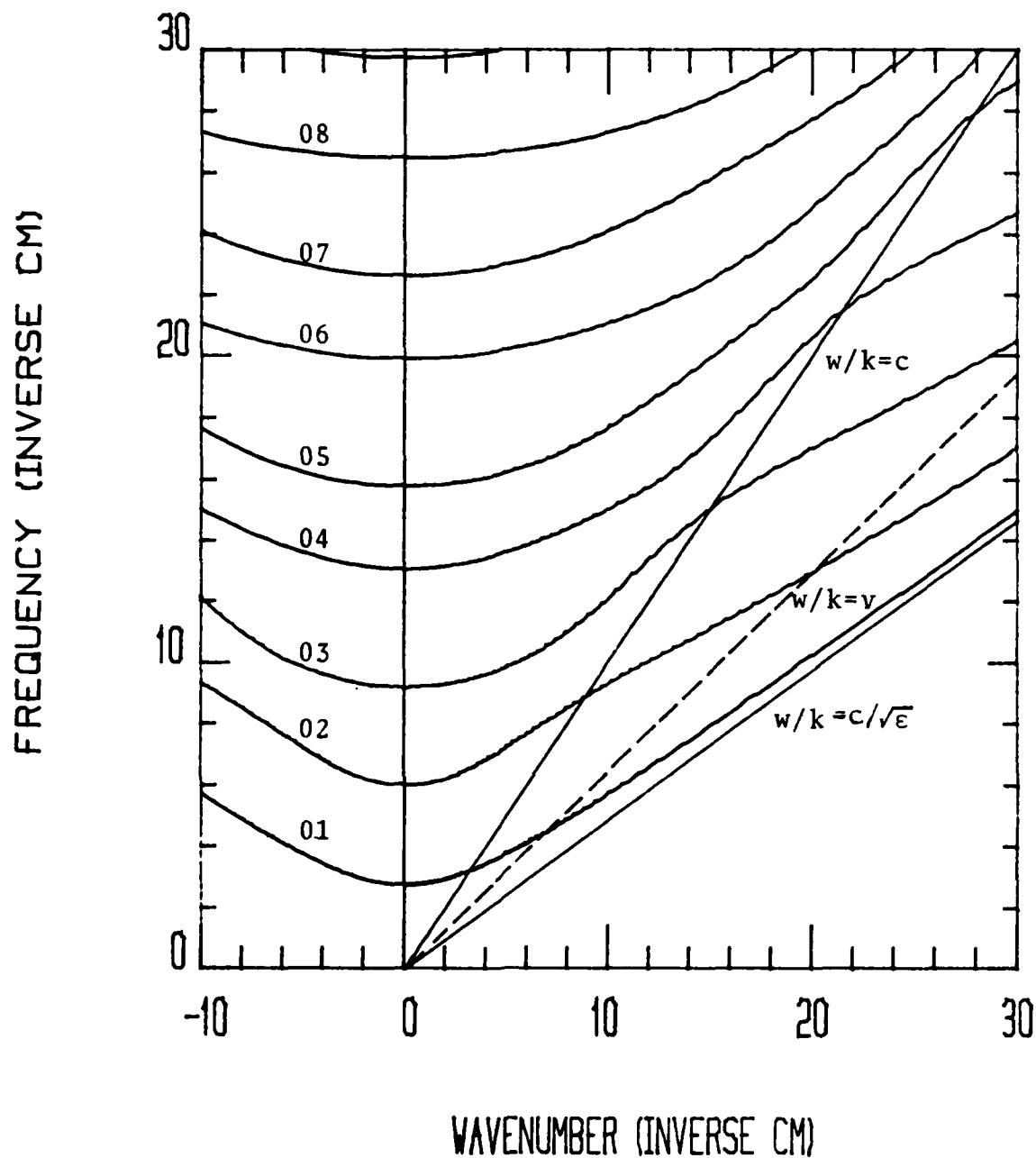


Fig. 2.1. TM_{00} dispersion curves for a 12.5 millimeter diameter waveguide with a two millimeter thick annular liner of boron nitride (dielectric constant=4.2). The beam line (dotted line) must lie between the vacuum and dielectric light lines (solid lines).

indicated by the points of intersection of the beam line with the dispersion curves in Fig. 2.1. Phase velocity synchronism allows the beam to interact with E_z , rather than having its effect averaged to zero by rapid fluctuations in the beam's rest frame. The synchronous condition can be derived by conserving energy and momentum for forward emission of a photon by an electron which loses a small fraction of its momentum.¹³

2.2 DISPERSION RELATIONS

Dispersion relations for uniform dielectric-lined guides have been derived elsewhere for the single slab,¹³ double slab¹² and cylindrical^{12,26} geometries. A short analysis is given here which accounts for the three geometries simultaneously and serves to illustrate their similarities and differences. The geometries are shown in Fig. 2.2.

Incorporating immediately the choice of modes (TM_{0n}), two of the boundary conditions (E_z symmetric at the origin and vanishing at $x=b$), and the harmonic temporal and longitudinal spatial dependence of the fields, $e^{i(\omega t - kz)}$, the solution to Maxwell's equations for the x or r dependence of the electric fields is given by

Fig. 2.2a.
Single slab geometry.

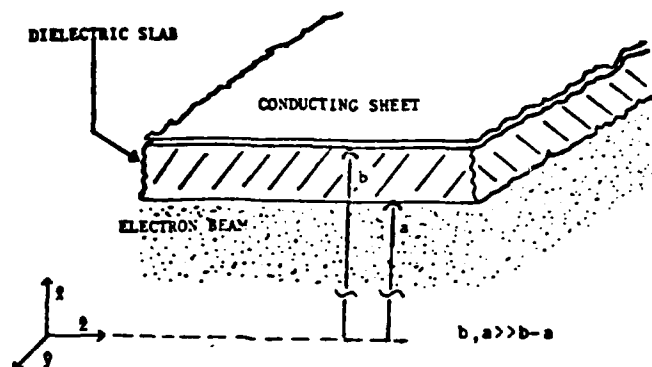


Fig. 2.2b.
Double slab geometry.

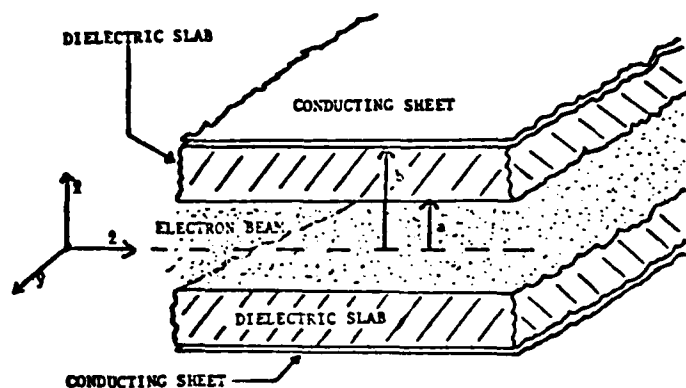
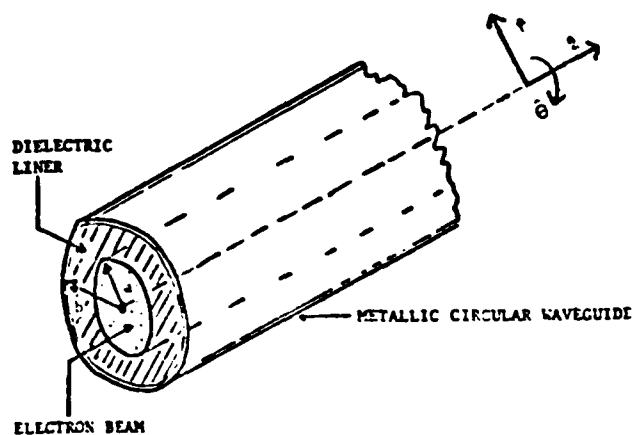


Fig. 2.2c.
Cylinder geometry.



$$E_z = \begin{cases} (A)\text{sn}(qx, qb) & a < x < b \\ (B)\text{Cs}(ipx, 0) & 0 < x < a \end{cases} \quad (2.1a)$$

$$E_x = \begin{cases} (ik/q)(A)\text{cs}(qx, qb) & a < x < b \\ (-k/p)(B)\text{Sn}(ipx, 0) & 0 < x < a. \end{cases} \quad (2.1b)$$

where x , for the single and double slab geometries and r , for the cylindrical geometry, are represented by x in these general expressions. The perpendicular wavenumbers, q and p , are given by $q^2 = \epsilon w^2/c^2 - k^2$ and $p^2 = k^2 - w^2/c^2$, where ϵ is the dielectric constant of the liner. Wave numbers, p and q , are real for the slow wave region, $c/\sqrt{\epsilon} < w/k < c$, within which the beam and wave may interact.

The generalized trigonometric functions sn , cs , and Sn and Cs are to be identified as follows. For the cylinder sn and cs are the small radial sine and cosine functions.

$$\text{sn}(u, v) = (J_0(v)Y_0(u) - Y_0(v)J_0(u))/(2/\pi v) \quad (2.2a)$$

$$\text{cs}(u, v) = (Y_0(v)J_1(u) - J_0(v)Y_1(u))/(2/\pi v). \quad (2.2b)$$

Sn and Cs are the large radial and cosine functions given by

$$\text{Sn}(u, v) = (J_1(v)Y_1(u) - Y_1(v)J_1(u))/(2/\pi v) \quad (2.3a)$$

$$\text{Cs}(u, v) = (J_1(v)Y_0(u) - Y_1(v)J_0(u))/(2/\pi v). \quad (2.3b)$$

Useful properties of these functions are given in Appendix 1. For the double slab and single slab geometries,

$$\text{sn}(u,v) = \text{Sn}(u,v) = \sin(v-u) \quad (2.4a)$$

$$\text{cs}(u,v) = \text{Cs}(u,v) = -\cos(v-u) \quad (2.4b)$$

Incorporating the other two boundary conditions (E_z and $\epsilon(x)E_x$ continuous at $x=a$) gives

$$(A)\text{sn}(qa,qb) = (B)\text{Cs}(ipa,0) \quad (2.5a)$$

$$\epsilon(Ai/q)\text{cs}(qa,qb) = -(B/p)\text{Sn}(ipa,0). \quad (2.5b)$$

The dispersion relation is the quotient of the above two equations.

$$(q)\text{tn}(qa,qb)(\text{Tn}(ipa,0)/i) = \epsilon p, \quad (2.6)$$

where $\text{tn} = -\text{sn}/\text{cs}$ and $\text{Tn} = \text{Sn}/\text{Cs}$. By substituting function definitions appropriate to each geometry, the familiar forms of the dispersion relations and field expressions can be recovered.

In general, it is suggested that any dielectric-lined guide, uniform in two orthonormal coordinates, will satisfy equations 2.1 and 2.6. The functions sn , cs , Sn , and Cs will be constructed from the independent solutions of the Helmholtz equation, in the appropriate set of orthonormal coordinates, and the derivatives of those solutions. Hereafter the names sn , cs , Sn , and Cs will normally be reserved for the radial trigonometric functions (Equations 2.2 and 2.3).

2.3 LIMITING CASES

The slow wave requirement can be expressed as $\cos\theta > 1/\sqrt{\epsilon}$, where θ is the Cerenkov angle defined by $\cos\theta = 1/\beta\sqrt{\epsilon}$. The sine of the angle of incidence for radiation in the liner impinging upon the dielectric-vacuum interface is equal to $\cos\theta$. Thus the slow wave requirement is equivalent to requiring total internal reflection at the dielectric-vacuum interface. The fields in the beam region must be evanescent, as can be seen by evaluating the field expressions. If the fields fall off sharply enough, it can be anticipated that the single slab expressions will describe the system. The fields fall off fastest for grazing incidence, where $\cos\theta = 1$ or $\beta = 1/\sqrt{\epsilon}$, that is, near the Cerenkov threshold. Fig. 2.1 indicates that a beam velocity near the Cerenkov threshold limit intersects the dispersion curve at large w and that $w = ck/\sqrt{\epsilon}$.

The single slab dispersion relation is

$$(q)\tan(qd) = \epsilon p \quad (2.7)$$

where $d=b-a$. In the single slab geometry the liner and conductor are located infinitely far out on the positive x axis so that $Tn(ipa,0) = \tanh(pa) = 1$.

The double slab dispersion relation is

$$(q)\tan(qd)\tanh(pa) = \epsilon p, \quad (2.8)$$

In the near-threshold limit, $\tanh(pa) \approx \tanh(wa\sqrt{\epsilon-1}) \approx 1$, giving $(q)\tan(qd) = \epsilon p$, the single slab dispersion relation. The cylinder dispersion relation is,

$$(q)\text{tn}(qa, qb)I_1(pa)/I_0(pa) = \epsilon p, \quad (2.9)$$

where I_1 and I_0 are modified Bessel functions of the first kind. Their ratio approaches unity for large arguments. Using $ct = 1/\text{tn}$, the general dispersion relation (Eqn. 2.6) becomes in this limit

$$ct(qa, qb) = q/\epsilon p. \quad (2.10)$$

The right hand side of Eqn. 2.10 approaches zero at threshold, implying that q is approaching one of the roots of $ct(qa, qb)$. Taylor expanding gives

$$(q - q_n)(d/dq)(ct(qa, qb))_{q=q_n} = q/\epsilon p, \quad (2.11)$$

or

$$q = q_n \left(1 - \frac{\text{sn}(q_n a, q_n b)}{\epsilon p (b \text{Sn}(q_n a, q_n b) - a \text{sn}(q_n a, q_n b))} \right), \quad (2.12)$$

where q_n is the n th root of $ct(qa, qb)$. The latter expression is used to evaluate growth rates along the dispersion curves near threshold. For the single and double slab Eqn. 2.12 becomes

$$q = ((2n+1)\pi/2d)(1 - 1/(\epsilon p d)). \quad (2.13)$$

Being near threshold is not a sufficient condition for the cylindrical expressions to approach the rectangular expressions. However, in the limit of high mode number, $n \gg 1$, or thin dielectric, $a, b \gg b-a$, $ct(qa, qb)$ evaluated for the cylinder approaches $\cot(qd)$.²⁶ Coupling to the beam in the region where these expressions are valid is difficult for lack of fields in the vicinity of the beam, as the growth rate results will confirm.

As the beam velocity approaches the speed of light, p approaches zero, q approaches infinity, and the small radial tangent, $tn(qa, qb)$, approaches $\tan(qd)$. The dispersion relation becomes

$$\text{single slab: } \tan(qd) = 0 \quad (2.14a)$$

$$\text{double slab: } \tan(qd) = \epsilon/qa \quad (2.14b)$$

$$\text{cylinder: } \tan(qd) = 2\epsilon/qa \quad (2.14c)$$

with $q = w\sqrt{\epsilon-1}/c$. The possibility of exploiting the wider mode spacing of the single slab geometry, as part of a scheme for an infrared Cerenkov device, has been examined.¹³

2.4 FREQUENCY MEASUREMENTS

Quartz ($\epsilon=3.78$), stycast ($\epsilon=5$), and boron nitride ($\epsilon=4.2$) have served as the liner material. An electron beam with a minimum diameter of three millimeters is provided by the beam focusing and collimating system shown in Fig. 2.3. The diverging beam is collected on the copper guide downstream from the liner and guide field. The radiation is guided through a transmitting teflon vacuum window and a circular to rectangular mode transducer into the detection hardware.

Frequency measurements are made with a mechanically driven, free space, Fabry-Perot interferometer (Fig. 2.4).²⁷ The drive speed of about ten microns per second, and the repetition rate for beam generation of about one Hz, insure that more than one pulse occurs within the 20 micron minimum linewidth of the interferometer.

For almost every liner used, the fundamental output frequency is near the frequency at which the TM_{01} mode is synchronous with the beam. Figures 2.5, 2.6, and 2.7 show the frequencies obtained in 12.5 millimeter diameter waveguide. A large systematic offset is noted for the three millimeter quartz and three millimeter stycast liners. A surface charge build-up on those liners is suspected of decelerating the beam to velocities synchronous with the observed output.

The charge per unit length, q/l , along the inner surface of the liner is limited by the dielectric strength of the

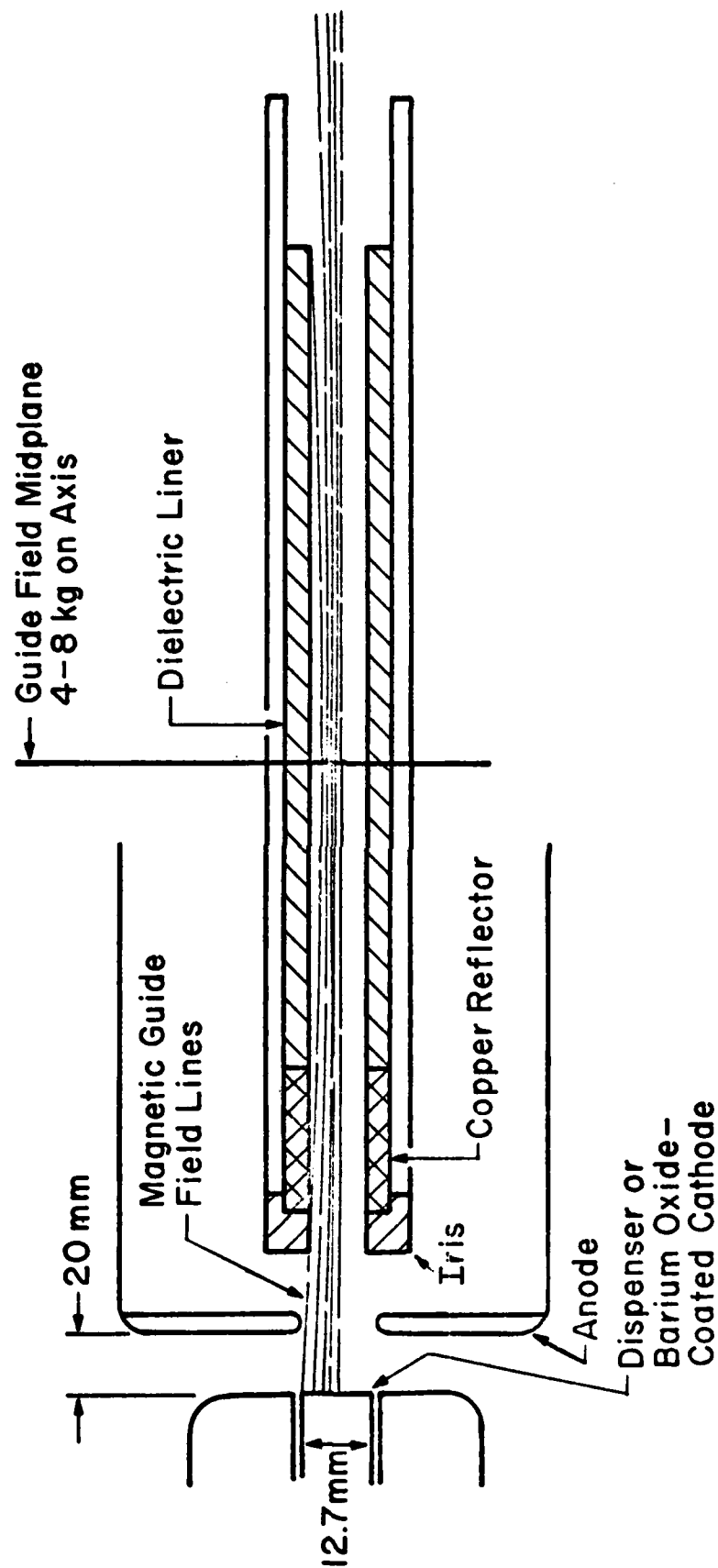


Fig. 2.3. Experimental cylindrical liner geometry.

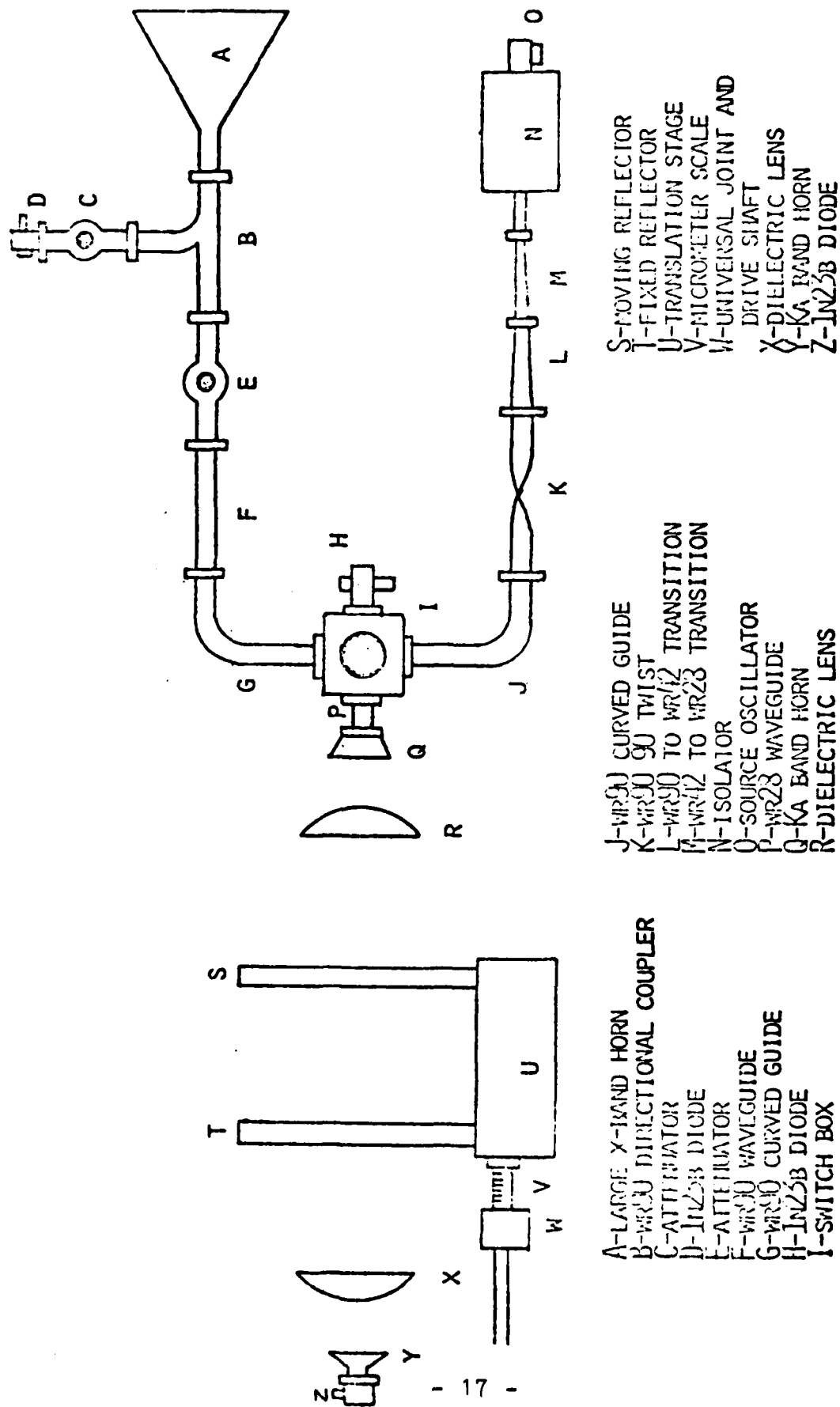


Fig. 2.4. Fabry-Perot interferometer (from ref. 27).

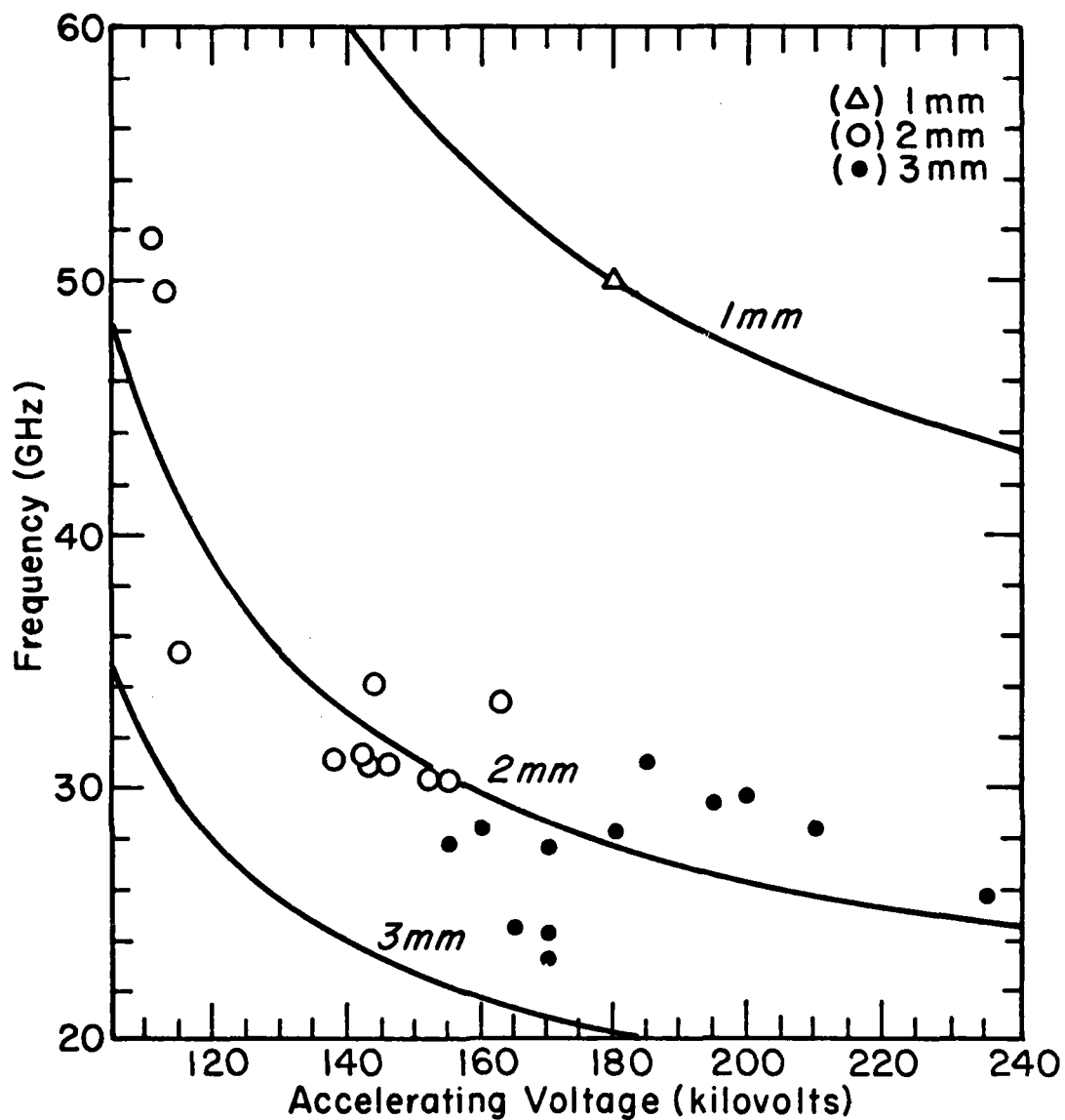


Fig. 2.5. The frequency of a coupling mode is plotted vs. the synchronous beam voltage to give a "tuning curve". The frequency measurements made with quartz liners of one, two, and three millimeter thicknesses are displayed along with the TM_{01} tuning curves for those liners. The guide diameter, $2b$, is 12.5 millimeters.

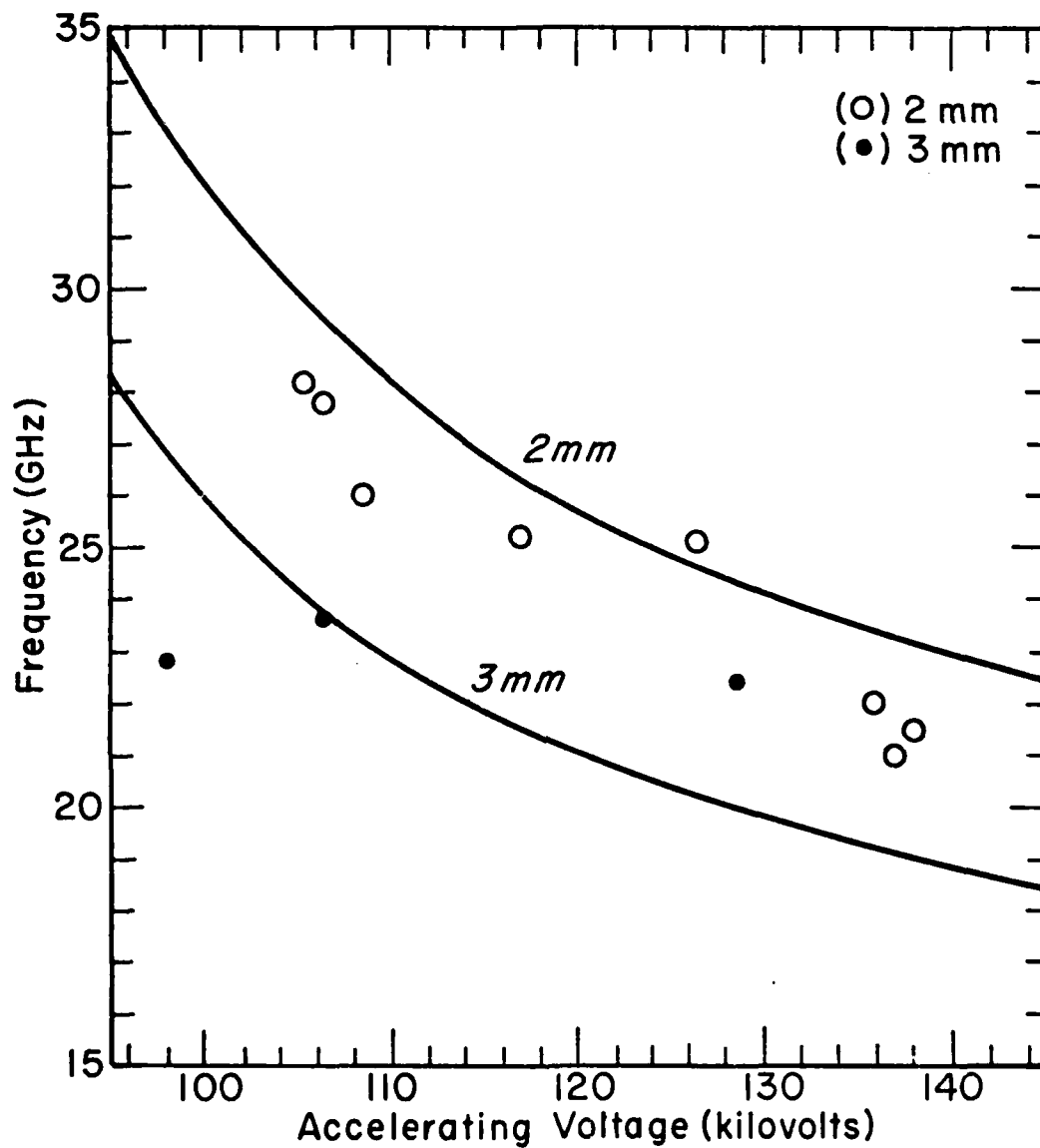


Fig. 2.6. Data and TM_{01} tuning curves for two and three millimeter thick boron nitride liners in 12.5 millimeter guide.

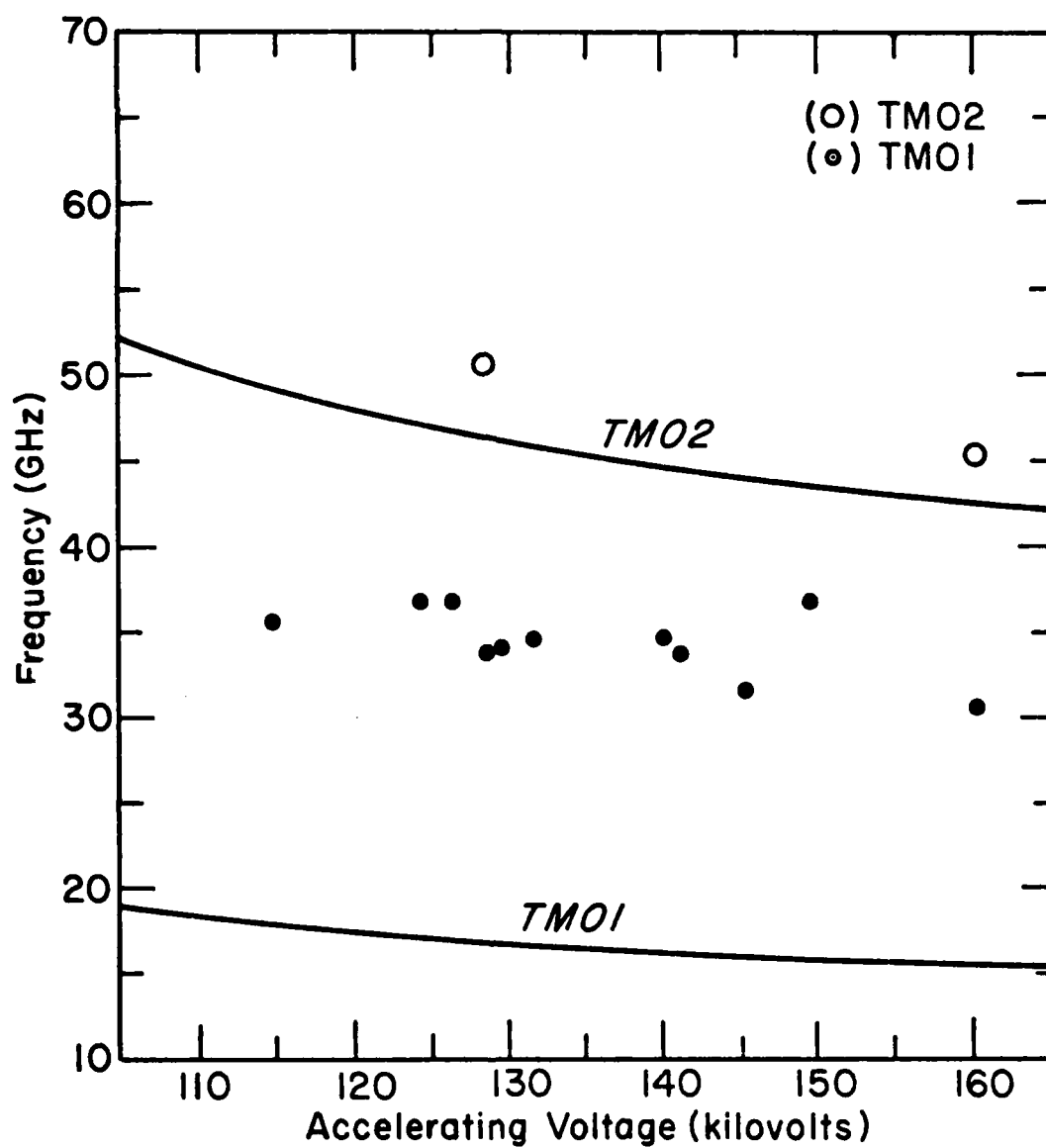


Fig. 2.7. TM_{01} and TM_{02} tuning curves and data for a three millimeter styrcast liner in 12.5 millimeter guide.

liner. Thus $q_{\max}/l = V_B/(2) \ln(b/a)$, where V_B is the breakdown voltage given by the dielectric strength times the thickness of the liner. The length, l , of the charged surface is at least $b-a$ due to surface breakdown. In approaching the charged section, an electron on the z axis gains a potential of q/a . For three millimeter liners $b=2a$, and $q_{\max}/a = q_{\max}/l = V_B/(2) \ln(2)$. For quartz, stycast, and boron nitride, V_B is 48, 36, and 60 kV, respectively, and the beam can lose a large fraction of its kinetic energy.

Quartz liners are frequently found to have suffered damage attributable to dielectric breakdown. The use of a thin conducting film to bleed off charge has been studied,²⁸ and other less drastic methods, such as a split liner, may prove helpful. So far, no coated liner has produced radiation.

If the charge is distributed over a longer section of liner, greater biasing is possible. If the dielectric surface has little tendency to hold charge, then q may remain much less than q_{\max} . For two millimeter liners $b=3a/2$, and $q_{\max}/a = q_{\max}/(2)l = V_B/(4) \ln(1.5)$, which is still 85% of the three millimeter value. However, the average gap between the beam and the liner is greater in the two millimeter geometry, and the biasing is less noticeable.

The longitudinal electric field associated with the one millimeter liner geometry is too weak to give good coupling for moderate beams. At the higher voltages and currents which

become necessary, the beam generator's performance is less consistent. Thus the probability of recording a noise-free interferogram, requiring approximately 1000 pulses, is low.

Since the phase velocity of any of the waveguide modes decreases with increasing frequency, a favorable scaling law is obtained for output frequency with respect to beam energy for a given dielectric liner. The range of frequencies obtainable on a single mode has reached nearly an octave (Fig. 2.5).

In some of the 12.5 millimeter diameter waveguide experiments and in a 9.5 millimeter waveguide experiment, it has been possible to suppress the TM_{01} mode and observe coupling to the TM_{02} mode (Figures 2.7 and 2.8). This can occur when the frequency is below the cutoff for the TM_{01} mode of the empty guide. Frequencies between 100 and 120 GHz have been attained. The power appears to be less than that obtainable on the TM_{01} mode, but still significant. Output of still lower apparent power has been observed through a 200 GHz filter with the two millimeter quartz liner in a 12.5 millimeter guide.

All the shorter wavelength power measurements are made with 1N53 diodes in a Ka band mount. This system is difficult to calibrate when it is far out of band. The voltage response generated at these short wavelengths would have corresponded to one tenth to one quarter of the power measured in the 8 mm region, if the wavelengths had been in the design band of the

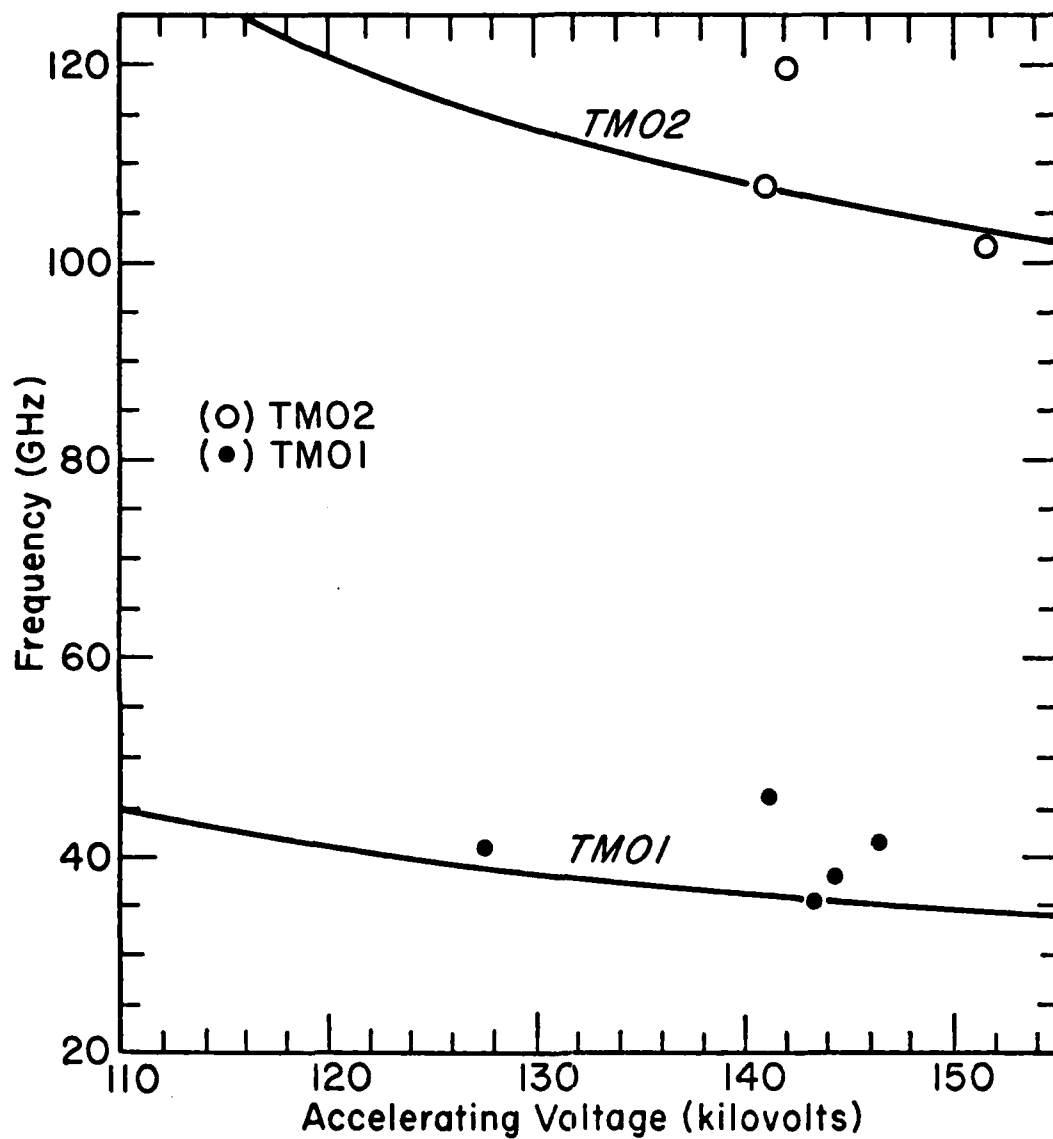


Fig. 2.8. TM_{01} and TM_{02} tuning curves and data for a 1.5 millimeter boron nitride liner in 9.5 millimeter guide.

mount. Hence, at the shorter wavelengths the output power would, at a minimum, be in the one kW range.

CHAPTER III

3.1 POYNTING FLUX, STORED ENERGY, AND THE DISPERSION FUNCTION

The dispersion relation can be expressed as $D(w,k)=0$, where $D(w,k)$ is identified as the dispersion function. Since the value of D is zero everywhere along a dispersion curve, the total derivative of D with respect to a displacement along the curve is also zero. In terms of partial derivatives,

$$0 = dD/dK = (\partial D/\partial w)(dw/dk) + \partial D/\partial k. \quad (3.1)$$

The group velocity, dw/dk can then be expressed as

$$dw/dk = (\partial D/\partial k)/(\partial D/\partial w), \quad (3.2)$$

the ratio of the partial derivatives of D .

The group velocity is also the ratio of the Poynting flux to the stored energy per unit length, giving

$$dw/dk = P/(U/L) = (\partial D/\partial k)/(\partial D/\partial w), \quad (3.3)$$

where the time averaged P and U are given by

$$P = (c/8\pi) \int d\vec{A} \cdot (\vec{E} \times \vec{H}^*) \quad (3.4a)$$

$$U = (1/16\pi) \int dV (\vec{E} \cdot \vec{D}^* + \vec{B} \cdot \vec{H}^*), \quad (3.4b)$$

or

$$U = (1/16\pi) L \int d\vec{A} (\vec{E} \cdot \vec{D}^* + \vec{B} \cdot \vec{H}^*), \quad (3.4c)$$

where L is the effective length of the region of interaction between the beam and lined guide, and the integrations are carried out over the cross sectional area of the guide.

Rearranging 3.3 gives

$$P/(\partial D/\partial k) = (U/L)/(\partial D/\partial w), \quad (3.5)$$

a ratio which can still be a function of w and k .

Assuming unity magnetic permeability and TM_{0n} mode symmetry we have

$$H_z = B_z = H_x = B_x = 0 \quad (3.6)$$

$$H_y = B_y = \begin{cases} (w/ck)E_x & 0 < x < a \\ (w\epsilon/ck)E_x & a < x < b \end{cases} \quad (3.7)$$

where x and y are the general transverse coordinates, perpendicular and parallel to the liner respectively. The P and U integrals can now be performed. The ratio, $P/(\partial D/\partial k) = (U/L)/(\partial D/\partial w)$, is found to be

$$\text{single slab: } B^2(w/16p)(\Delta y/\epsilon\pi q)(1/\sin qd) \quad (3.8a)$$

$$\text{double slab: } B^2(w/8p)(\Delta y/\epsilon\pi q)\cosh(pa)\sinh(pa)/\sin qd \quad (3.8b)$$

$$\text{cylinder: } B^2(w/8p)(a/q)I_0(pa)I_1(pa)/\text{sn}(qa,qb), \quad (3.8c)$$

where B is the electric field coefficient defined by 2.1 and Δy is the spatial extent of the interaction in the \hat{y} direction. The derivatives are

double slab:

$$\partial D/\partial k = kS\{b-a(1-\epsilon)\cos^2 - a(1-q^2/\epsilon p^2)\sin^2 + (1/q)(1-q^2/p^2)\text{sincos}\} \quad (3.9a)$$

$$\partial D/\partial w = (w/c^2)S\{\epsilon b - a(\epsilon - q^2/\epsilon p^2)\sin^2 + (1/q)(\epsilon - q^2/p^2)\text{sincos}\} \quad (3.9b)$$

single slab:

$$\partial D/\partial k = kS\{d + (1/q)(1-q^2/p^2)\text{sincos}\} \quad (3.9c)$$

$$\partial D/\partial w = (w/c^2)S\{\epsilon d + (1/q)(\epsilon - q^2/p^2)\text{sincos}\} \quad (3.9d)$$

$$\sin = \sin(q(b-a)) = \sin qd \quad \cos = \cos(q(b-a)) = \cos qd$$

cylinder:

$$\partial D/\partial k = kS\{b^2/a - a(1-\epsilon)c^2 - a(1+q^2/\epsilon p^2)\text{sn}^2 - (2/q)(1+q^2/p^2)\text{sn}cs\} \quad (3.9e)$$

$$\partial D/\partial w = (w/c^2)S\{\epsilon b^2/a - a(\epsilon + q^2/\epsilon p^2)\text{sn}^2 - (2/q)(\epsilon + q/p^2)\text{sn}cs\} \quad (3.9f)$$

$$sn = sn(qa, qb) \quad cs = cs(qa, qb),$$

where $S = \epsilon p(Ct(ipa, 0)/i) / ((q)sn(qa, qb))$ in each case, and a convenient form is used for D ,

$$D(w, k) = -(q)sn(qa, qb) - (\epsilon p)cs(qa, qb)(i(Ct(ipa, 0))). \quad (3.10)$$

3.2 COLLECTIVE VS. SINGLE ELECTRON GROWTH RATE

The results of the previous section are used in Section 3.3 for the calculation of growth rates. In this section beam space charge interactions and beam energy spread are discussed with respect to the growth rate. It is concluded that the present experiment may be characterized by a cold, collective growth rate.

Assuming the Cerenkov radiation due to the beam and the axial bunching of the beam interact as a linear feedback system, the radiation field will grow exponentially. The growth rate can be recovered from the time averaged stored field energy, U , given by Eqn. 3.4c. Then

$$w'' = (dU/dt)/2U, \quad (3.11)$$

where w'' , the growth rate, is the imaginary part of the frequency, $w = w_0 + w' + iw''$. The no-beam solutions are now designated w_0, k_0 where $D(w_0, k_0) = 0$.

The growth rate is actually temporal only in the electron beam's rest frame. The spatial gain in the lab frame is given by $k'' = w''/v$. In the beam frame the Poynting flux is uniform in space, resulting in no net radiative power flow out of a longitudinal section of guide. The increase in stored energy, dU/dt , is then due entirely to the energy given up by the electrons to the fields, $-(1/2)\text{Re}\int dV(\mathbf{J}^* \cdot \mathbf{E})$. The modulated portion of the current density, the only portion which contributes to this integral, is related to the electric field through Vlasov's equation for the electron phase space distribution function.

In the single electron case the direct interaction of electrons with one another is ignored. The spatial modulation of the electron distribution enters the problem only through Vlasov's equation. A positive growth rate is possible for an electromagnetic wave whose phase velocity is slightly less than the beam velocity. A cold beam analysis has been performed.²⁹ The dependence of the growth rate on the velocity difference for a cold beam is a well known result and is independent of the wave supporting structure. The dependence of the growth rate on the detuning parameter, $(w - kv)(L/2v)$, is shown in Fig. 3.1.

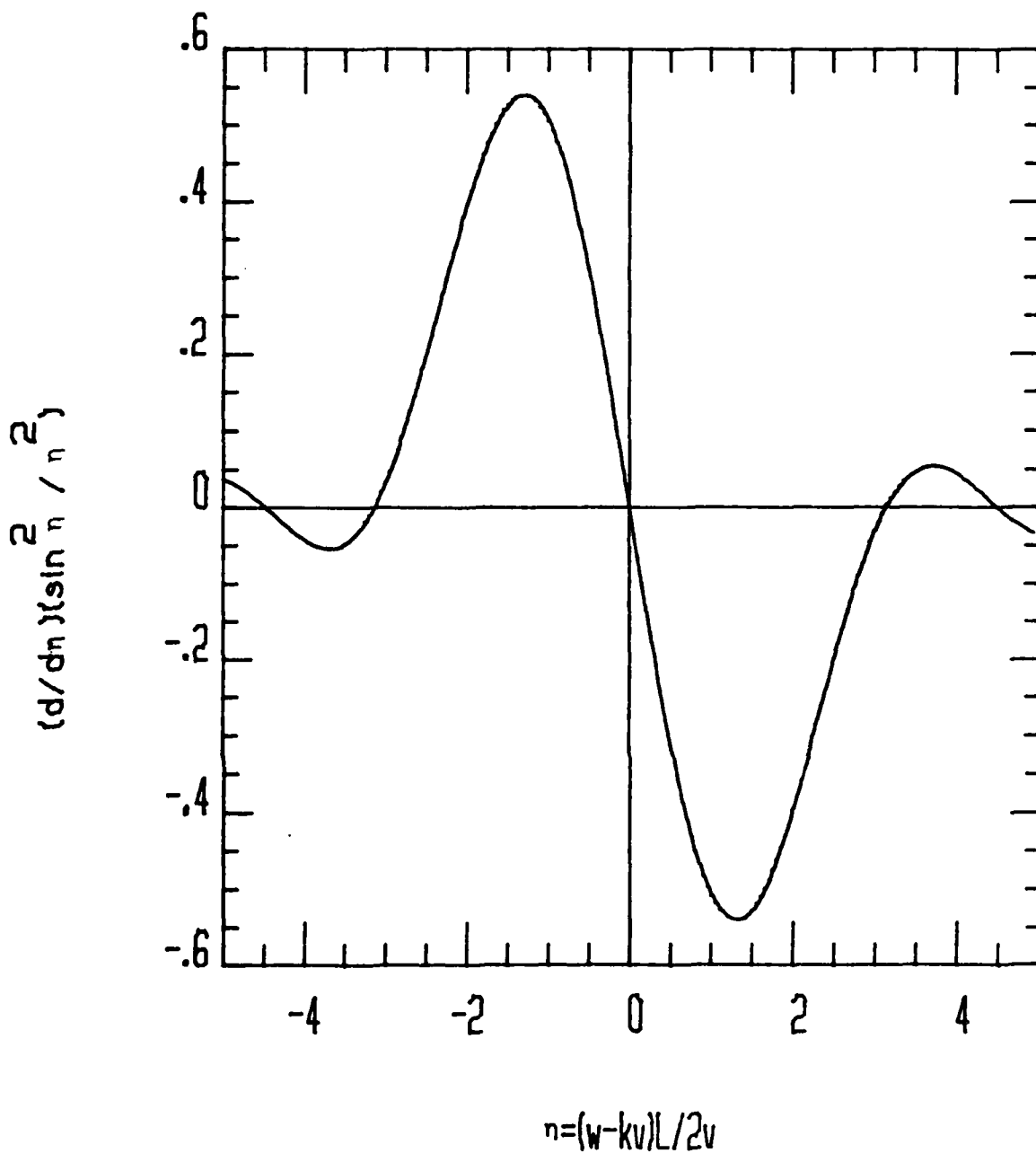


Fig. 3.1. Dependence of the single particle growth rate on the total phase shift of the radiation as seen by the beam during a transit of the liner.

Electrons may influence one another through the space charge interaction (Poisson's equation) if given sufficient time. Space charge oscillations can serve to enhance bunching. The transit time of electrons through the interaction region, L/v , must exceed the time required for a plasma oscillation, $2\pi\gamma^{3/2}/\omega_p$, where $\omega_p^2 = 4\pi ne^2/m$. In this case the growth rate can exceed that which is calculated from Vlasov's equation alone.

A direct calculation of dU/dt is now less convenient. Instead, the beam can be treated as a dielectric medium, and the beam dispersion function becomes coupled to the passive guide dispersion function. A new dispersion function is calculated, and its roots can have imaginary parts for phase velocities less than the beam velocity.

The procedure for calculating the dispersion function is analogous to the usual derivation of electrostatic plasma oscillations.^{12,30} In the cold beam limit the Vlasov equation reduces to the simple continuity equation (Eqn. 4.3). The electron density and velocity perturbations are assumed small, permitting linearization. The guide boundary conditions must still be satisfied. The dispersion functions for the single slab,³¹ double slab,¹² and cylinder¹² have been calculated. The result is given as

$$D(\omega, k, \omega_p^2) = (q) \text{tn}(qa, qb) (\text{Tn}(ipa\sqrt{\epsilon_b}, 0)/i) - p/\sqrt{\epsilon_b}, \quad (3.12)$$

where

$$\epsilon_b = 1 - w_p^2 / (\gamma^3 (w - kv)^2). \quad (3.13)$$

In the absence of a beam, Eqn. 3.12 clearly gives the earlier result (Eqn. 2.6) for $D(w, k) = D(w, k, 0)$. The roots of $D(w, k, w_p)$ are shifted from the roots of $D(w, k, 0)$ along the real and imaginary axes.

In the absence of a dielectric, Eqn. 3.12 for $D=0$ reduces to

$$(p' / \sqrt{\epsilon_b}) \text{Ct}(p' b \sqrt{\epsilon_b}, 0) = 0, \quad (3.14)$$

where $\epsilon=1$ and $a=b$. The definition $p'^2 = w^2/c^2 - k^2$ is used in anticipation of fast waves. This gives an empty guide dispersion function,

$$D(w, k, w_p^2) = (1 - w_p^2 / (\gamma^3 (w - kv)^2)) (w^2/c^2 - k^2 - x_n^2/b^2), \quad (3.15)$$

where x_n is the n th root of $\text{Ct}(x, 0)$,

$$\text{cylinder: } J_0(x_n) = 0 \quad (3.16a)$$

$$\text{double and single slabs: } \cos(x_n) = 0. \quad (3.16b)$$

The roots of Eqn. 3.15 are all real, implying no growth. For the single slab, b is taken to be infinitely large. The

usual dispersion function for electrostatic plasma oscillations, $1 - w_p^2 / (\gamma^3 (w - kv)^2)$, results, implying that a half space bounded by an infinite conducting sheet is not a waveguide.

The no-guide dispersion relation is satisfied by two modes,

$$w = kv \pm w_p^2 / \gamma^{3/2}, \quad (3.17)$$

the fast (+) and slow (-) space charge modes. Modes of this nature exist in the presence of the guide as well. Only the slow space charge (negative energy) mode can couple energy from the beam into the radiation field. The frequency spread due to the beam's velocity spread, $k\Delta v$, must be less than $2w_p^2 / \gamma^{3/2}$ in order to resolve the slow space charge mode from the fast space charge mode. This criterion can also be expressed as an upper limit on the beam's fractional energy spread,

$$\Delta\gamma / \gamma < (\beta\gamma)^2 (2w_p^2 / w\gamma^{3/2}). \quad (3.18)$$

For the typical experimental parameters, $\gamma = 1.2$, $w_p = 10^{10} \text{ sec}^{-1}$, and $w = 2 \times 10^{11} \text{ sec}^{-1}$,

$$\Delta\gamma / \gamma < .05 \quad (3.19)$$

is necessary. The real part of the beam-induced frequency shift, or detuning, is negative for the growing solution to $D(\omega, k, \omega_p^2) = 0$. Thus it can help to resolve the space charge modes.³¹ This shift is of the order of the growth rate and, as will be seen, can be a significant fraction of ω_p . A negative shift also means that the phase velocity of the wave is slightly less than the beam velocity.

In Section 3.3 the single electron growth rate is compared to the collective growth rate. For this reason the restriction on beam energy spread pertaining to the single electron case is stated below. For significant growth the detuning parameter should have the value which gives the large maximum in Fig. 3.1. Expressed as a frequency, the optimum detuning found for the single electron analysis is $-\pi v/L$. This detuning must be resolved with respect to $k\Delta v$. Thus

$$\Delta\gamma/\gamma < (\beta\gamma)^2 (\pi v/wL) \quad (3.20a)$$

or

$$\Delta\gamma/\gamma < (\beta\gamma)^2 (\lambda/2L) \quad (3.20b)$$

or

$$\Delta\gamma/\gamma < .02 \quad (3.20c)$$

for the experimental parameters above.

Energy spread is unavoidable when producing collimated charge beams, although $\Delta\gamma/\gamma = 10^{-3}$ is possible with existing technology. A particle simulation code is available to

calculate the trajectories of charged particles in the vicinity of potential surfaces and magnetic field which have rectangular or cylindrical symmetry (see App. III).³² The charges are moved a small distance in the direction of $\vec{E} + (\vec{v}/c) \times \vec{B}$. Then, the electric potential field is adjusted to satisfy Poisson's equation at all the mesh points of the simulation for the new charge distribution. Self magnetic fields are added to the external field.

The code was run for a simplified model of the beam focusing system. Mesh points were .5 millimeters apart. The maximum transverse energy is acquired by electrons at the maximum beam radius (Figures 3.2 and 3.3). It is

$$\Delta\gamma/\gamma = .023. \quad (3.21)$$

The average transverse energy, weighted by the beam density profile given by the simulation (Fig. 3.4), is

$$\Delta\gamma/\gamma = .01. \quad (3.22)$$

Thus the cold beam criteria for the collective and single electron regimes are just satisfied by the simulated beam.

The transit time of the beam through the resonator lies in the range

$$0.6 \text{ nsec} < L/v < 1.0 \text{ nsec}. \quad (3.23)$$

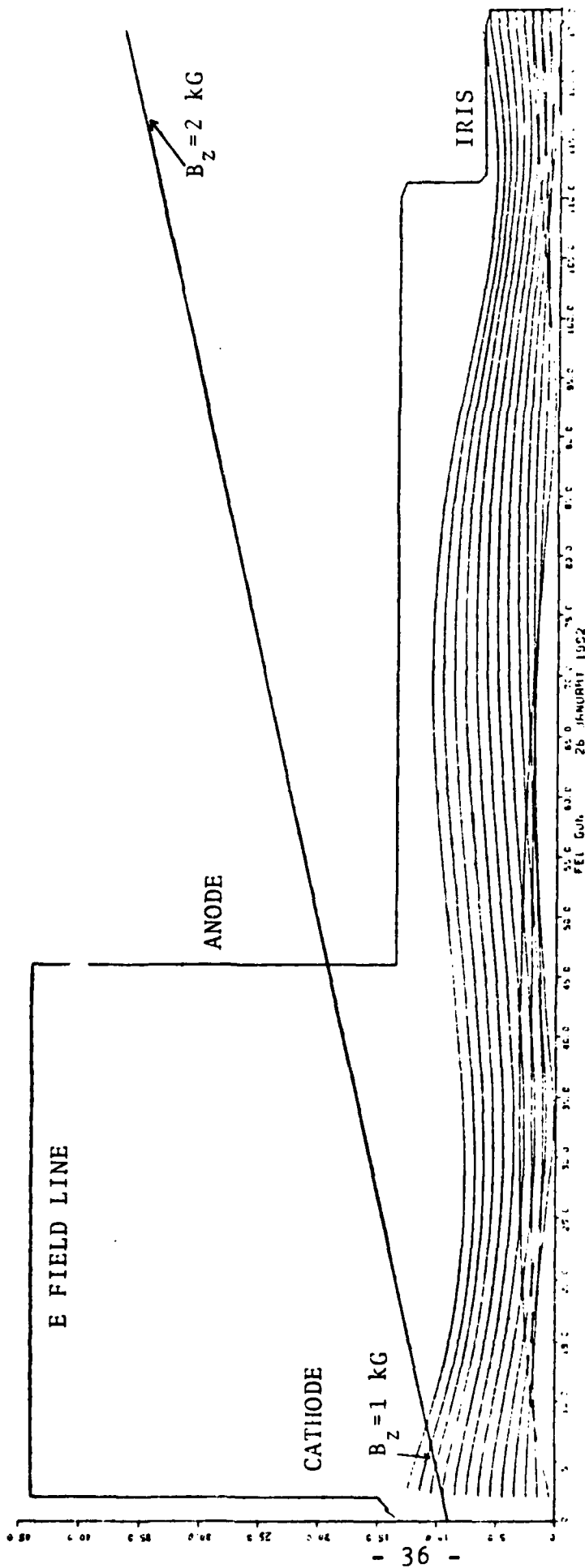


Fig. 3.2. Radius as a function of the longitudinal coordinate for beam electrons with thirteen equally spaced initial radii (far left). The outermost trajectories are least well aligned with the guiding magnetic field. The coordinates are given in mesh units. A mesh unit is defined to be .5 millimeters for this run of the particle trajectory code.

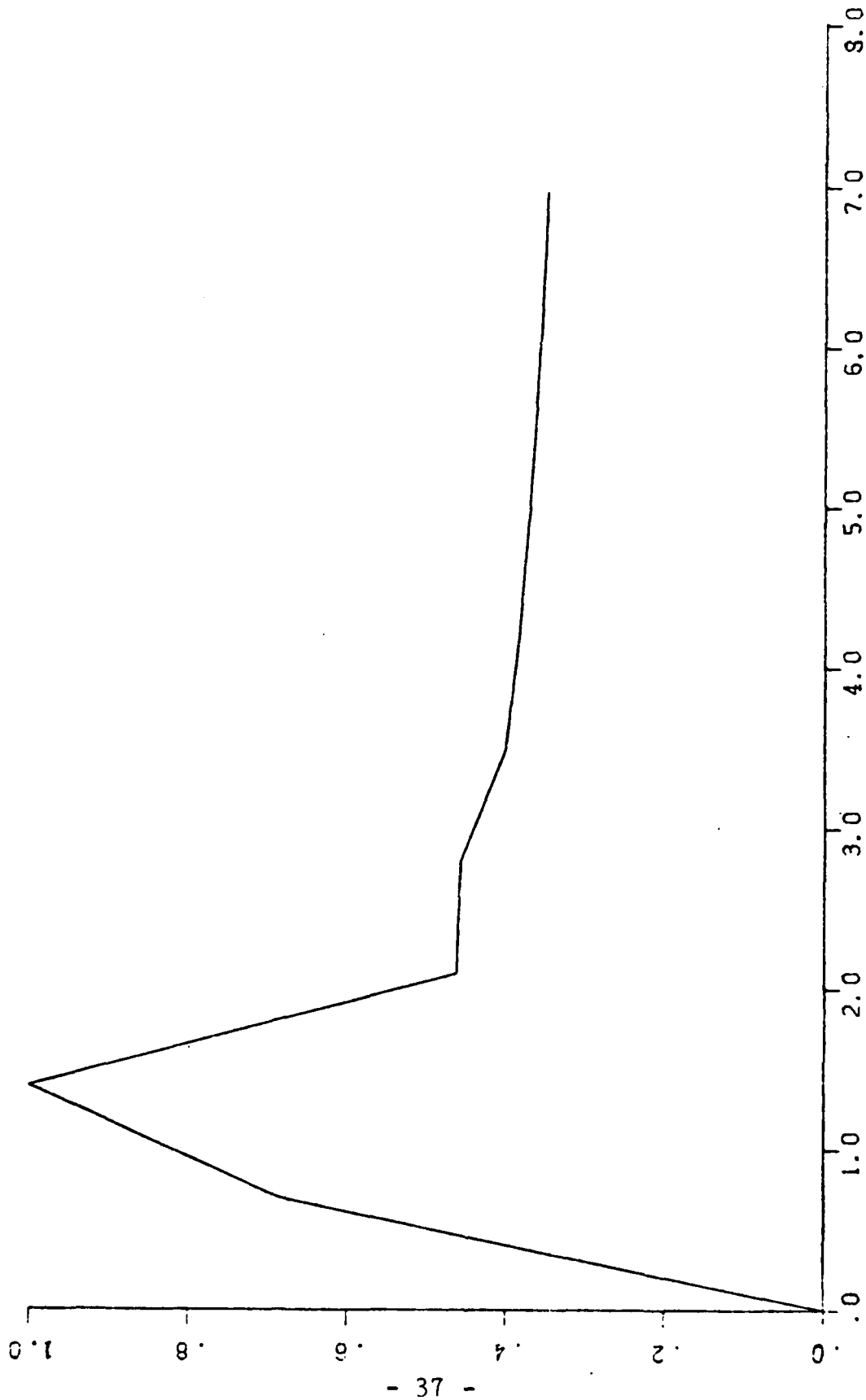


Fig. 3.3. $\text{ALPHA} = dr/dz$ is given as a function of the final radius (in mesh units) for the thirteen trajectories calculated.

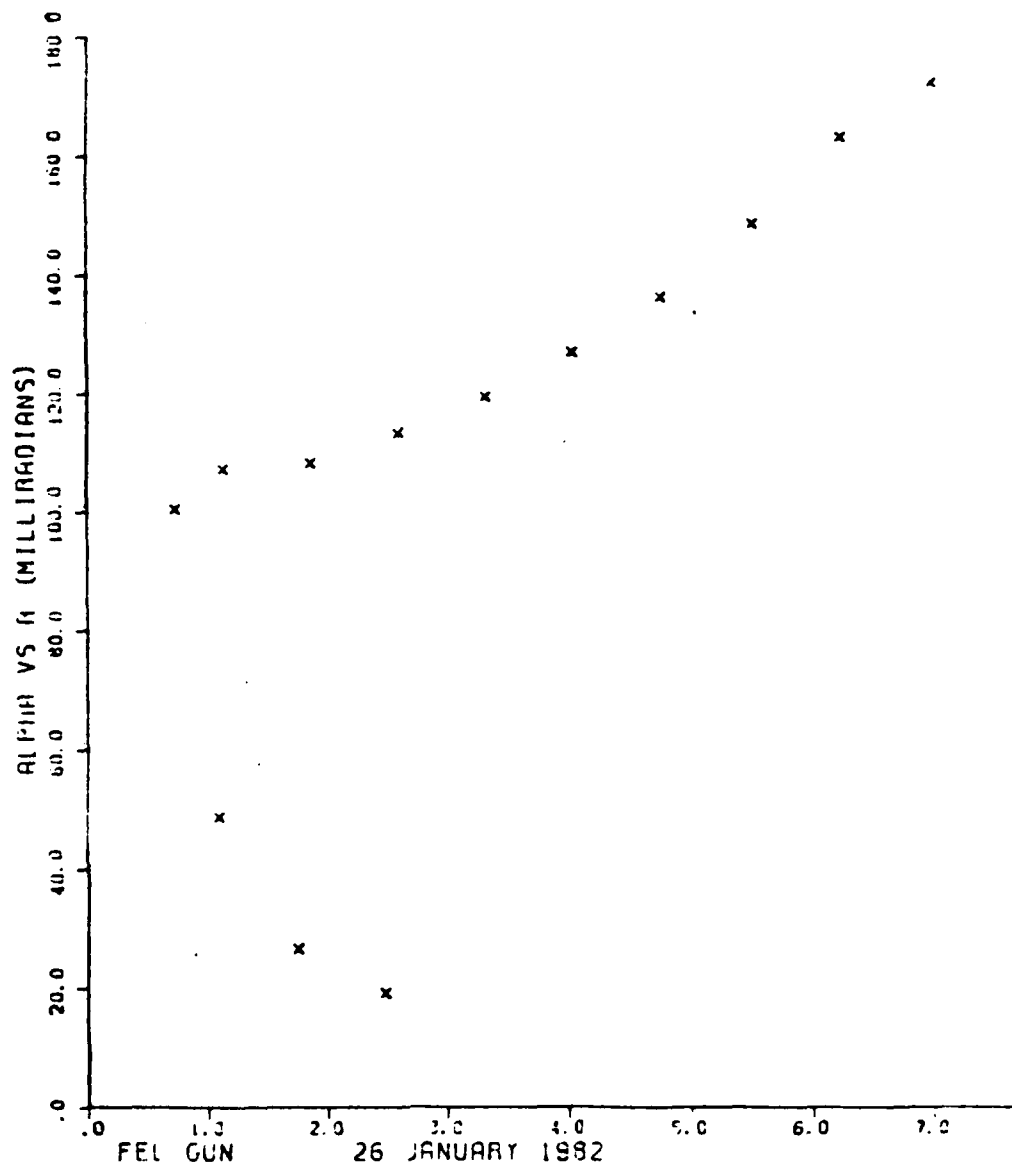


Fig. 3.4. Final simulation beam current density as a function of radius, normalized to the maximum value.

The time required for a plasma oscillation lies in the range

$$0.2 \text{ nsec} < 2\pi \gamma^{3/2} / w_p < 1.7 \text{ nsec.} \quad (3.24)$$

There is hope, then, that the space charge interaction may contribute to the growth rate.

3.3 GROWTH RATES FOR THE CYLINDER

To evaluate the collective growth rate, the complex solution to the combined dispersion relation, Eqn. 3.12, must be found. At present, codes are available which find the real solutions to the no-beam dispersion relation, Eqn. 2.6, (Appendix III). They are not capable of solving Eqn. 3.12, but could possibly be adapted to do so. Equation 3.12 has been solved in the weak beam approximation for the single slab³¹ and double slab.¹² In this approximation the detuning and growth rate due to the beam are assumed to be small with respect to w_0 . Thus $D(w, k, w_p^2)$ may be Taylor expanded about w_0, k_0 with respect to w and with respect to beam density, w_p^2 .

$$D(w, k, w_p^2) = D_0 + (w - w_0) \partial D_0 / \partial w + (w_p^2) \partial D_0 / \partial (w_p^2), \quad (3.25)$$

$$D_0 = D(w_0, k_0, 0).$$

The dispersion relation becomes

$$w - w_0 = w_p^2 (\partial D(w_0, k_0, 0) / \partial (w_p^2)) / (\partial D(w_0, k_0, 0) / \partial w). \quad (3.26)$$

For the cylinder

$$\partial D / \partial (w_p^2) = -(1/2\gamma^3 (w - kv)^2) (\epsilon p I_0(pa) / q \operatorname{sn}) (q^2 a \operatorname{sn}^2 / \epsilon - \epsilon p^2 a \operatorname{cs}^2), \quad (3.27)$$

using $D(w, k, w_p^2) = q\sqrt{\epsilon_b} I_1(p\sqrt{\epsilon_b} a) \operatorname{sn} - \epsilon p I_0(p\sqrt{\epsilon_b} a) \operatorname{cs}$. It is further assumed that the roots are near synchronism, $w \approx kv$, $k \approx k_0$.

Already knowing $\partial D / \partial w$ (Eqn. 3.9f), we have

$$(w - w_0)^3 = \frac{-w_p^2 c^2 a}{2\gamma^3 w} \cdot \frac{q^2 \operatorname{sn}^2 / \epsilon - \epsilon p^2 \operatorname{cs}^2}{(\epsilon b^2 / a) - a(\epsilon - q^2 / \epsilon p^2) \operatorname{sn}^2 - (2/q)(\epsilon - q^2 / p^2) \operatorname{sn} \operatorname{cs}} \quad (3.28)$$

$$q = w/c\sqrt{\epsilon - 1/\beta^2}, \quad p = w/c\beta\gamma.$$

Equation 3.28 has three roots for $w - w_0$: w' , $w' + iw''$, and $w' - iw''$. The detuning, w' , and the growth rate, w'' , are given by

$$w' = |(w - w_0)^3|^{1/3} \quad (3.29a)$$

$$w'' = (\sqrt{3}/2)w', \quad (3.29b)$$

The no-beam dispersion curves of Fig. 2.1 are replotted in Fig. 3.5 for the lowest TM_{0n} modes, along with $w''(k)$. The

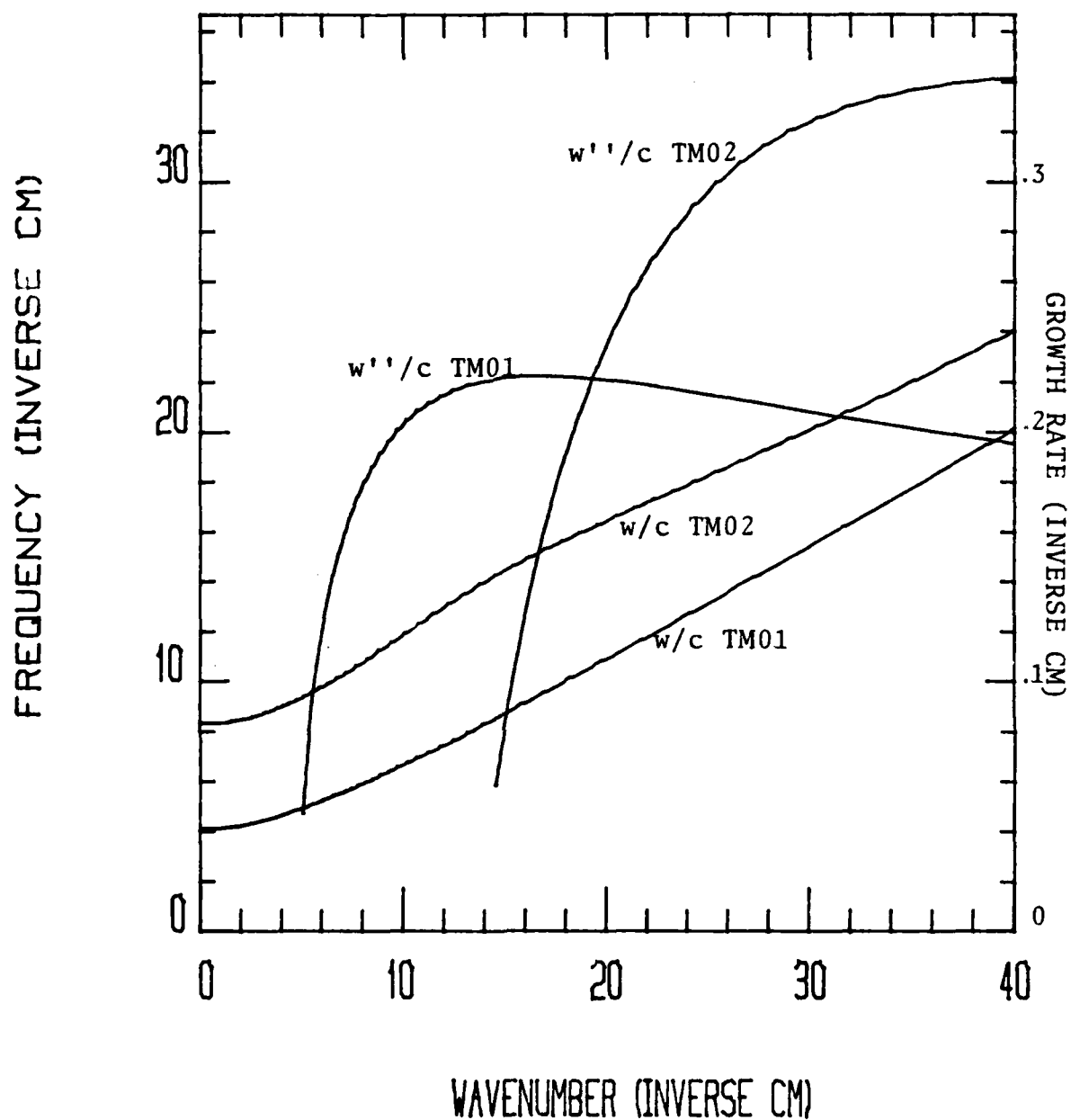


Fig. 3.5. The two lowest TM_{0n} no-beam dispersion curves and associated growth rates. At each wavenumber the beam is chosen to have a velocity synchronous with the no-beam mode and an electron density of 10^{10} cm^{-3} . The liner is two millimeter thick boron nitride in 12.5 millimeter guide.

synchronous beam velocity is assumed at each wavenumber. A significant growth rate for the TM_{02} mode is indicated and has led to output. The frequencies corresponding to TM_{02} and higher mode coupling (Fig. 3.6) lead to violation of the cold beam criteria (Equations 3.18 and 3.20). Including warm beam effects will reduce the calculated growth rates.^{13,31}

The peak gain as a function of velocity is plotted in Fig. 3.7 for several dielectric constants. Liner dimensions and electron density are chosen for comparison to a previous double slab calculation (Fig. 3.8).¹² The cylinder exhibits a sharper turn-on at threshold and a slower fall-off than the double slab. The optimum dielectric constant drops from about four to about three.

The double slab growth rate expression is given for comparison as well.

$$(w-w_0)^3 = \frac{-w_p^2 c^2}{2\gamma^3 w} \cdot \frac{a((q^2/\epsilon)\sin^2 - \epsilon p^2 \cos^2) + q \sin \cos}{(\epsilon b - a(\epsilon + q^2/\epsilon p^2)\sin^2 + 1/q(\epsilon + q^2/p^2)\sin \cos)}, \quad (3.30)$$

where $\sin = \sin(qd)$ and $\cos = \cos(qd)$. Conventional trigonometric functions replace the radial trigonometric functions. The cross term in the numerator no longer vanishes, as in the cylinder expression, and the cross term in the denominator changes by a factor of -2. The $\epsilon b^2/a$ term in the denominator of Eqn. 3.28 is now ϵa as a result of the difference in

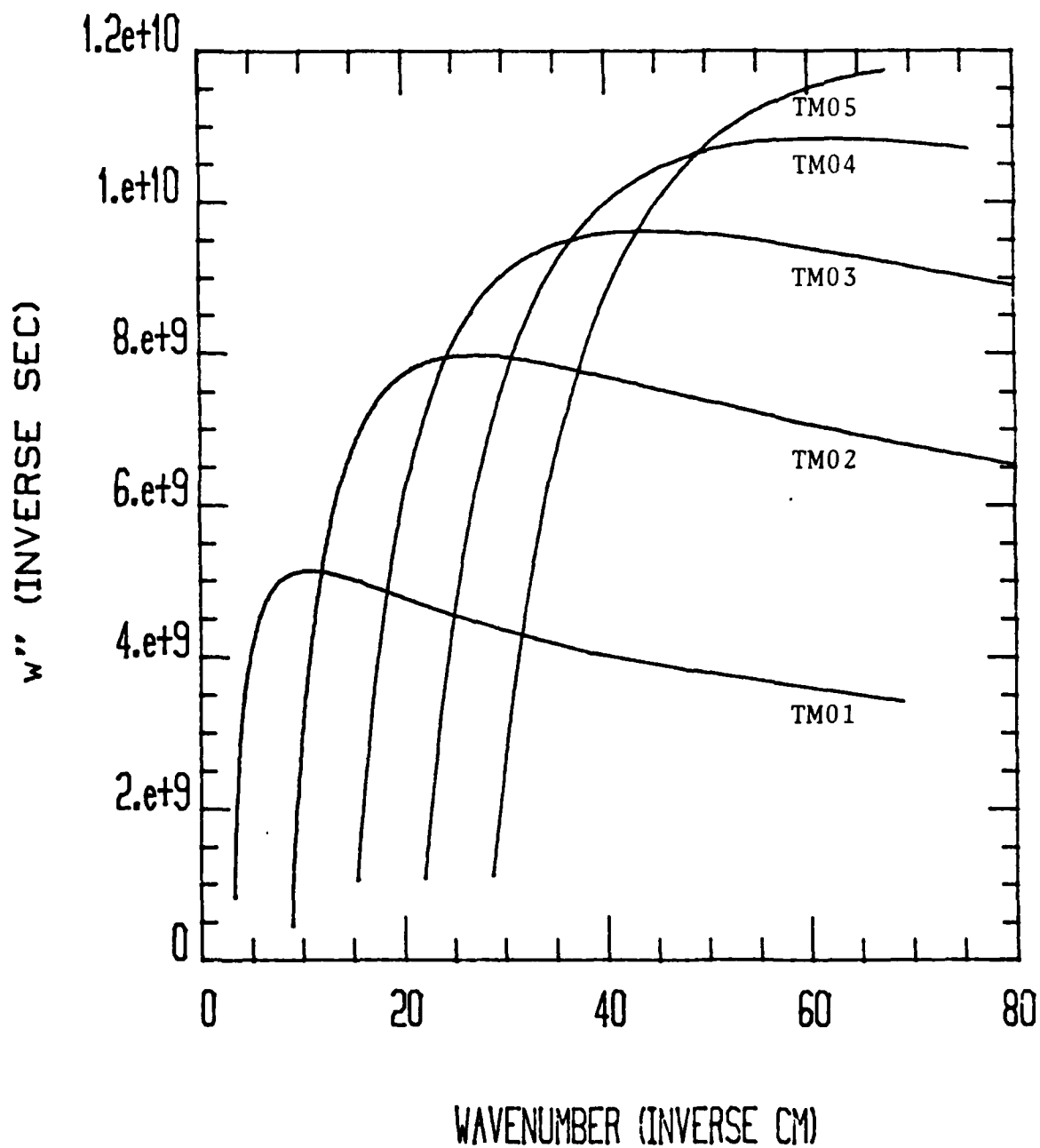


Fig. 3.6. Higher mode collective growth rates for the parameters of the previous figure.

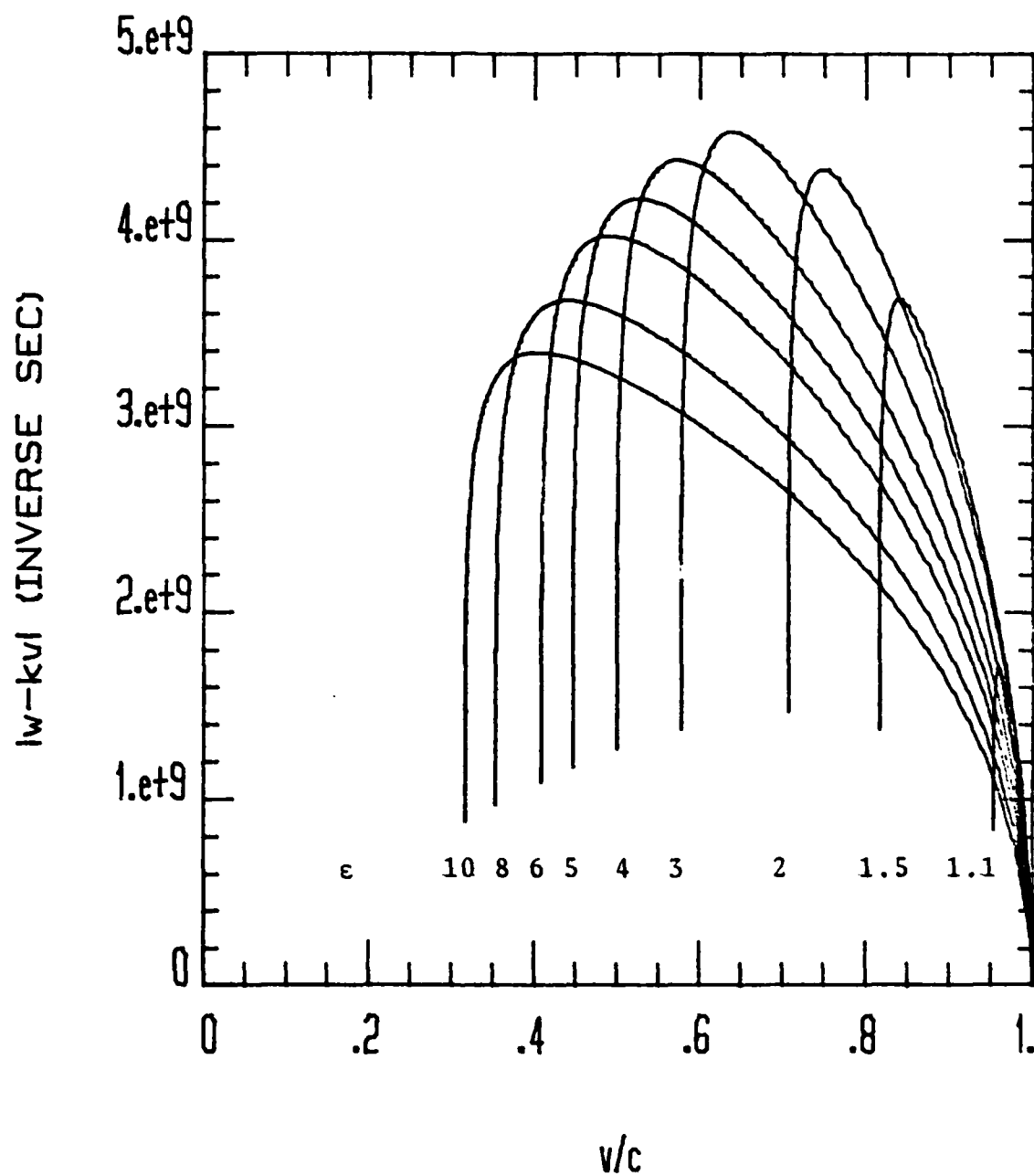


Fig. 3.7. Growth rate as a function of velocity for the TM_{01} mode of a 2.5 millimeter thick liner in ten millimeter diameter guide; $n=10^{10} \text{ cm}^{-3}$. The dielectric constant is allowed to vary. A value of three is about optimum.

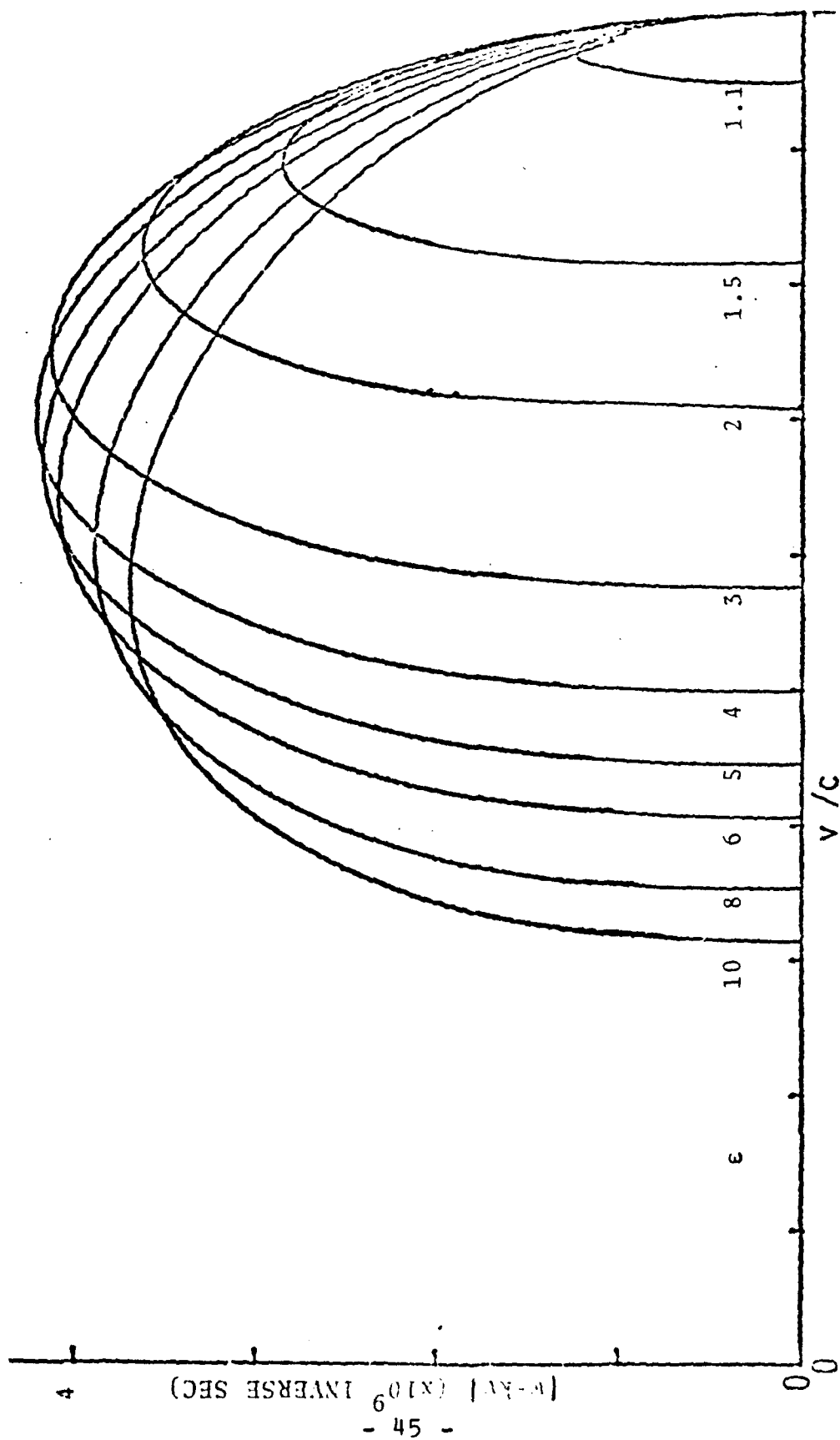


Fig 3.8. Growth rate as a function of velocity for the TM_{01} mode in the double slab geometry. The slabs are 3.5 millimeters thick; the conductors are ten millimeters apart; $n=10$ cm⁻³. The dielectric constant is allowed to vary. A value of four is about optimum. (From ref. 12).

normalization between the radial and rectangular trigonometric functions (Eqn. A1.4).

Taking the single slab limit of Eqn. 3.30 gives

$$(w-w_0)^3 = \frac{w_p^2 c^2}{2\gamma^3 w} \cdot \frac{a(\epsilon p^2 \cos^2 - (q^2/\epsilon) \sin^2) - q \sin \cos}{\epsilon d + (a/p^2)(\epsilon p^2 \cos^2 - (q^2/\epsilon) \sin^2) - (1/q)(\epsilon + q^2/p^2) \sin \cos} \quad (3.31)$$

The single slab dispersion relation gives

$$\epsilon p^2 \cos^2 - (q^2/\epsilon) \sin^2 = 0. \quad \text{Thus}$$

$$(w-w_0)^3 = \frac{w_p^2 c^2}{2\gamma^3 w} \cdot \frac{q^2}{\epsilon q d + \epsilon + q^2/p^2} = \frac{w_p^2 w}{2\gamma^3} \cdot \frac{1}{\beta^2} \cdot \frac{\epsilon \beta^2 - 1}{\epsilon q d + \gamma^2 (\epsilon - 1)} \quad (3.32)$$

The fall-off of the growth rate at threshold and at high energy, indicated by Figures 3.7 and 3.8 for the cylinder and double slab, is apparent in the expression for the single slab.

Experimentally, liner thickness is varied as well as dielectric constant. A thicker liner always results in a higher calculated growth rate, assuming the beam current can be maintained for the smaller hole diameter. Furthermore, a smaller hole sees less of the curvature present in the guide field now in use. The radial magnetic field at the ends of the liner increases with radius and with distance from the mid-plane of the guide field. This guide field curvature leaves a gap between the beam and the dielectric, degrading

AD-A122 683

CERENKOV MASER AND CERENKOV LASER DEVICES(U) DARTMOUTH
COLL HANOVER N H DEPT OF PHYSICS AND ASTRONOMY
J E WALSH DEC 82 ARO-16572.3-PH DARG29-79-C-8203

3/3

UNCLASSIFIED

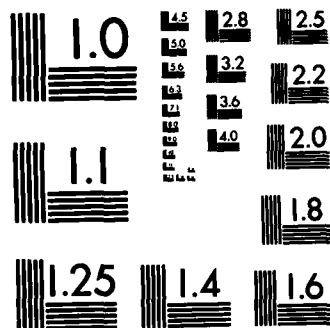
F/G 28/5

NL

END

FORMED

DTIC



MICROCOPY RESOLUTION TEST CHART
NATIONAL BUREAU OF STANDARDS-1963-A

the growth rate. The gap is largest at the mid-plane and is largest overall for a thin liner.

In order to choose a liner thickness for optimum growth rate with a particular beam generating system, the growth rate should somehow account for beam-dielectric gaps and for non-uniform beam cross sections (Fig. 3.4). In principle, one could derive a new dispersion relation for a beam, gap, and lined guide by matching the new boundary conditions for E_z and E_r at the beam-vacuum and vacuum-dielectric interfaces.³³ However, to account for beam-dielectric gaps and nonuniform beams in a more convenient manner, an effective beam parameter can be used.

An effective beam density,

$$n' = n \int_0^{r_b} E_z^2(r) r dr / E_z^2(0) \pi b^2, \quad (3.33)$$

for a solid uniform beam has already been incorporated into the calculation of a single electron growth rate for the cylinder. For the single electron case, n' is an exact effective beam density. The reason for this is that, in the Vlasov analysis for a weak beam, electrons lose energy at a rate proportional to the square of the local longitudinal electric field amplitude.

In the collective case n' serves as an approximate effective beam density. An alternate form, more useful for the collective case, is

$$n' = n \int_0^{r_b} E_z^2(r) r dr / \int_0^a E_z^2(r) r dr, \quad (3.34)$$

as $n'=n$ when the beam just fills the hole.

Without presenting any of the details of the single electron calculation, the growth rate will be evaluated in the cylindrical geometry for comparison to the collective growth rate. A general single electron expression resulting from the cold-beam Vlasov analysis²⁹ is directly quoted as

$$w'' = \frac{w}{(\beta\gamma)^3} \cdot \frac{I_b}{I_A} \cdot \frac{L^3}{V_m n} \cdot \frac{n' F \partial}{\partial n} \left(\frac{\sin^2 n}{n^2} \right). \quad (3.35)$$

Some definitions are required. I_b is the beam current, and I_A is the Alfvén current, $ec/r_0 = 17$ kA, where r_0 is e^2/mc^2 , the classical radius of an electron. V_m is the mode volume, taken to be $\pi b^2 L$ for the cylinder. n is the dimensionless single electron detuning parameter, $(w - kv)(L/2v)$, introduced in Fig. 3.1. The maximum value of the n -dependent factor, known as the lineshape function, is seen in Fig. 3.1 to be about .55. F and n' are the geometry-dependent factors.

Using Eqn. 3.33,

$$n'/n = (r_b^2/b^2)(I_0^2(pr_b) - I_1^2(pr_b)). \quad (3.36)$$

F is the ratio of the mode energy density on axis due to E_z , $|E_z(0)|^2/8\pi$, to the average total energy density, U/V_m . For the cylinder

$$F = \frac{(b^2/a)(q^2 c^2 / \epsilon w^2)(sn^2 / I_0^2(pa))}{\epsilon b^2/a - a(\epsilon + q^2/\epsilon p^2)sn^2 - (2/q)(\epsilon + q^2/p^2)sn cs}, \quad (3.37)$$

where again $sn=sn(qa, qb)$ and $cs=cs(qa, qb)$.

The resulting velocity dependence of the growth rate with the lineshape function held at .55 is shown in Fig 3.9 for the parameters of Figures 3.7 and 3.8. The growth rates are low but not insignificant. The optimum dielectric constant is about seven in this case.

In Fig. 3.10 the liner thickness is varied while holding the beam radius and guide diameter constant. The growth rates fall off sharply as the gap between the beam and the liner widens. Use of the single electron effective beam density (Eqn. 3.34) for the collective calculation gives similar behavior (Fig. 3.11). In both cases, the peak growth rate shifts to higher velocities as the gap widens and milder E_z evanescence becomes more important.

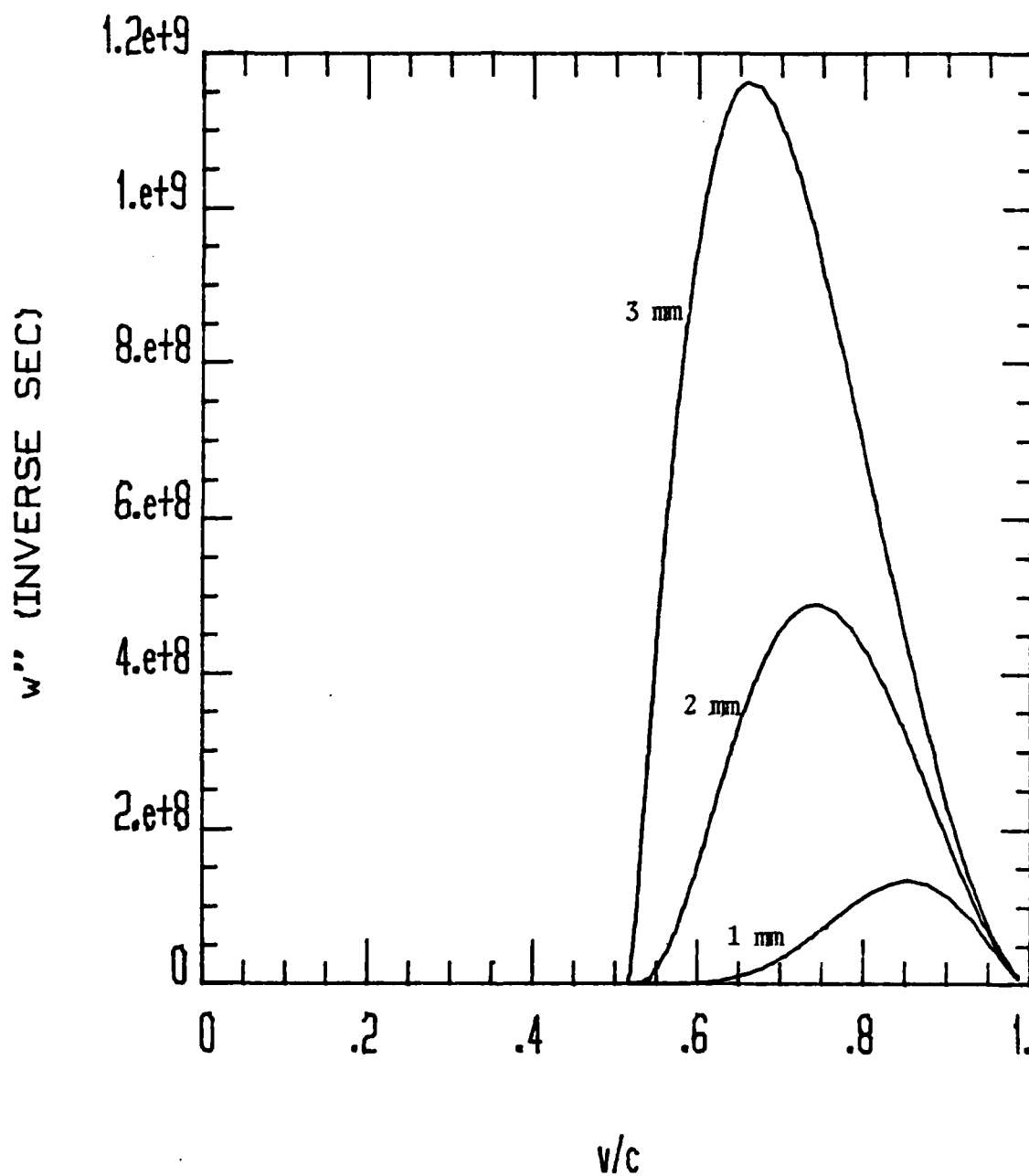


Fig. 3.10. Single electron growth rate for different liner thicknesses. The beam radius is held at three millimeters. The guide diameter is 12.5 millimeters.

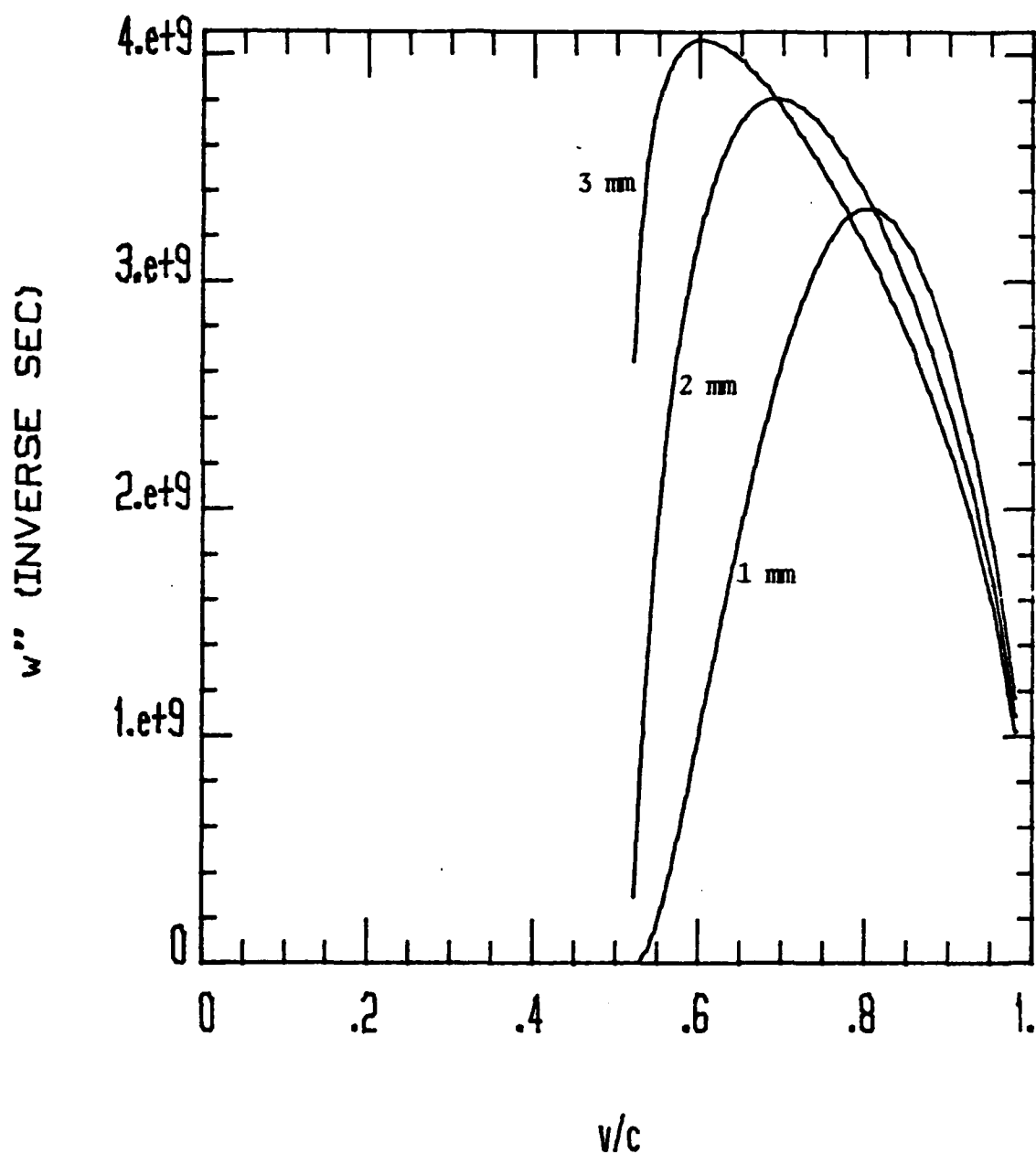


Fig. 3.11. Collective growth rate ($w'' = 3/2|w - kv|$) for different liner thicknesses. The beam radius is held at three millimeters. The guide diameter is 12.5 millimeters. An effective beam density is used to account for the gap between the beam and the dielectric.

CHAPTER IV

4.1 FEEDBACK

In order for the present device to produce high power, it must operate as a feedback oscillator. The guide field geometry restricts the interaction region to a maximum length of about 15 cm. This severely limits the power available through single pass amplification.

Experimental evidence for multiple passes through the liner by the radiation helps to explain the observation of large output signals. Most noticeable is the increased beam energy necessary for oscillation when the impedance mismatch at either end of the liner section is made less drastic. Also, output is preferred at a set of discrete beam velocities, coupling to the appropriate TM_{01} synchronous frequencies. This set of discrete frequencies must be those for which the multiply reflected waves traveling downstream add constructively.

In a multiple pass, oscillator system the round trip growth must exceed the round trip loss. The beam is assumed not to interact with waves traveling upstream. Thus

$$w'T > -\ln R_d - \ln R_u, \quad (4.1)$$

where T is the one-way transit time, L/v , and R_u and R_d are the fractions of incident power left in the original mode after reflection upstream and downstream respectively. All losses due to absorption are assumed to be negligible. Ideally, R_u should be unity if all the power is to be coupled out downstream. The fields are concentrated in the liner for $w/k < c$, allowing a reflective washer to achieve high R_u at the upstream end of the liner.

A scheme for adiabatically compressing an annular beam in the region between an on-axis reflector and the liner has been proposed.³⁴ Such a scheme presents difficulties with respect to beam dynamics and millimeter wave optics, but the added efficiency may be worth the effort for some applications.

Reflections from several downstream elements are possible. Tapers, bends, and horns should reflect a negligible amount; the vacuum window and the circular to rectangular mode transducer may contribute a bit more. The reflections from the downstream end of the liner section and the Fabry-Perot interferometer are the most significant and help to explain some experimental observations.

The liner geometry is shown in Fig. 2.3. An upper limit to the reflection obtained at the interface between the lined and empty guides will be that obtained at an infinite dielectric-vacuum interface.³⁵ The angle of incidence is non-zero for TM modes. In terms of the longitudinal wavenumbers, k and k' , for the dielectric and the vacuum,

$$R_d = ((k/\epsilon - k')/(k/\epsilon + k'))^2. \quad (4.2)$$

The same expression is obtained for the junction of a completely filled guide and an empty guide with k and k' evaluated for the TM_{01} modes.³⁶

The reflection at the end of the lined guide is actually lower for two reasons: (1) because not all of the electric field is in the liner, the effective dielectric constant in the lined guide is less than ϵ ; and (2), the radial non-uniformity of the lined guide will cause higher TM_{0n} modes to be launched and reflected. These reduce the power reflected in the TM_{01} mode in a way not described by Eqn. 4.2.

The data in Fig. 4.1 indicate a dependence on end reflectivity for the threshold beam voltage. The tapered end is less reflective than the square end, and a check can now be made as to whether or not feedback from the end of the square end liner is sufficient to explain the output at the lower voltage.

The dispersion relations for the lined and empty guides give k and k' . For the loss at the end of the liner, $-10 \log R_d$, the value 9.5 dB is obtained at 50 GHz and 10.8 dB at 30 GHz. The additional loss obtained by tapering the end would be at least 10 dB for a final liner thickness of zero.³⁷ However, the final thickness achieved was still about half the original thickness. Thus only a few dB of additional loss are guaranteed.

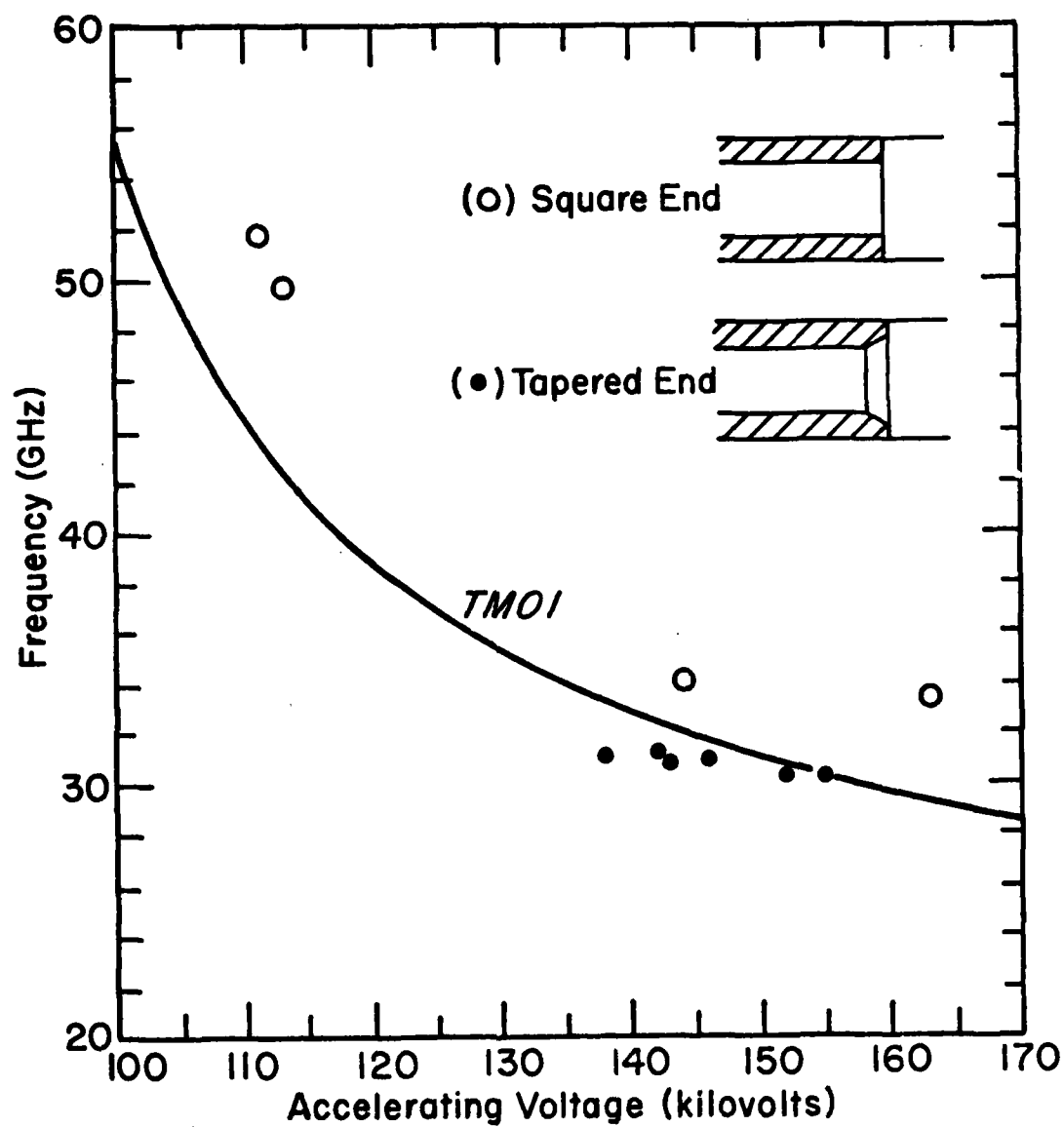


Fig. 4.1. Frequency measurements for two different two millimeter thick quartz liners in 12.5 millimeter guide.

The growth rate for the lower voltage, 50 GHz, output is significantly lower than the growth rate for the higher voltage, 30 GHz output, if the gap between the beam and the liner is accounted for by an effective beam density. The gap is about one millimeter. The middle curve in Fig. 3.11 gives these growth rates assuming $n=10^{10} \text{ cm}^{-3}$ (e.g. a 7.5 ampere beam of uniform cross section with velocity $.55c$ and radius three millimeters).

The square end liner experiment employed a 20 ampere beam (Fig. 4.2) with $L=15 \text{ cm}$ giving $w''T=8.4 \text{ dB}$ at 50 GHz and $w''T=13.2 \text{ dB}$ at 30 GHz. Thus the oscillation criterion, Inequality 4.1, is almost satisfied by the square end liner at 50 GHz and well satisfied at 30 GHz. The approximations made in calculating w'' may have led to an artificially low result. The detuning and the plasma frequency which are assumed to be small, are each about 4% of w_0 .

If the 50 GHz oscillation is assumed to take place just above threshold, then a few dB of additional loss due to tapering will quench it, but can still permit oscillation in the higher growth rate region near 30 GHz, as the data indicate. Removal of the upstream copper reflector will also increase losses and, indeed, was found to increase the voltage threshold.

The interferometer (Fig 2.4) can be a source of feedback. The reflectivity of the perforated brass mirrors is well above 90% at 35 GHz. The largest uncontrolled loss of signal is by

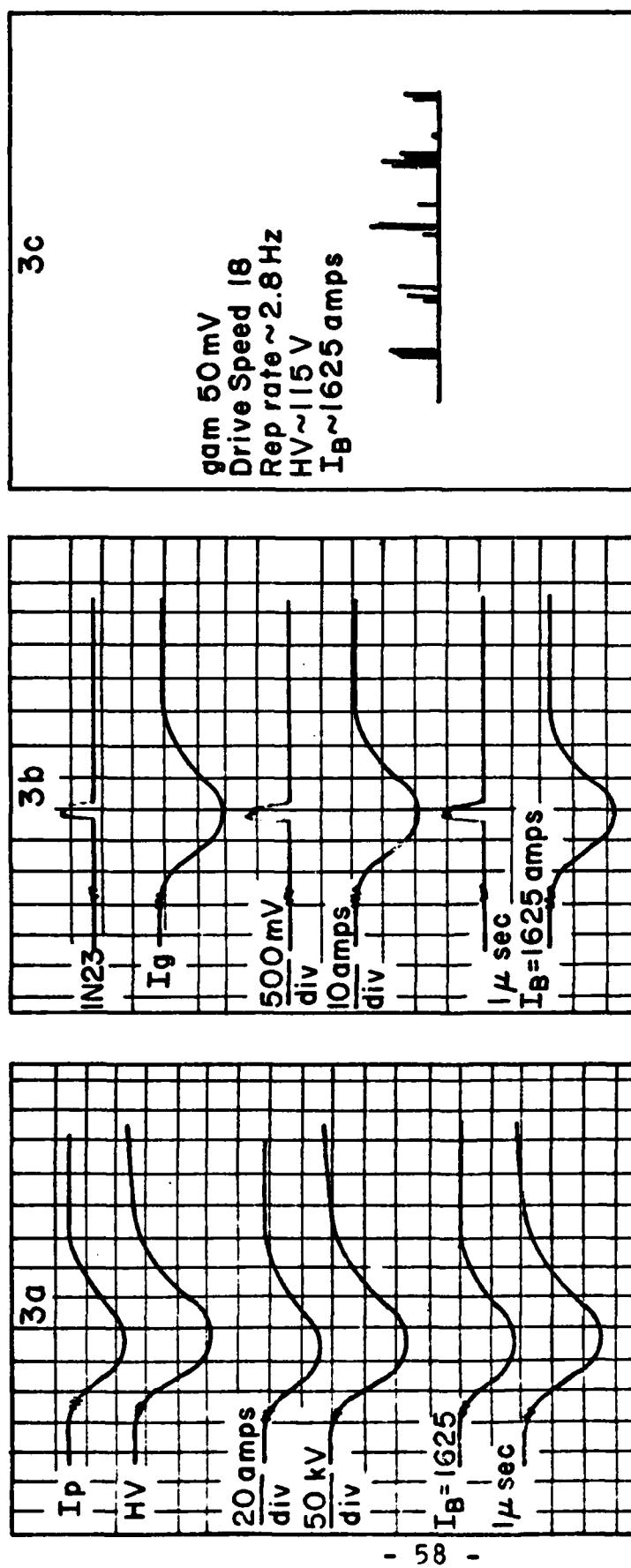


Fig. 4.2. (a) The time dependence at one microsecond per division of the current (I_p) and voltage (HV) at the cathode. (b) The microwave signal on a 1N23 detector diode in coupled off X-band waveguide and the current (I_g) collected on the downstream waveguide. (c) The throughput of the interferometer peaks at every three millimeters of mirror separation, indicating an output wavelength of six millimeters (50 GHz). (Taken 09-28-81.)

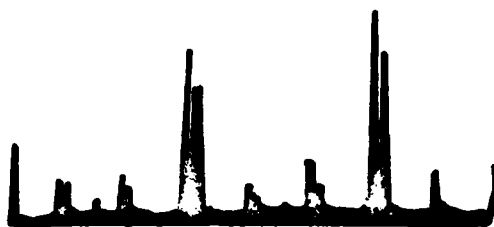
scattering out of the open cavity formed by the launching horn, collimating lens, and upstream mirror. Feedback is normally reduced further by a waveguide attenuator, intended primarily to protect the diode detector of the interferometer. Even so, a reflected signal only 10 dB down is possible.

When the interferometer is tuned to the output, both the transmission through to the detector and the reflection back to the liner are maximized. Amplified feedback should, in this configuration, result in line-narrowing. The interferograms in Fig. 4.3 have narrower than normal linewidths. They also have signals at mirror separations tuned to harmonics of the output, which are simply higher order modes of the interferometer. The presence of harmonics is enhanced for a sharply tuned driving signal. This effect is important to the operation of frequency-doubled and frequency-tripled lasers and musical instruments.

Once the threshold oscillation condition, Inequality 4.1, is satisfied, whatever the source of feedback, the beam pulse duration of 100 to 1000 transit times guarantees the survival of only self-reproducing cavity modes. At a given point in the waveguide, the signal will have the same phase after each round trip. The TM_{01} or TM_{02} fields can satisfy this condition only at a discrete set of frequencies or longitudinal modes.

Observation of this effect is simplified by the slow rise time of the single stage pulse forming network currently in

23 Nov. '81 4C
Rep Rate 3.5
Drive Speed 20



30 Nov '81 11C
Rep Rate 5 Hz
Drive Speed 18
Gain 5 mV

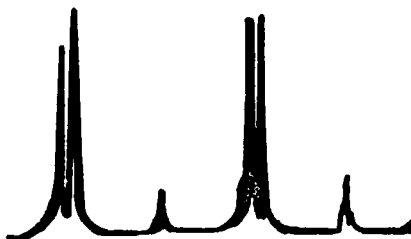
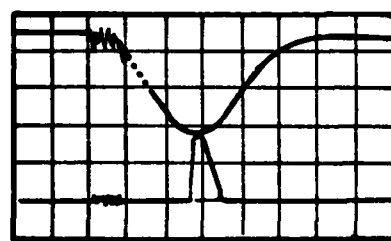


Fig. 4.3. Interferograms for two millimeter thick boron nitride indicating some control over the signal by the interferometer.

use. Output is most often generated when the beam is at its peak voltage as in Fig. 4.4a. A small increase in the peak voltage, which is insufficient to reach synchronism with the adjacent longitudinal mode, often leads to output on the original mode. However, the output is now generated when the beam voltage is at its original peak value, earlier or later in the pulse than the new peak, or both earlier and later. (Figures 4.4b, 4.4c, and 4.4d).

Fig. 4.5 shows the signal behavior as the beam voltage is swept from oscillation threshold to about twice that value. Only three values of the beam voltage correspond to output. When such a value is realized for only a short time, as on the rise of the beam pulse, the duration of the output is shorter. The synchronous frequencies corresponding to these voltages are spaced a few GHz apart as confirmed by interferograms. Normally, when Inequality 4.1 is satisfied, the single pass gain is high enough to generate output, masking the multiple pass behavior somewhat.

The frequency measurements for the tapered liner (Fig. 4.1) show little variation over a wide voltage range. Preference for a particular axial mode is indicated by these measurements and by the output pulse locations, with respect to the peak beam voltage, during the same measurements.



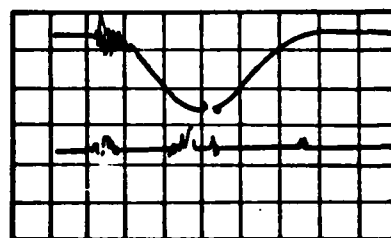
50 kV/div, 20 mV/div

(a)



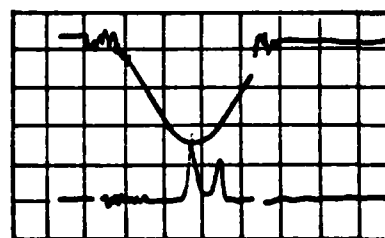
50 kV/div, 100 mV/div

(b)



100 kV/div, 50 mV/div

(c)



50 kV/div, 50 mV/div

(d)

Fig 4.4. With a three millimeter thick stycast liner, output occurs when the beam is synchronous with one of the axial modes of the resonating cavity, not necessarily at the peak beam voltage. The top trace shows the beam voltage. (One microsecond per division.) (Taken 10-28-81.)

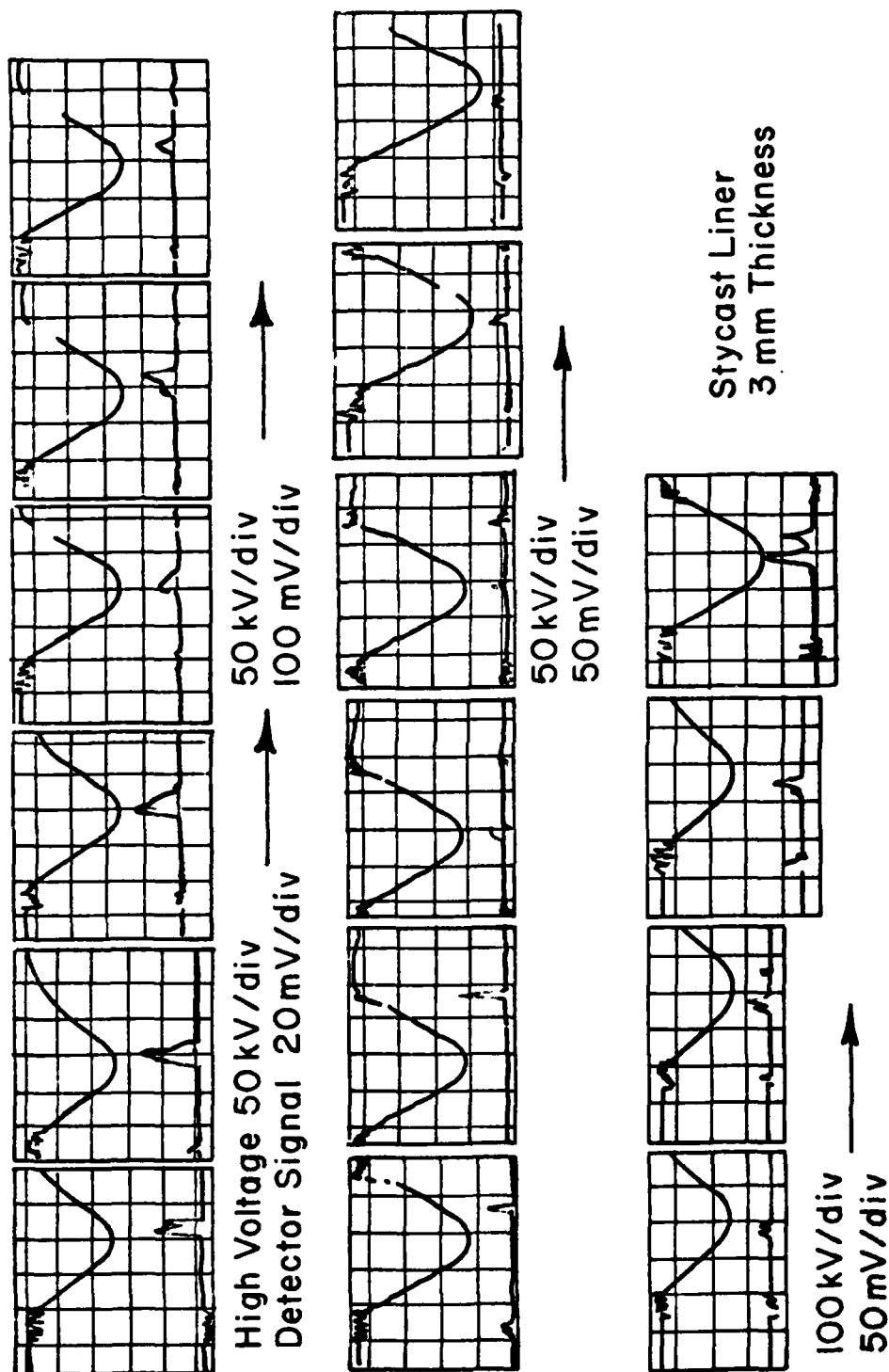


Fig. 4.5. The behavior of the styrcast liner output as the beam voltage is gradually increased (from left to right and top to bottom). (Taken 10-28-81.)

4.2 OUTPUT POWER

Having determined that the feedback and growth rate are sufficient for oscillator operation, an estimate of the output power is necessary. It is noted that, for single pass amplification, the output power should scale as $e^{w'T}$. Since an input signal is not provided, the coefficient of this exponential depends on the degree of pre-modulation undergone by the beam during acceleration and focusing, and is difficult to predict. Multiple passes lead to much larger power. The restrictions on exponential growth lead to an estimate of the achievable power.

The linearized analysis which gives the collective dispersion function, Eqn. 3.12, assumed an electron density of the form $n_0 + n_1 e^{i(\omega t - kz)}$, $n_1 \ll n_0$.¹² As the radiation field amplitude grows, so does the bunched portion of the beam, n_1 . Eventually, $n_0 = 0$, contrary to the assumption, and the dispersion function is no longer correct.

The continuity equation,

$$\partial n / \partial t + \nabla \cdot (n \vec{v}) = 0, \quad (4.3)$$

becomes

$$(-i\omega + ikv_0 + ikv_1)n_1 = 0. \quad (4.4)$$

where $v = v_0 + v_1 e^{i(\omega t - kz)}$. Equation 4.4 is satisfied when kv_1 is equal to the original detuning, $\omega - kv_0$.

The force equation, $\partial(\gamma m v)/\partial t = -eE_z$, which assumes v_0 and v_1 parallel to the strong guiding magnetic field, now gives the electric field in terms of known quantities.

$$\vec{E}_{\text{saturating}} = i(m/e)\gamma^3(\omega - kv_0)v_1^2 \quad (4.5a)$$

or

$$|\vec{E}_{\text{sat}}| = (m/e)\gamma^3(\omega - kv_0)^2/k, \quad (4.5b)$$

where Eqn. 3.28 is used to evaluate $\omega - kv_0$. When the longitudinal electric field component reaches this value, the collective gain mechanism begins to saturate.

The entire beam cross section will see a field at least as large as that given by Eqn. 4.5b when the field at $r=0$ reaches that value. With this convention, the saturating power is given by multiplying Eqn. 3.8c by Eqn. 3.9e. The coefficient, B , in Eqn. 3.8c is set equal to $|\vec{E}_{\text{sat}}|$. Fig. 4.6 shows the behavior of the saturating power along a dispersion curve. Figures 4.7 and 4.8 show the voltage and current dependence. If only the beam cross-sectional r.m.s. average E_z is required to reach $|\vec{E}_{\text{sat}}|$, the power at saturation will be less, as shown in Figures 4.9, 4.10, and 4.11. A beam radius of six millimeters corresponds to a one millimeter gap.

At a fixed voltage the growth rate is proportional to $I_b^{1/3}$, regardless of the choice of saturation criterion.

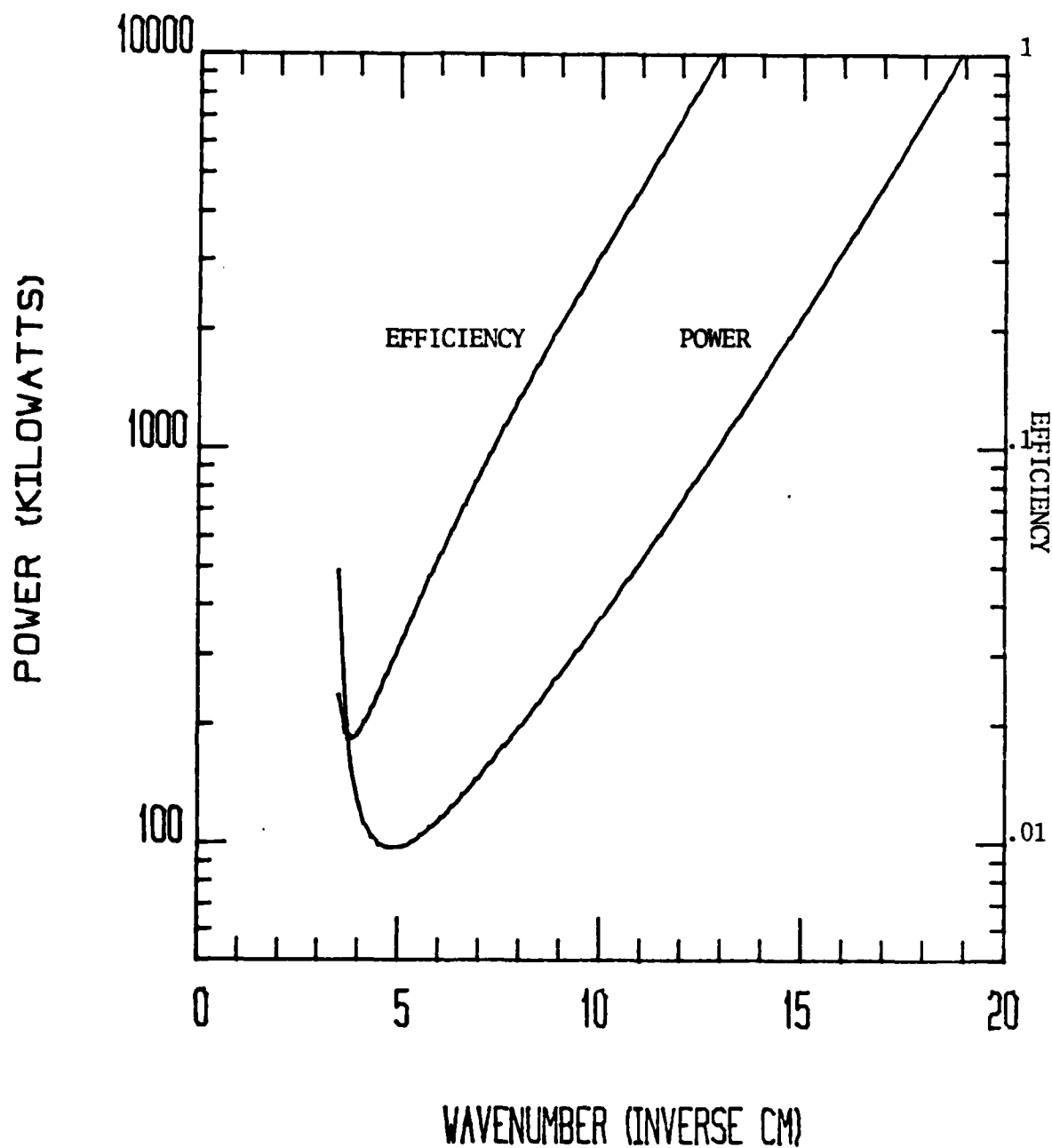


Fig. 4.6. The saturating power and efficiency, defined as the saturating power divided by the beam power, for a two millimeter thick boron nitride liner in 12.5 millimeter guide. The beam current is held at ten amperes.

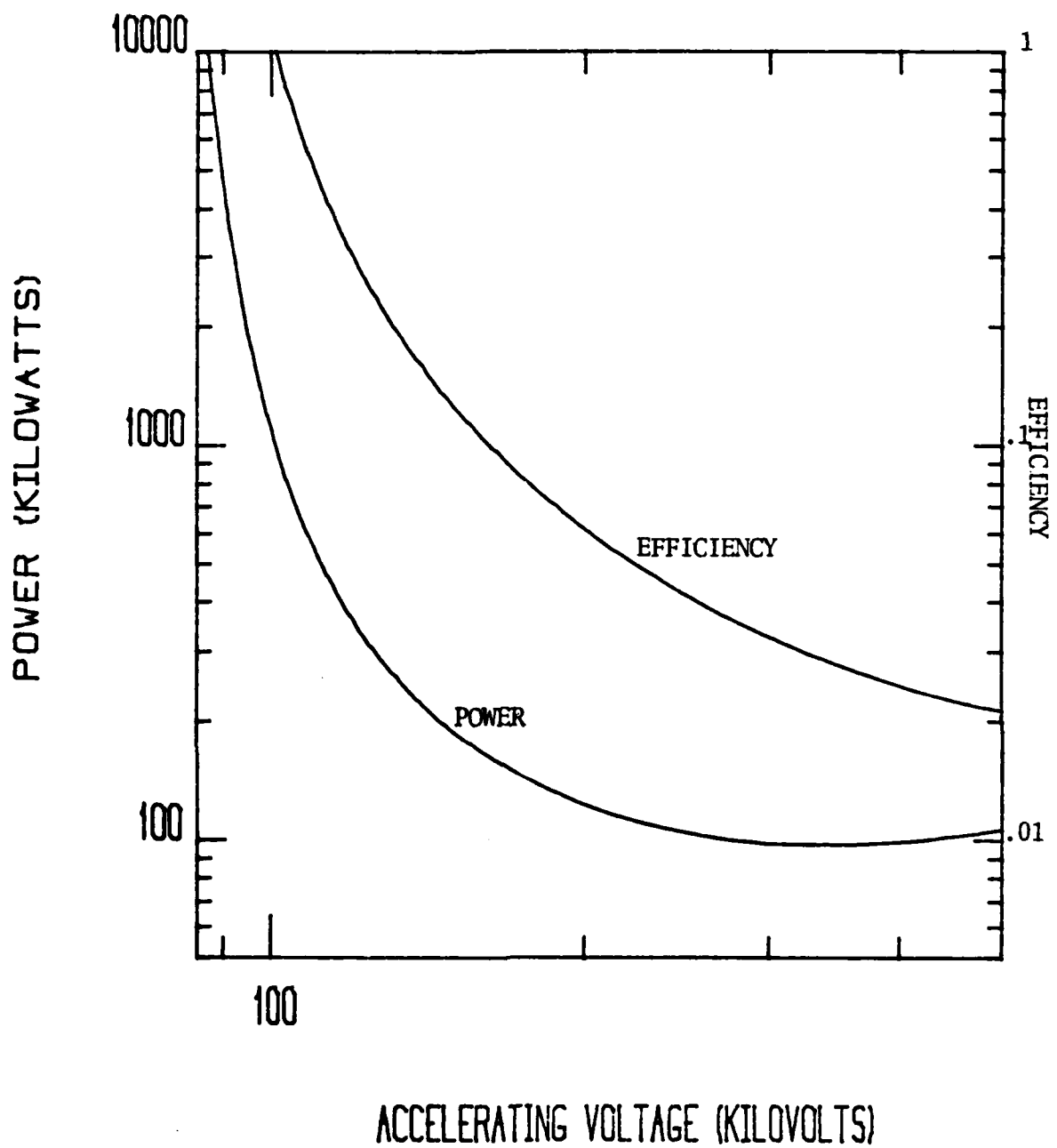


Fig. 4.7. The saturating power and efficiency from the previous figure as a function of beam voltage.

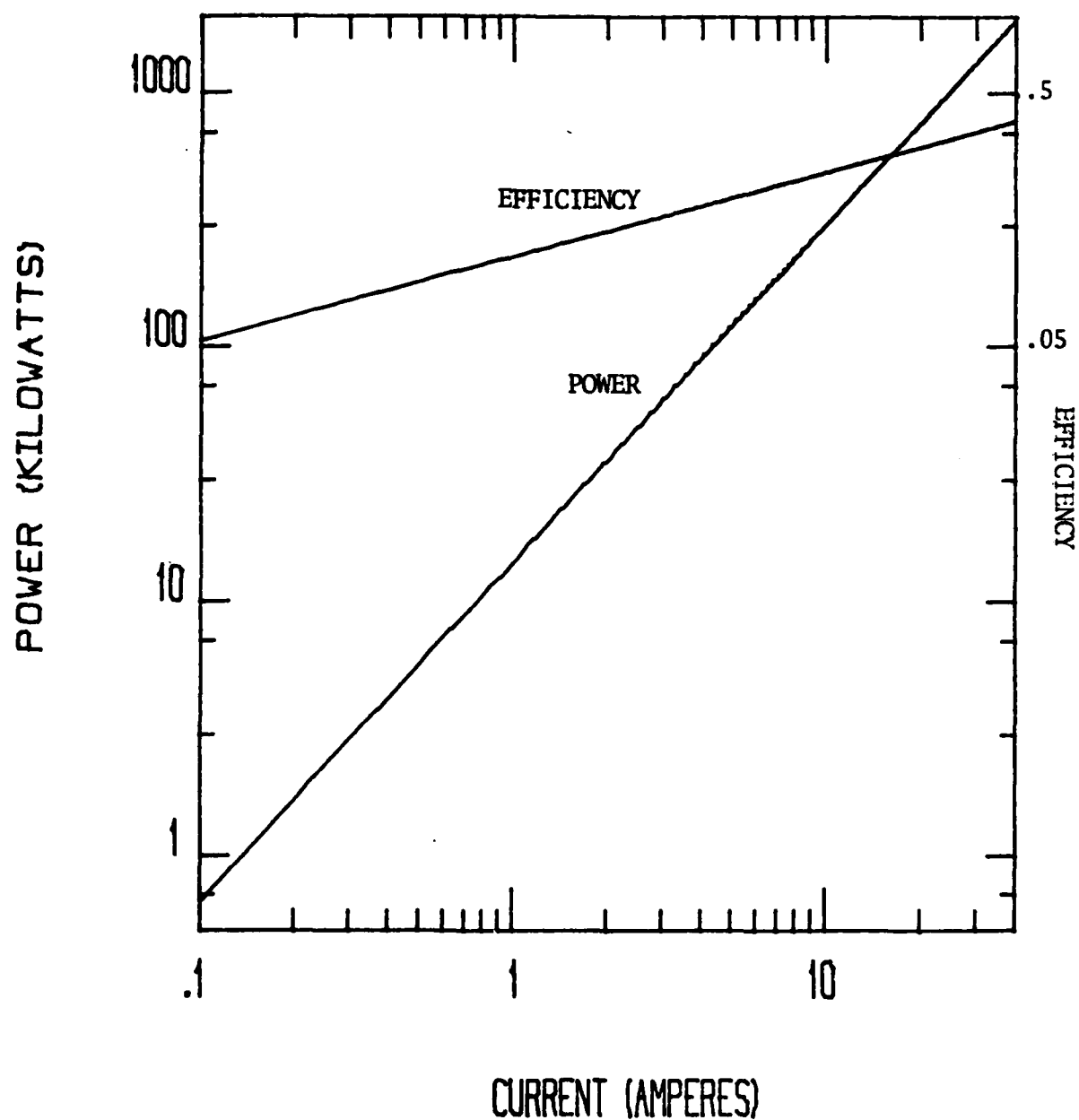


Fig. 4.8. Saturating power and efficiency vs. current for a two millimeter thick boron nitride liner in 12.5 millimeter guide and a constant 125 keV beam.

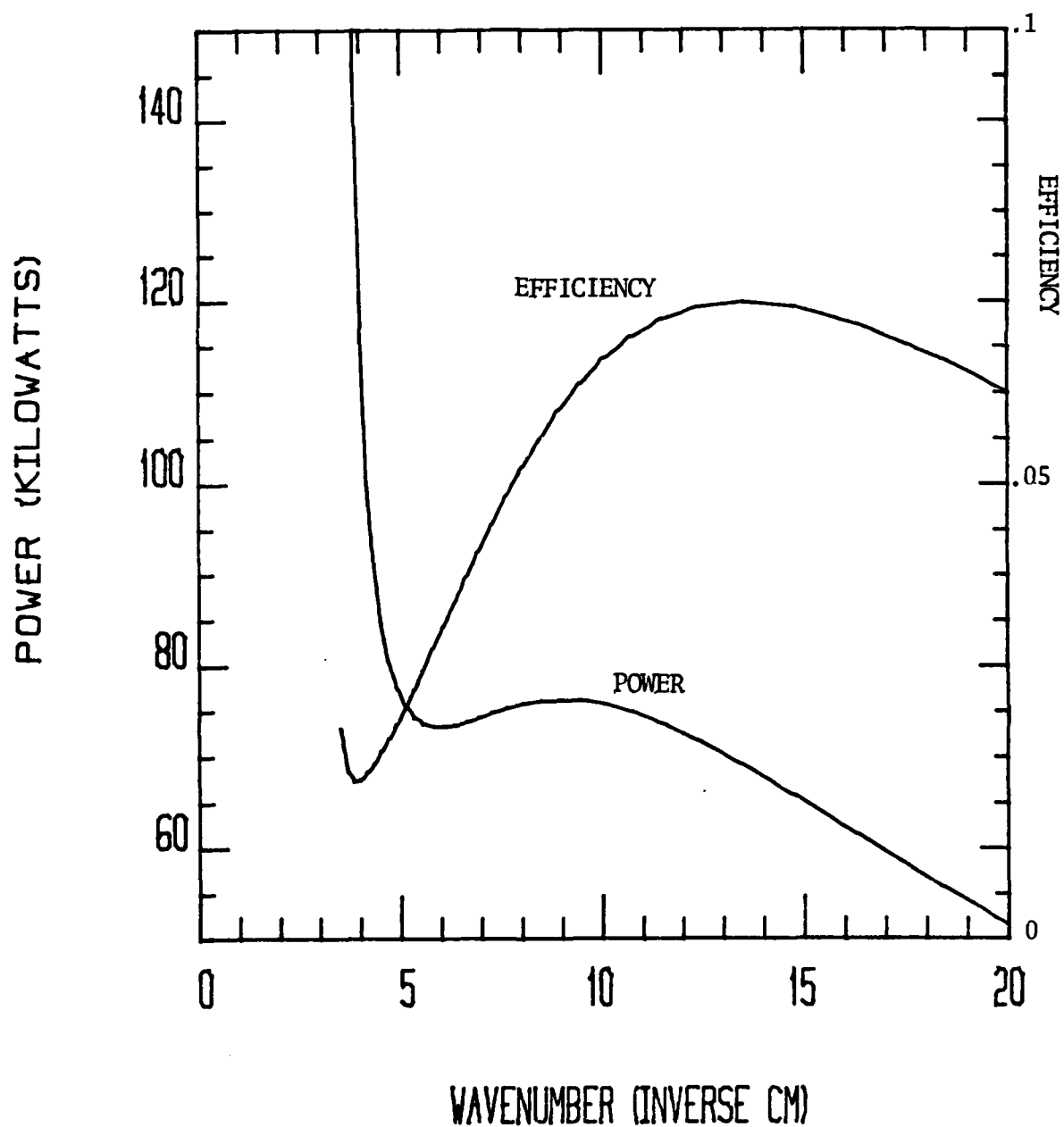


Fig. 4.9. Saturating power and efficiency for a two millimeter boron nitride liner. An effective beam density is used to account for a beam diameter of six millimeters. The gap between the beam and the dielectric is about one millimeter.

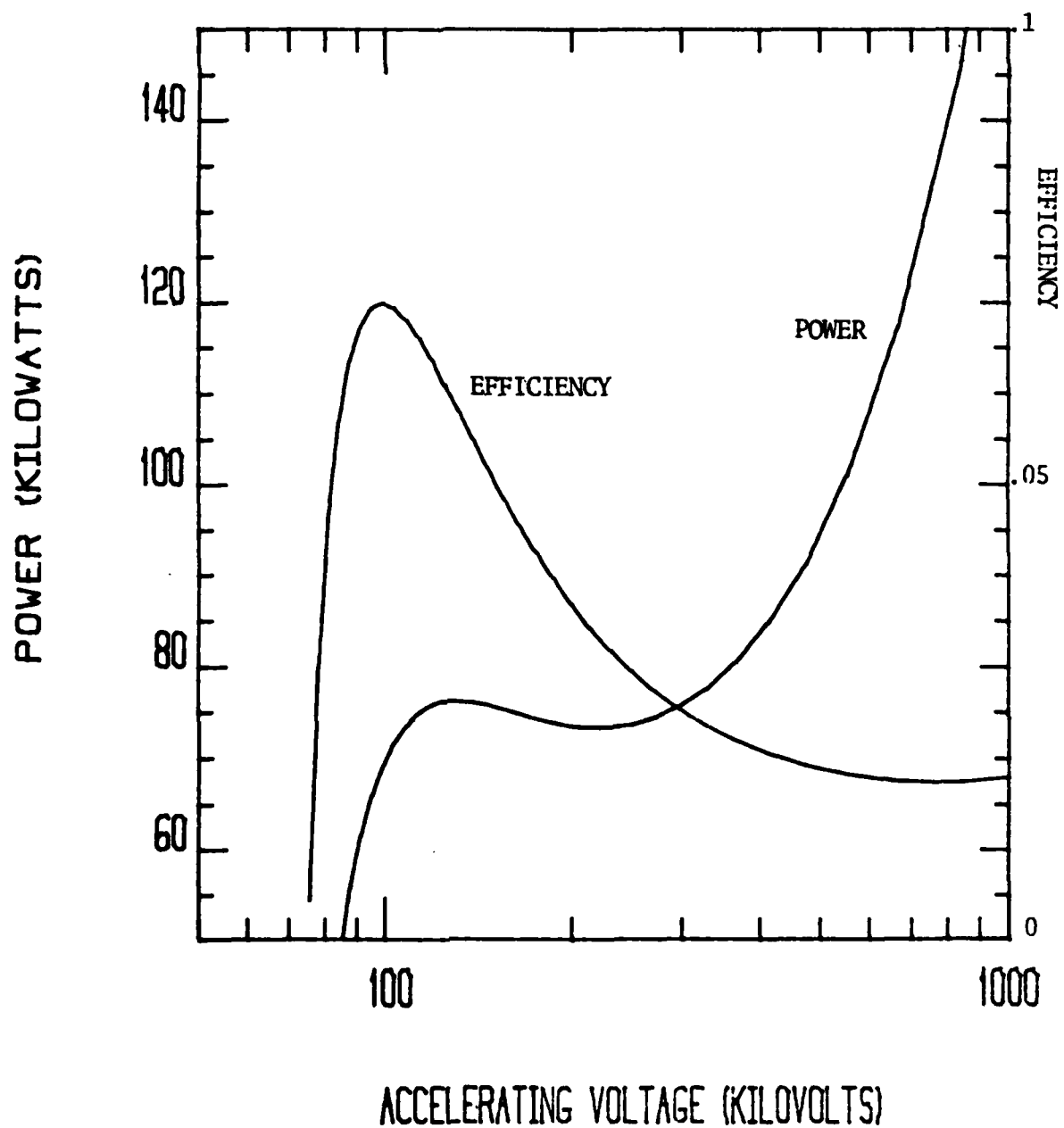


Fig. 4.10. The saturating power and efficiency from the previous figure as a function of beam voltage.

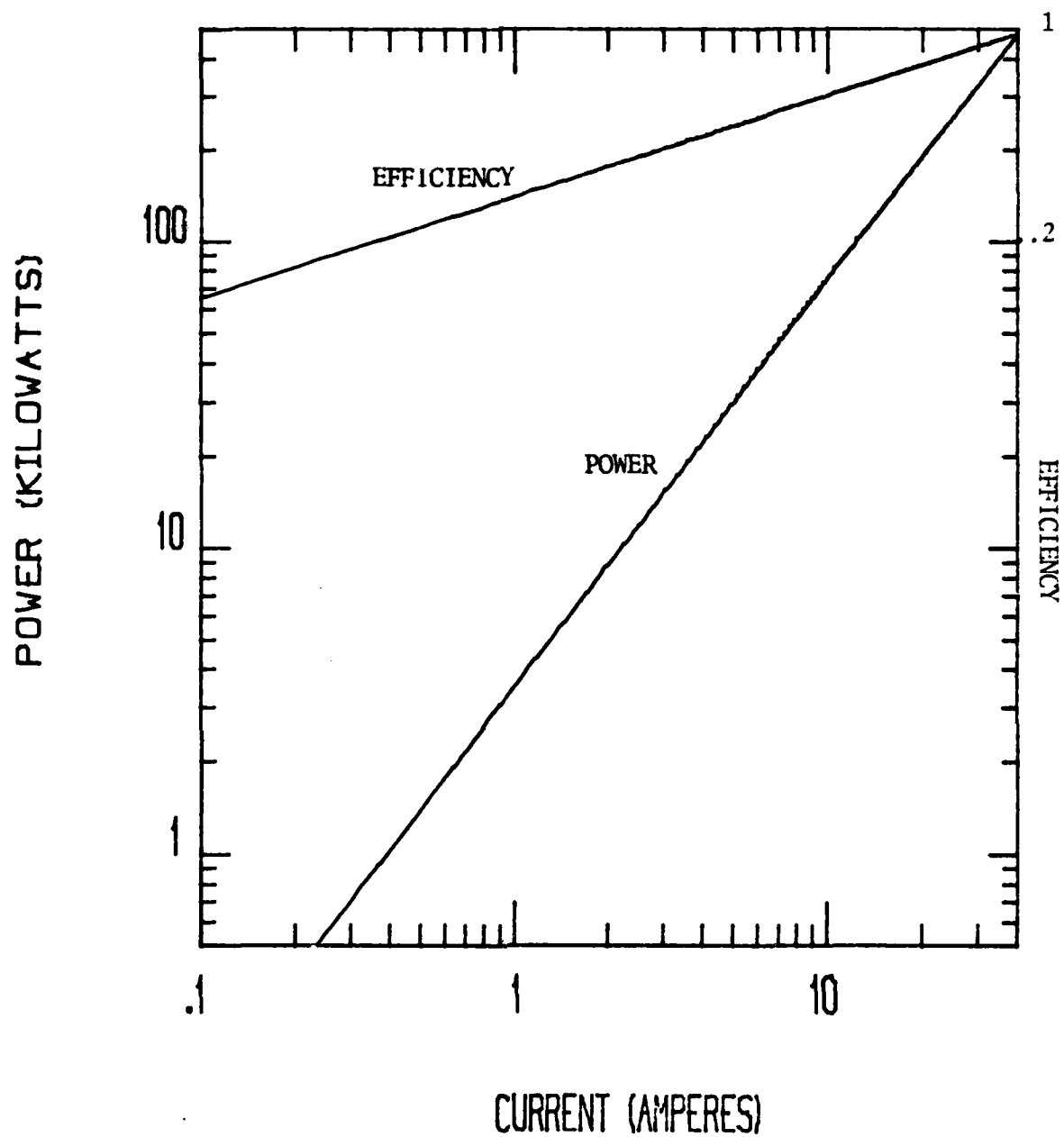


Fig. 4.11. Saturating power and efficiency vs. current for a two millimeter boron nitride liner in 12.5 millimeter guide and a constant 125 keV, six millimeter diameter beam.

The power and efficiency are proportional to $I_b^{4/3}$ and $I_b^{1/3}$, respectively.

4.3 POWER MEASUREMENTS

Power measurements are made with calibrated lengths of a lossy material (Emerson & Cuming eccosorb AN72), conventional Ka band (21-42 GHz) variable waveguide attenuators, and square-law detector diodes in Ka band mounts. Radiation is guided from the circular to rectangular transducer through the attenuation to the diode. As the power increases, attenuation is added, avoiding nonlinear diode response.

At least a factor of two uncertainty is present in these measurements. The waveguide attenuators, used in measurements with quartz, and the diode mounts are designed for the TE_{10} mode of the rectangular guide. The actual mode structure is probably TM_{11} . A fixed amount of eccosorb in a fixed position was used in the quartz measurements.

In measurements with boron nitride the amount of eccosorb was changed between readings; the variable attenuators were not used. This technique should be less sensitive to mode structure. However, the standing wave pattern in the detection hardware is sensitive to the position of the eccosorb. Thus measurements are uncertain by a factor of the standing wave ratio.

The general behavior of the power as a function of beam current for the two millimeter quartz liner is shown in Fig. 4.12. A calibration was obtained with the same liner geometry. A 12 ampere, 115 kilovolt beam generated 30 kilowatts of radiation at 50 Ghz.

Power vs. current data for two millimeter boron nitride are given in Fig. 4.13. The frequency is 21 GHz, and the maximum power is 36 kilowatts. Powers up to 100 kilowatts (10% efficiency) were obtained for three millimeter thick boron nitride in the 12.5 millimeter diameter waveguide (Fig. 4.14). Power is often sufficient to cause atmospheric breakdown in X-band waveguide.

The kilowatt level power measurements correspond well with estimates of the saturating power. Signal levels two and three orders of magnitude lower are also observed and may correspond to single pass operation. Different mechanisms may dominate at different times during the output pulse.

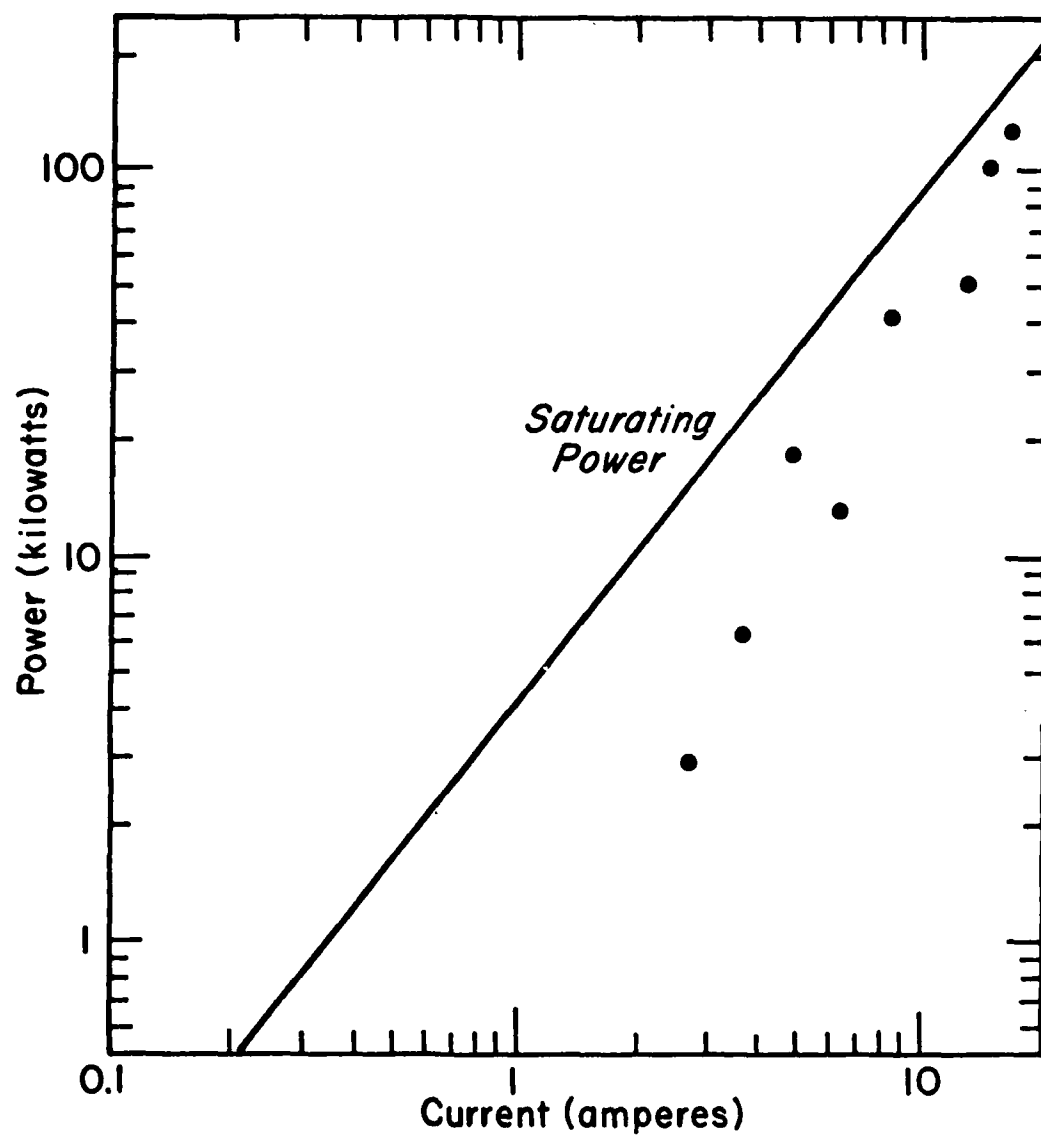


Fig. 4.12. Saturating power and measurements (●) for two millimeter quartz with a 150 keV beam. The saturating power is evaluated assuming a six millimeter beam diameter.

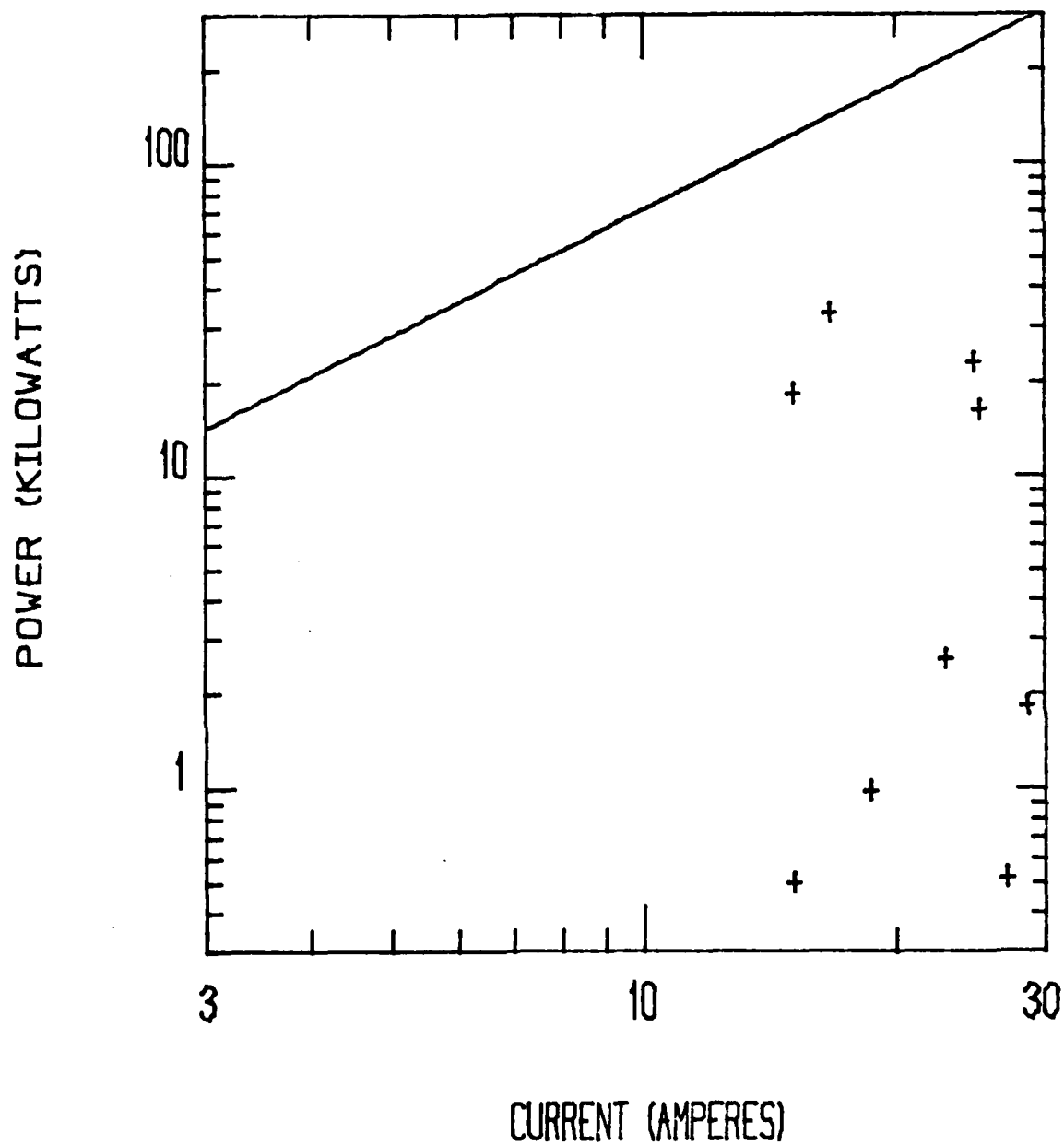


Fig. 4.13. Saturating power and measurements (+) for two millimeter boron nitride with a 150 keV beam. The saturating power is evaluated assuming a six millimeter beam diameter.

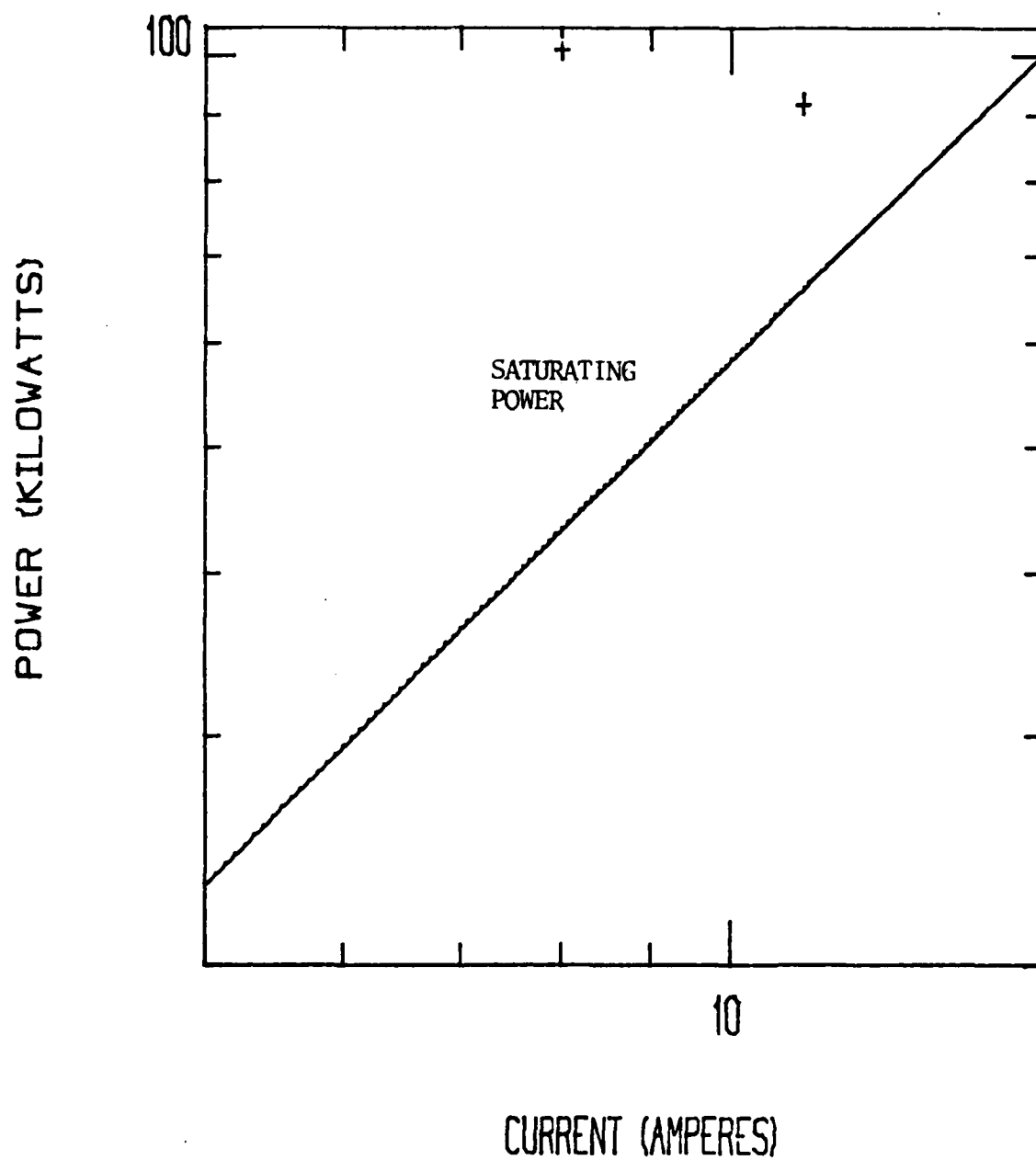


Fig. 4.14. Saturating power and measurements (+) for three millimeter boron nitride with a 114 keV beam. The saturating power is evaluated assuming a six millimeter beam diameter.

CHAPTER V

5.1 CONCLUSION

Knowledge of the cold, collective growth rate for the cylinder is useful to the present experimental effort. The onset of multiple pass operation and subsequent saturating power can be estimated.

Planned for the future are experiments which will employ a colder, more dense (more collective) beam. The beam cross-sectional profile will be more uniform in the z direction. Modifications to the pulse forming network can make the beam energy more uniform in time and provide information about the possible DC operation of Cerenkov masers. With these improvements the calculated growth rate will be subject to less uncertainty.

The growth rate related measurements will be more accurate as well. A low power, swept source is available for passive resonator feedback measurements, and methods for controlling the feedback externally are under development. Better power diagnostics and, eventually, beam calorimetry will be implemented.

All of this information can be used to optimize the length of a liner for a given cross-sectional, beam-liner

geometry and, with a little more effort, to design a beam-liner geometry of variable cross section. The resulting large energy extraction combined, possibly, with a beam recovery system should lead to an efficient, high power, tunable, millimeter source.

APPENDIX I

A1.1 RADIAL TRIGONOMETRIC FUNCTIONS

Definitions:

$$sn(u,v) = (J_0(v)Y_0(u) - Y_0(v)J_0(u))/(2/\pi v) \quad (A1.1a)$$

$$cs(u,v) = (Y_0(v)J_1(u) - J_0(v)Y_1(u))/(2/\pi v) \quad (A1.1b)$$

$$Sn(u,v) = (J_1(v)Y_1(u) - Y_1(v)J_1(u))/(2/\pi v) \quad (A1.1c)$$

$$Cs(u,v) = (J_1(v)Y_0(u) - Y_1(v)J_0(u))/(2/\pi v) \quad (A1.1d)$$

$$\begin{aligned} Sn(u,0) &= \lim(v \rightarrow 0) Sn(u,v) \\ &= J_1(u) \lim(v \rightarrow 0) (-Y_1(v)/(2/v)) = J_1(u) \quad (A1.2a) \end{aligned}$$

$$\begin{aligned} Cs(u,0) &= \lim(v \rightarrow 0) Cs(u,v) \\ &= J_0(u) \lim(v \rightarrow 0) (-Y_1(v)/(2/v)) = J_0(u). \quad (A1.2b) \end{aligned}$$

Identities:

$$sn(u,u) = Sn(u,u) = 0 \quad (A1.3a)$$

$$cs(u,u) = Cs(u,u) = \sqrt{v/u} \quad (A1.3b)$$

$$sn(u,v)Sn(u,v) + cs(u,v)Cs(u,v) = v/u. \quad (A1.4)$$

Derivatives:

$$(d/du)sn(u,v) = cs(u,v) \quad (A1.5a)$$

$$(d/du)cs(u,v) = Sn(u,v) \quad (A1.5b)$$

$$(d/du)Sn(u,v) = Cs(u,v) - Sn(u,v)/u \quad (A1.5c)$$

$$(d/du)Cs(u,v) = -Sn(u,v) \quad (A1.5d)$$

$$(1/(2/\pi qb))(d/dq)((2/\pi qb)sn(qa,qb)) = (a)cs - (b)Cs \quad (A1.6a)$$

$$(1/(2/\pi qb))(d/dq)((2/\pi qb)cs(qa,qb)) = -(a)sn + (b)Sn - cs/q. \quad (A1.6b)$$

APPENDIX II

A2.1 ANISOTROPIC DIELECTRIC LINERS

Dielectric tubes and sheets are manufactured which have a lower dielectric constant along the short (x) axis than that along the other two axes (Union Carbide "Boralloy" boron nitride). Such a material suggests the possibility of operating at a low phase velocity and high frequency with milder evanescence of the longitudinal electric field. Preliminary analysis indicates that some advantage may be gained.

The wave equation for E_z becomes more complicated, since the substitution $\nabla \cdot \vec{E} = 4\pi ne$ is no longer possible. The fields are now given as

$$E_z = \begin{cases} (A)\text{sn}(q'x, q'b) & a < x < b \\ (B)\text{Cs}(ipx, 0) & 0 < x < a \end{cases} \quad (\text{A2.1a})$$

$$E_x = \begin{cases} (ikq'/q_x^2)(A)\text{cs}(q'x, q'b) & a < x < b \\ (-k/p)(B)\text{Sn}(ipx, 0) & 0 < x < a, \end{cases} \quad (\text{A2.1b})$$

where $q'^2 = \epsilon_z w^2/c^2 - (\epsilon_z/\epsilon_x)k^2$, $q_x^2 = \epsilon_x w^2/c^2 - k^2$, and $p^2 = k^2 - w^2/c^2$.

The dispersion relation is now

$$(q_x^2/q') \operatorname{tn}(qa, qb) (\operatorname{Tn}(ipa, 0)/i) = \epsilon_x p. \quad (\text{A2.2})$$

Equations A2.1 and A2.2 reduce to to Equations 2.1 and 2.6 when $\epsilon_x = \epsilon_z$.

Fig. A2.1 shows dispersion curves for isotropic liners with dielectric constants of 3.4 and 5.12 and the curve for an anisotropic liner with $\epsilon_x = 3.4$ and $\epsilon_z = 5.12$. At small wavenumbers the mode of the anisotropic liner has a phase velocity nearly as slow as the phase velocity of the mode of the $\epsilon = 5.12$ isotropic liner. At large wavenumbers it approaches the $\epsilon = 3.4$ phase velocity. The group velocity of the anisotropic mode, however, is quite a bit larger than that of either of the isotropic modes in the range of wavenumbers shown. The experimental wavenumbers fall in this range. The growth rate of the collective Cerenkov instability is connected to the group velocity as described in Section 3.1, and may also be larger for the anisotropic case.

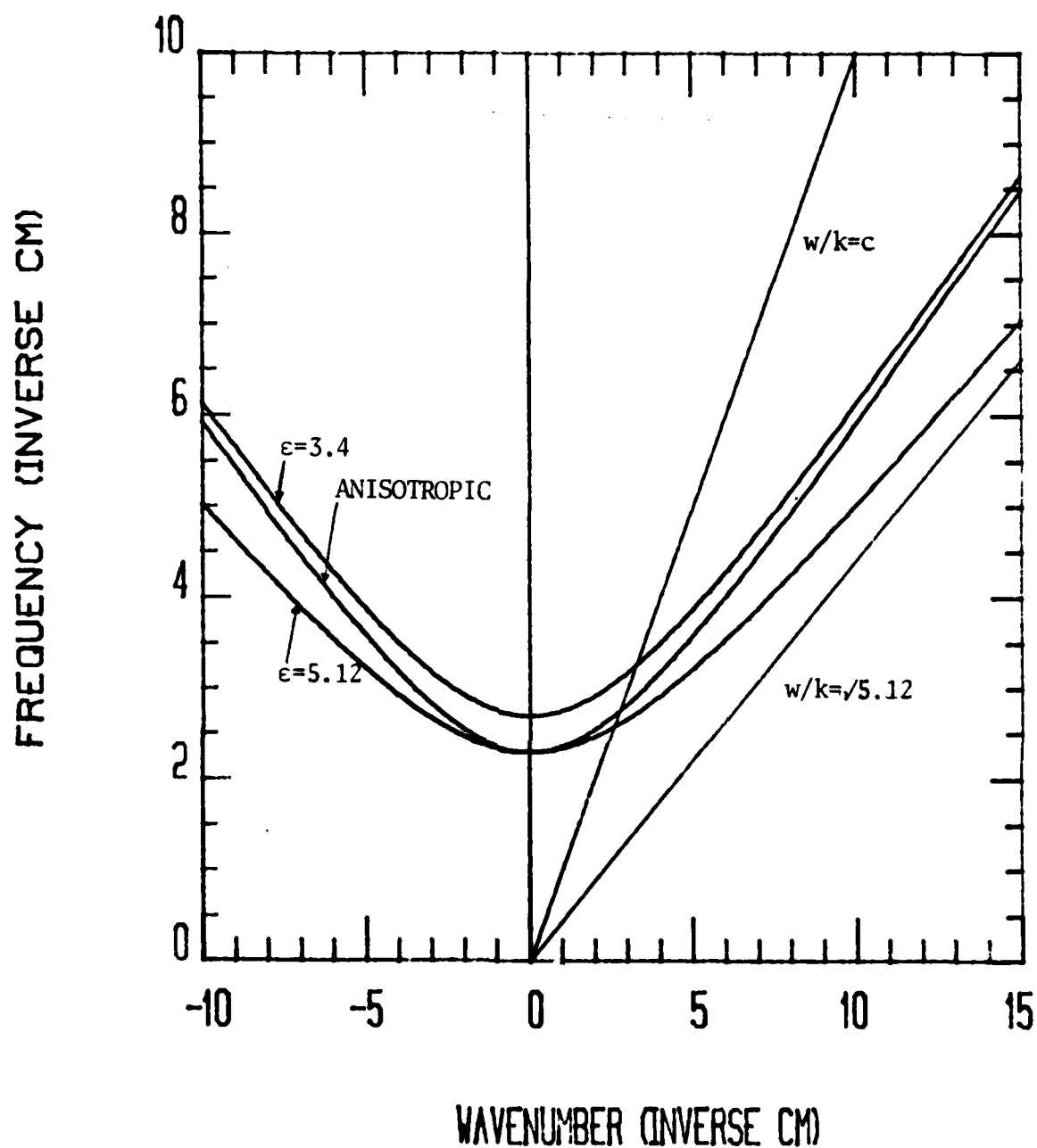


Fig. A2.1 Dispersion curves for the TM_{01} modes of two isotropic liners and an anisotropic liner with $\epsilon_\theta = \epsilon_r = 3.4$ and $\epsilon_z = 5.12$. The liner thickness is three millimeters, r , and the guide diameter is 12.5 millimeters.

APPENDIX III

A3.1 SOFTWARE

The following programs and catalogs are stored in the catalog *D11140:FELCAT and on tape Q1172.

2SLABCAT: Catalog containing double slab dispersion program and related software.

ANIS.DIS: CYLDIS modified to account for a radial dielectric constant different from that along the other axes of the liner.

COLGNEFF: Program to calculate the cylinder growth rate using an effective beam density (Eqn. 3.34) to account for a gap between the liner and a three millimeter radius beam. The guide dispersion curve is read from files CYLTM0n. Liner parameters are read from CYLTMCO. When the program reaches the end of the dispersion file, it attempts to continue the calculation by using an approximation (Eqn. 2.12). The roots of $ct(qa, qb)$, necessary for the

approximation, are read from CT.ZEROS. Growth rates are output to COLGAINn.

COLLGAIN: Operates exactly as COLGNEFF assuming no gap.

CTZEROER: Calculates roots of $ct(qa, qb)$ and stores them in CT.ZEROS (compiled).

CUTOFFS: Calculates cutoff frequencies for the TE_{0n} and TM_{0n} modes of the cylinder. The liner parameters and frequencies are stored in CYLTECO or CYLTMCO (compiled).

CYLDIS: Calculates dispersion curves for the TE_{0n} and TM_{0n} modes of the cylinder. The curves are stored one point ($k \text{ cm}^{-1}$, $w \text{ cm}^{-1}$) to a line in terminal format files CYLTEOn and CYLTMOn, $n=1, \dots, 9$. Liner parameters and cutoff frequencies are read from CYLTECO or CYLTMCO (bound).

IMSL8: The public fortran Bessel routines used by the various cylinder programs were recovered from IMSLLIB***:EDITION8, appended together, compiled under XF84, and saved in FELCAT under this name. The routines are accessed by basic7 programs by the

statement LIBRARY "IMSL8". Fortran programs can use the statement \$LIBRARY "IMSLLIB***:IMSL8".

PLOT: Calls GRAPHLIB*** routines to perform various plotting tasks. For example, empty guide dispersion curves, beam lines, and axes appropriate for dispersion curves can be drawn with simple commands after the "dispersion" or "d" command.

POWER: Calculates growth rate using effective beam density and uses it to calculate the saturating power. The saturating electric field can be equated to the field at $r=0$ or the r.m.s. average field. Either current or voltage can be varied. Input files are CYLTMCO and CYLTMOn. POWERDAT is the output file.

RAMANCAT: Catalog containing programs for converting dispersion curves to tuning curves when the intersecting beam line is shifted by the cyclotron frequency or the pump wavenumber.

SCODELIB: Catalog containing source code for compiled programs.

SPGAIN: Calculates single electron growth rate. Reads liner parameters from CYLTMCO, dispersion curves from

CYLTM0n, and attempts to approximate using CT.ZEROS.

Growth rates are output to SPGAINn.

TUNECONV: Converts a dispersion curve to a tuning curve
(voltage,frequency).

The Herrmannsfeldt electron trajectory program and related programs are stored in the first six positions on tape Q-773 (format Gcos, seven track) at Kiewit Computation Center, Dartmouth College.

REFERENCES

1. Nikolaus, B., Zhang, D. Z., and Toschek, P. E., Phys. Rev. Lett., 47, 171 (1981).
2. Walling, J. C., Peterson, O. G., Jenssen, H. P., Morris, R. C., and O'Dell, E. W., IEEE J. Quant. Electron., vol. QE-16, 1302 (1980).
3. Colson, W. B., private communication (1982).
4. Elias, L. R., Phys. Rev. Lett., 42, 977 (1979).
5. Walsh, J. E., "Cerenkov and Cerenkov-Raman Radiation Sources," in "Physics of Quantum Electronics," Addison-Wesley, Reading, Mass., vol. 7, 255 (1980).
6. Palevsky, A. and Bekefi, G., Phys. Fluids, 22, 986 (1979).
7. Andronov, A. A., Flyagin, V. A., Gapanov, A. V., Gol'denberg, A. L., Petelin, M. I., Usov, V. G., and Yulpatov, V. K., Infrared Phys., 18, 385 (1978).
8. Jory, H. R., private communication (1982).
9. Deacon, D. A. G., Elias, L. R., Ramian, G. J., Schwettman, H. A., and Smith, T. I., Phys. Rev. Lett., 38, 892 (1977).
10. Sprangle, P., Smith, R. A., and Granatstein, V. L., NRL Memorandum Report 3911 (1978).
11. Harvey, A. F., "Coherent Light," Wiley-Interscience, New York, 1970.
12. Felch, K. L., Ph.D. thesis (1980) - available from Dartmouth College Dept. of Physics and Astronomy.
13. Murphy, J. B., Ph.D. thesis (1982) - available from Dartmouth College Dept. of Physics and Astronomy.
14. Jacobs, S., Sargent, M., and Scully, M. (editors), "Physics of Quantum Electronics," Addison-Wesley, Reading, Mass., vol. 5 (1978).

15. Jacobs, S., Pilloff, H., Sargent, M., Scully, M., and Spitzer, R. (editors), "Physics of Quantum Electronics," Addison-Wesley, Reading, Mass., vol. 7 (1980).
16. Jelly, J. V., "Cerenkov Radiation and Its Applications," Pergamon Press, New York, (1958).
17. Button, K. (editor), "Infrared and Millimeter Waves, Sources of Radiation," Academic Press, New York, vol. 1 (1979).
18. Ginzburg, V. L., Dokl. Akad. Nauk SSSR, 56, no. 3, 253 (1947).
19. Lashinsky, H., J. App. Phys., 27, 631 (1956).
20. Lashinsky, H., "Cerenkov Radiation at Microwave Frequencies," in "Advances in Electronics and Electron Physics," Academic Press, New York, vol. 14, 265 (1961).
21. Pierce, J. R., J. App. Phys., 26, 627 (1955).
22. Bolotovskii, B. M., Usp. Fiz. Nauk, 75, 295 (1961).
23. Walsh, J. E., Marshall, T. C. and Schlesinger, Phys. Fluids, 20, 709 (1977).
24. Felch, K. L., Busby, K. O., Layman, R. W., Kapilow, D. and Walsh, J. E., Appl. Phys. Lett., 38, 601 (1981).
25. Von Laven, S., Branscum, J., Golub, J., Layman, R., and Walsh, J. E., Proc. IEEE Int. Conf. on Plasma Science (1982).
26. Marcuvitz, N. (editor), MIT Rad. Lab. Series, McGraw-Hill, New York, vol. 10 (1951).
27. Wise, D., Master's thesis (1981) - available from Dartmouth College Thayer School of Engineering.
28. Branscum, J., Honors thesis (1981) - available from Dartmouth College Dept. of Physics and Astronomy.
29. Walsh, J. E. and Murphy, J. B., to be published.
30. Krall, N. and Trivelpiece, A., "Principles of Plasma Physics," McGraw-Hill, New York (1973).
31. Walsh, J. E., "Stimulated Cerenkov Radiation," in "Advances in Electronics and Electron Physics," Academic Press, New York, vol. 58, 271 (1982).

32. Herrmannsfeldt, W. B., SLAC-Report-226 (1979) - description of code available from SLAC Information Center.
33. Uhm, H. S., NSWC TR-139 (1981) - available from the Naval Surface Weapons Center.
34. Thode, L. E., private communication (1981).
35. Feynman, R. P., Leighton, R. B., Sands, M., "The Feynman Lectures on Physics," Addison-Wesley, Reading, Mass., vol. 2 (1966).
36. Montgomery, C. G. and Montgomery, D. D. (editors), MIT Rad. Lab. Series, McGraw-Hill, New York, vol. 8 (1948).
37. Collin, R. E., "Fundamentals of Microwave Engineering," McGraw-Hill, New York (1966).

Cerenkov radiation in dielectric-lined waveguides

K. L. Felch, K. O. Busby, R. W. Layman, D. Kapilow, and J. E. Walsh
Dartmouth College, Hanover, New Hampshire 03755

(Received 16 June 1980; accepted for 4 February 1981)

Using a dielectric-lined waveguide in combination with a relativistic electron beam, we are able to produce 1 kW of Cerenkov microwave radiation. We have observed the dependence of the output microwave frequency on the beam voltage. In addition, we have detected microwave radiation in excess of 150 GHz, corresponding to higher-order mode interaction.

PACS numbers: 32.30.Bv

The need for a high-power source of short-wavelength microwave radiation for use in communications, plasma heating, etc., has motivated much experimental work. Recently, work has been directed toward making the cyclotron maser (gyrotron)¹ and the free-electron laser² into viable short-wavelength microwave generators. The Cerenkov radiation experiments presented in this letter represent a slightly different approach to the problem of producing short-wavelength microwaves at significant power levels.

Ginzburg first suggested using the Cerenkov effect to produce microwave radiation in 1947,³ and Abele⁴ pointed out that Cerenkov radiation produced in a waveguide would lead to a discrete spectrum. Since then several experiments have substantiated Ginzburg's predictions.⁵⁻⁷ These early experiments produced only small amounts of power and generally used prebunched electron beams. In 1977, Walsh, Marshall, and Schlesinger used an intense relativistic electron beam (0.5 MeV, 10 kA) in combination with a dielectric-lined waveguide and produced approximately 1 MW of microwave radiation at 60 GHz.⁸ The present experiments have been performed in an effort to investigate the viability

of using modest electron beams (150 kV, 20 A) in studying the Cerenkov radiation produced in dielectric-lined waveguides and in scaling such a device up to higher frequency operation.

Cerenkov radiation is produced when a charged particle is directed through or in close proximity to a dielectric material, at a speed in excess of the speed of light in the dielectric. The resulting "shock" radiation is generally very weak and is emitted in a continuous spectrum. However, if a resonant structure such as a dielectric-lined waveguide is used in combination with a relativistic electron beam, the resulting Cerenkov instability bunches the electron beam in the waveguide and makes it possible to obtain high-power microwave radiation at discrete frequencies.

The frequency of the Cerenkov radiation produced in a dielectric-lined waveguide is approximately the synchronous frequency of the electron beam and the partially filled waveguide modes, as shown in Fig. 1. Transverse magnetic waveguide modes with aximutal symmetry, TM_{0N} modes, will be the modes excited by the axially directed electron beam. It can be seen that by varying the dimensions of the

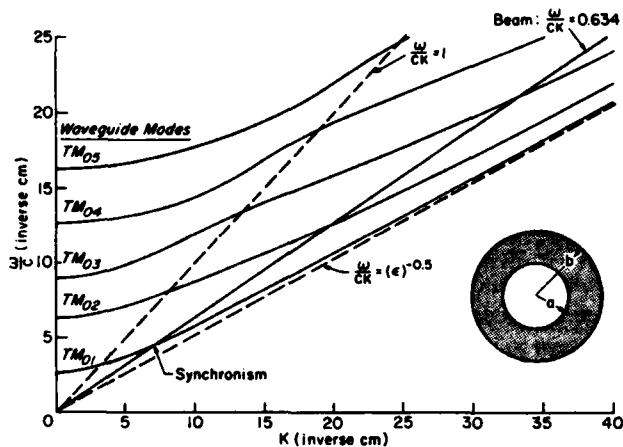


FIG. 1. Plot of the dispersion relation of a dielectric-lined waveguide for TM_{0N} waveguide modes, showing the synchronous frequencies of the waveguide modes and a 150-keV electron beam.

dielectric liner or by changing the electron velocity the synchronous frequency may be tuned to both higher and lower values. In addition, if one is able to couple to higher-order waveguide modes, one is able to obtain extremely high frequencies. The gain obtainable on the higher branches will, however, usually be smaller than that on the fundamental branch.

A schematic diagram of the electron beam generator and resonator structure is shown in Fig. 2. The cathode is either a dispenser or a barium-oxide-cathode, which provides a solid, cylindrical electron beam of up to 30 A. A pulse from a pulse forming network is fed into a high-voltage pulse transformer with bifilar secondary windings. The output voltage pulse may be varied between 0 and -300 kV and is between 4 and 6 μ s in width. The machine is fired 1 to 7 times per second and has the ability to operate at 200 pps. The electron beam is accelerated from the cathode through a hole in the molybdenum anode and into the quartz-lined ($\epsilon = 3.78$) cylindrical waveguide. The beam is held on the axis of the waveguide by an axial magnetic field of between 2.5 and 8 kG. As the electron beam emerges from the dielectric-lined waveguide it follows diverging magnetic field lines until it is deposited on the waveguide walls.

Microwaves produced in the resonator are fed out the end of the machine where power and frequency measurements are carried out. Power measurements are made using crystal detectors and attenuators in suitable waveguide

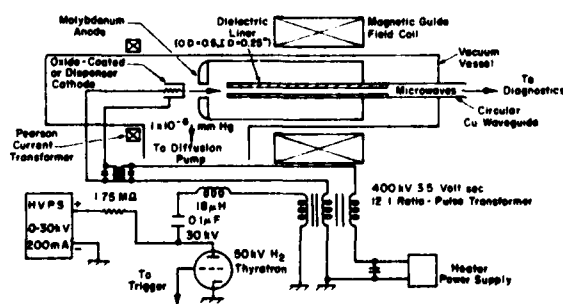


FIG. 2. Schematic diagram of the experimental apparatus for the Cerenkov microwave generation experiments.

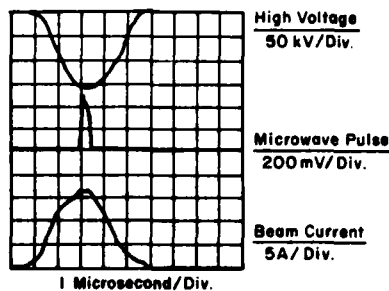


FIG. 3. Oscilloscope traces of the electron beam current and voltage and the resultant Cerenkov microwave pulse.

mounts, and frequency measurements are made by using a series of high pass filters or by using a microwave Fabry-Perot interferometer.

Data from a typical shot are shown in Fig. 3. The microwave pulses usually occur on or near the peak of the high-voltage pulse after a certain voltage threshold has been reached. The Cerenkov threshold for quartz ($\beta^2\epsilon > 1$, $\epsilon = 3.78$) is about 85 kV, but we do not observe microwave output until voltages of about 120 kV have been reached. The value of the guiding magnetic field has no effect on the microwave output other than the fact that it must be present to enable the electrons to pass through the resonator. Electron beam currents as low as 500 mA are sufficient for microwave generation, while higher currents serve to enhance the power and pulse width of the microwave signal. For a typical 150-kV, 10-A electron beam, we detect peak microwave powers of 1 kW.

The inset in Fig. 4 shows an interferogram obtained using a Fabry-Perot interferometer consisting of two screens, one fixed and one movable. The interferogram is the result of hundreds of successive shots while the moving screen is slowly swept through a distance of 3-5 cm. The distance between successive maxima in the interferogram is a direct measurement of one-half the free-space wavelength of the radiation.

A series of such interferograms was taken for numerous different voltages. A plot of the output frequency versus beam voltage is shown in Fig. 4. Included in Fig. 4 is a theoretical plot of the synchronous frequency of the beam-waveguide system as a function of beam voltage. We note that the

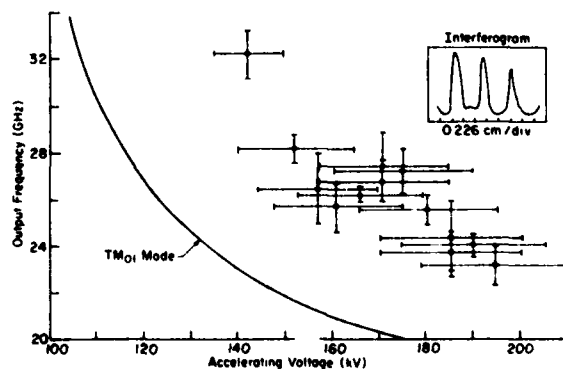


FIG. 4. Plot of the output microwave frequency, obtained using the Fabry-Perot interferometer (a typical interferogram is shown in the inset), as a function of beam voltage. The theoretical plot of the synchronous frequencies for the TM_{01} mode is shown for comparison.

data plot has the same general shape as the theoretical one, but that it is displaced to higher voltages. We find that by dividing the observed voltage by a factor of 1.3, the data will fit on the theoretical curve. As of yet, we have found no direct reason for this discrepancy.

Using high-frequency filters, we have been able to detect radiation in excess of 150 GHz with the present resonator structure. These high-frequency signals are probably due to the interaction of the electron beam with higher-order waveguide modes, since the gain, although smaller, is not negligible. The power of the 150-GHz signals is 1 W at the diode junction and may be much higher if one takes into account the sensitivity of the detector diode [1N53] at 150 GHz.

In conclusion, the above experiments have demonstrated the ability to use the Cerenkov interaction produced when a relativistic electron beam is accelerated through a dielectric-lined waveguide, as a tunable source of high-power, short-wavelength radiation. We have observed the basic de-

pendence of the output frequency on electron beam energy and have detected microwave signals in excess of 150 GHz at significant power levels.

We would like to acknowledge the support of the U.S. Army, Grant No. DAAG-29-79-C0203.

¹J. L. Hirshfield, "Gyrotrons," in *Infrared and Millimeter Waves*, edited by Kenneth J. Button (Academic, New York, 1979), Vol. 1.

²P. Sprangle, R. A. Smith, and V. L. Granatstein, "Free Electron Lasers and Stimulated Scattering from Relativistic Electron Beams," in Ref. 1.

³V. L. Ginzburg, Dok. Akad. Nauk SSSR **56**, 253 (1947).

⁴M. Abele, Nuovo Cimento **9**, 207 (1952).

⁵M. Danos, S. Geschwind, H. Lashinsky, and A. van Trier, Phys. Rev. **92**, 828 (1953).

⁶P. D. Coleman and C. Enderby, J. Appl. Phys. **31**, 1695 (1960).

⁷R. Ulrich, Z. Phys. **199**, 171 (1967).

⁸J. E. Walsh, T. C. Marshall, and S. P. Schlesinger, Phys. Fluids **20**, 709 (1977).

END

FILMED